

On power system automation

Synchronised measurement technology supported power system situational awareness

Naglic, Matija

DOI

[10.4233/uuid:33a9138f-7224-4734-a326-d90a9d5980c1](https://doi.org/10.4233/uuid:33a9138f-7224-4734-a326-d90a9d5980c1)

Publication date

2020

Document Version

Final published version

Citation (APA)

Naglic, M. (2020). *On power system automation: Synchronised measurement technology supported power system situational awareness*. [Dissertation (TU Delft), Delft University of Technology].
<https://doi.org/10.4233/uuid:33a9138f-7224-4734-a326-d90a9d5980c1>

Important note

To cite this publication, please use the final published version (if applicable).
Please check the document version above.

Copyright

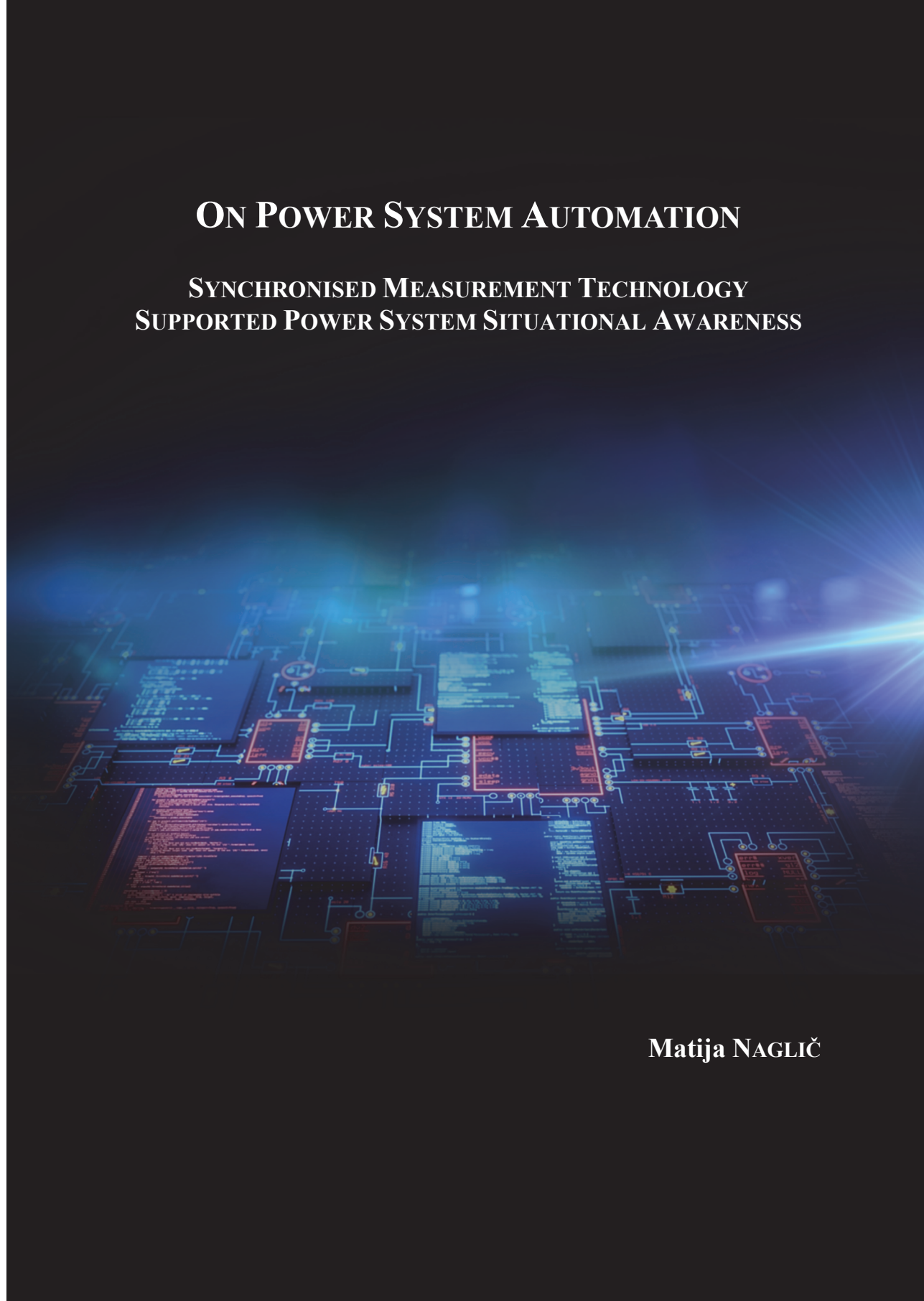
Other than for strictly personal use, it is not permitted to download, forward or distribute the text or part of it, without the consent of the author(s) and/or copyright holder(s), unless the work is under an open content license such as Creative Commons.

Takedown policy

Please contact us and provide details if you believe this document breaches copyrights.
We will remove access to the work immediately and investigate your claim.

ON POWER SYSTEM AUTOMATION

SYNCHRONISED MEASUREMENT TECHNOLOGY SUPPORTED POWER SYSTEM SITUATIONAL AWARENESS



Matija NAGLIČ

ON POWER SYSTEM AUTOMATION

SYNCHRONISED MEASUREMENT TECHNOLOGY
SUPPORTED POWER SYSTEM SITUATIONAL AWARENESS

Dissertation

for the purpose of obtaining the degree of doctor
at Delft University of Technology,
by the authority of the Rector Magnificus prof. dr. ir. T.H.J.J. van der Hagen,
Chair of the Board for Doctorates,
to be defended publicly on
Monday 30 March 2020 at 10:00 a.m.

by

Matija NAGLIČ
univerzitetni diplomirani inženir elektrotehnike,
The University of Ljubljana, Slovenia,
born in Kranj, Slovenia

This dissertation has been approved by the promotor.

Composition of the doctoral committee:

Rector Magnificus,
Prof. ir. M.A.M.M. van der Meijden
Dr. Dipl.-Ing. M. Popov

Chairperson
Delft University of Technology, promotor
Delft University of Technology, promotor

Independent members:

Prof. Dr. P. Palensky
Prof. Dr. V. Terzija
Prof. Dr. M. Paolone
Prof. Dr.-Ing. M. Luther
Ir. M. Abbenhuis
Prof. Dr. P. Bauer

Delft University of Technology
The University of Manchester
Swiss Federal Institute of Technology of Lausanne
Friedrich-Alexander-Universität Erlangen-Nürnberg
TenneT TSO B.V.
Delft University of Technology, reserve member

This research was financially supported by the Dutch Research Council (NWO) within the program of Uncertainty Reduction of Smart Energy Systems (URSES).



ISBN 978-94-6384-118-4

Keywords: energy transition, power system automation, synchronised measurement technology, situational awareness, phasor measurement unit, disturbance detection, slow coherency, control room of future

Copyright © 2020 by Matija Naglič
Cover design by Matija Naglič
Cover photo copyright © 2020 by Shade Lite @ bigstockphoto

All rights reserved. No part of the material protected by this copyright notice may be reproduced or utilized in any form or by any means, electronic or mechanical, including photocopying, recording or by any information storage and retrieval system, without written permission of the author.

An electronic version of this dissertation is available at <http://repository.tudelft.nl/>

Printed in The Netherlands by Ipskamp Printing, Enschede

*“Always be brave, John, like that little boy. Stand your ground and follow your dreams. They will lead you to your destiny. Follow your destiny, it will lead you into the wonders of the universe. And always follow the wonders of the universe, for they will lead you to a special garden, filled with roses.”*¹

In memory of my grandfather Peter Naglič.

¹ R. Sharma. *The Monk Who Sold his Ferrari*. London, United Kingdom: HarperCollins Publishers, 1997

SUMMARY

This thesis aims to provide insight into the necessary power system operation and control developments to facilitate a sustainable, safe and reliable electric power supply now and in the future. The primary objective is *to enhance the interconnected power system situational awareness with the aim of reinforcing the reliability of power systems*. First, the thesis elaborates on the existing and emerging operational challenges of modern power systems and identifies the required power system developments to overcome them. Next, it focuses on state-of-the-art *Synchronised Measurement Technology* (SMT) supported *Wide-area Monitoring Protection and Control* (WAMPAC) of power systems. In this context, a cyber-physical experimental testbed for online evaluation of the emerging WAMPAC applications under realistic conditions is developed. The testbed consists of a real-time power system digital simulator and actual SMT components that are connected with the simulator as Hardware-In-Loop (HIL). As a part of the testbed, a new web-based SMT monitoring platform is developed for online monitoring of Phasor Measurement Unit (PMU) measured power grid dynamics and alarming purpose. Following, the reasons and the shortcomings of conventional software simulated bus measurements for WAMPAC application design and validation are discussed. To address the shortcomings and fill the scientific gap between the IEEE Std. C37.118-2005 (communication part) and IEEE Std. C37.118.2-2011 specifications and their implementation, a *MATLAB* supported *Synchro-measurement Application Development Framework* (SADF) is developed. The SADF for the first time enables online receiving and parsing of PMU generated machine-readable messages into a human-friendly *MATLAB* format. In this context, a robust data receiver communication technique with integrated fall-back procedures, and an efficient online receiving and parsing methodology of the encapsulated machine-readable configuration and data frames are proposed. Next, to improve situational awareness of power systems, two SMT-supported algorithms are proposed. The first algorithm is suitable for online detection of disturbances, observed as excursions in PMU measurements, in AC and HVDC power grids. Notably, PMUs are utilised for the first time to deliver synchro-measurements of an HVDC grid. The proposed algorithm features adaptive thresholds for immunity to measurement variance, fast response, and low computational burden, making it suitable for near real-time operation, as a part of backup protection schemes and monitoring applications. For the evaluation purpose of the algorithm, in particular, to determine the associated disturbance detection time delay, noteworthy attention is paid to time-synchronisation of the supporting systems of the testbed. Further, the second proposed algorithm is suitable for online identification of grouping changes of slow coherent generators in an interconnected power system. Hereby, a series of proposed solutions,

addressing unresolved and newly identified challenges, is compound into the adaptive algorithm, enabling robust and near-real-time tracking of grouping changes of slow coherent generators during quasi-steady-state and the electromechanical transient period following a disturbance. The algorithm, for the first time, detects and removes the interfering pre-event measurements in an observation window and adaptively tracks grouping changes of slow coherent generators, leading to improved accuracy and more robust results, respectively. Moreover, the improved similarity method leads to the identification of areas with different frequencies; meanwhile, the new AP preference adjustment method adaptively determines the optimal number of slow coherent groups and partitions the outlier generators as independent clusters. All together in combination with the novel adaptive observation window method, which determines the minimum number of samples to be processed for near real-time coherency identification, facilitates the design of fast-acting and adaptive emergency control schemes. Finally, in conclusions, the main findings of this thesis are summoned, and further research directions towards the *Control Room of Future* are presented.

SAMENVATTING

Dit proefschrift heeft als doel inzicht te verschaffen in de noodzakelijke ontwikkelingen in de werking en het bedienen van het energiesysteem om een duurzame, veilige en betrouwbare elektrische energievoorziening nu en in de toekomst mogelijk te maken. Het primaire doel is om *het situationele bewustzijn van het onderling verbonden elektrische energiesysteem te verbeteren met als doel de betrouwbaarheid van elektrische energiesystemen te vergroten*. Ten eerste gaat het proefschrift in op de bestaande en in opkomst zijnde operationele uitdagingen van moderne elektrische energiesystemen en identificeert het de voor het elektrische energiesysteem vereiste ontwikkelingen om deze uitdagingen aan te kunnen. Vervolgens concentreert het zich op de meest geavanceerde *Wide-area Monitoring Protection and Control* (WAMPAC) ondersteund door *Synchronised Measurement Technology* (SMT) van elektrische energiesystemen. Een cyber-fysieke experimentele proefopstelling is in deze context ontwikkeld voor online evaluatie van de in opkomst zijnde WAMPAC-toepassingen onder realistische omstandigheden. De proefopstelling bestaat uit een real-time digitale simulator van een elektrisch energiesysteem en werkelijke SMT-componenten die met de simulator zijn verbonden als Hardware-In-Loop (HIL). Als onderdeel van de proefopstelling is een nieuw internet gebaseerd SMT-monitoringsplatform ontwikkeld voor de online monitoring van de door Phasor Measurement Unit (PMU) gemeten dynamiek van het elektrische energienetwerk en alarmsystemen. Hierop volgend worden de redenen voor en de tekortkomingen van conventionele met software gesimuleerde busmetingen voor het ontwerpen en valideren van WAMPAC-toepassingen besproken. Om de tekortkomingen aan te pakken en de wetenschappelijke kloof tussen de specificaties van IEEE Std. C37.118-2005 (communicatiedeel) en IEEE Std. C37.118.2-2011 en de implementatie daarvan te overbruggen, is een *Synchro-measurement Application Development Framework* (SADF) ontwikkeld die ondersteund wordt door *MATLAB*. De SADF maakt voor het eerst online ontvangst en ontleding mogelijk van door PMU gegenereerde voor een machine leesbare berichten in een mensvriendelijk *MATLAB*-formaat. In deze context worden een robuuste communicatietechniek voor gegevensontvangers met geïntegreerde uitwijkprocedures voorgesteld en een efficiënte online ontvangst- en ontleedmethodologie van de bijgesloten door een machine leesbare configuratie en gegevensframes. Vervolgens worden twee door SMT ondersteunde algoritmen voorgesteld om het situationeel bewustzijn van elektrische energiesystemen te verbeteren. Het eerste algoritme is geschikt voor de online detectie van storingen, waargenomen als afwijkingen in PMU-metingen, in AC- en HVDC-elektriciteitsnetwerken. Opmerkelijk is dat PMU's voor het eerst gebruikt worden om synchroonmetingen van een HVDC-netwerk te leveren. Het voorgestelde

algoritme beschikt over adaptieve drempelwaarden voor immuniteit voor meetafwijkingen, snelle respons en lage rekenlast, waardoor het geschikt is voor vrijwel real time functioneren, als onderdeel van back-up beveiligingsschems's en applicaties voor monitoring. Er wordt uitvoerig aandacht besteed aan tijdsynchronisatie van de ondersteunende systemen van de proefopstelling met het doel om het algoritme te evalueren, in het bijzonder om de gerelateerde vertraging in de storingsdetectie vast te stellen. Verder is het tweede voorgestelde algoritme geschikt voor de online identificatie van veranderingen in groepering van traag coherente generatoren in een onderling verbonden elektrisch energiesysteem. Hierbij is een reeks voorgestelde oplossingen, die onopgeloste en nieuw geïdentificeerde uitdagingen aanpakt, samengevoegd tot een adaptief algoritme, waardoor het mogelijk wordt om robuust en vrijwel real-time veranderingen in groepering van langzaam coherente generatoren te volgen tijdens een quasi-stationaire fase en tijdens de elektromechanische transitieperiode volgend op een storing. Het algoritme detecteert en verwijdert, voor het eerst, de interfererende metingen voorafgaand aan een gebeurtenis in een observatievenster en volgt adaptief veranderingen in groepering van langzaam coherente generatoren, hetgeen respectievelijk leidt tot een verbetering in nauwkeurigheid en robuustere resultaten. Bovendien leidt de verbeterde similariteitsmethode tot de identificatie van gebieden met verschillende frequenties; ondertussen bepaalt de nieuwe AP-methode voor het bijstellen van voorkeuren adaptief het optimale aantal traag coherente groepen en verdeelt de afwijkende generatoren als onafhankelijke clusters. Dit alles samen, in combinatie met de nieuwe adaptieve methode met het observatievenster, die het minimum aantal te verwerken monsters bepaalt voor vrijwel real-time identificatie van coherentie, vergemakkelijkt het ontwerp van snel in werking tredende en adaptieve schema's voor noodbesturing. Tenslotte worden in de conclusies de belangrijkste bevindingen van dit proefschrift samengevat en worden verdere onderzoeken richting de *Control Room of Future* gepresenteerd.

PREFACE

This thesis is submitted to the Delft University of Technology (TUD) in partial fulfilment of the Doctoral Programme requirements for the degree of Doctor. This research work has been performed during the period August 2014 – September 2019, in the group of Intelligent Electrical Power Grids at the department of Electrical Sustainable Energy at TUD in Delft, Netherlands. Prof. ir. Mart A.M.M. van der Meijden, TUD and TenneT TSO B.V., and Dr. Dipl.-Ing. Marjan Popov, TUD, have been the promotor.

The research work presented in this thesis is conducted in the frame of the *Uncertainty Reduction in Smart Energy Systems* (URSES) research program², funded by the Dutch Scientific Council NWO and Shell International B.V.. The primary aim of the URSES program is to contribute to the uncertainty reduction in modern energy systems by developing novel solutions for a faster transition towards reliable, affordable and sustainable energy systems. The research work of this thesis is motivated mainly by the scope of *PMU Supported Frequency-Based Corrective Control of Future Power Systems* URSES project under 408-13-025 project number. This project aims to develop a wide-area intelligent system, which empowers Synchronised Measurement Technology for online assessment of system-wide vulnerability and development of timely remedial actions based on system-wide consideration. The research scope of the project was divided into three parts, two Ph.D. and a postdoc research positions, with colleagues M.Sc. Ilya Tyuryukanov and Dr. Jose Chavez Muro in the lead of the other two parts, respectively.

² NWO, Uncertainty Reduction In Smart Energy Systems, 2014. [Online]. Available: <https://www.nwo.nl/en/research-and-results/programmes/URSES+-+Uncertainty+Reduction+in+Smart+Energy+Systems>

TABLE OF CONTENTS

Summary	xi
Samenvatting	xiii
Preface	xv
Chapter 1 Introduction	1
1.1 Thesis Background	2
1.1.1 Traditional power system operation and control	2
1.1.2 Evolving power systems and emerging operational challenges	5
1.2 Problem Definition	9
1.3 Research Objective and Approach	11
1.4 Thesis Outline	13
Chapter 2 Cyber-Physical Experimental Testbed	15
2.1 Introduction	15
2.2 Synchronised Measurement Technology	16
2.2.1 Phasor measurement unit	17
2.2.2 Time synchronisation	23
2.2.3 Phasor data concentrator	24
2.2.4 Wide area telecommunication network	27
2.3 Wide Area Monitoring Protection And Control	27
2.3.1 State-of-the-art WAMPAC applications	28
2.3.2 Existing WAMPAC systems worldwide	29
2.3.3 WAMPAC system implementation challenges	31
2.4 WAMPAC-ready Cyber-physical Experimental Testbed	31
2.4.1 Motivations for the testbed	32
2.4.2 State-of-the-art	33
2.4.3 Components of the testbed	34
2.4.4 Validation of the testbed	38
2.5 Concluding Remarks	39

Chapter 3	Synchro-measurement Application Development Framework	41
3.1	Introduction	41
3.1.1	Motivations for the SADF	42
3.1.2	State-of-the-art	43
3.2	Overview of IEEE Std. C37.118.2-2011	43
3.2.1	Communication framework	44
3.2.2	Communication mode	44
3.2.3	Frame structure and message type	45
3.2.4	Typical data exchange	47
3.3	Structure of SADF Software Library	48
3.3.1	Connection establishment for data exchange	48
3.3.2	Frame integrity validation	51
3.3.3	Frame parsing	51
3.4	Compliance and Performance Evaluation	54
3.4.1	Simulation testbed	54
3.4.2	Compliance verification against IEEE Std. C37.118.2-2011	55
3.4.3	SADF processing performance evaluation	58
3.4.4	Example application: online voltage magnitude monitoring	60
3.5	Concluding Remarks	61
Chapter 4	Online Disturbance Detection	63
4.1	Introduction	63
4.1.1	State-of-the-art	63
4.1.2	Challenges and motivations	64
4.2	Proposed Methodology	65
4.2.1	Data acquisition in AC and HVDC	65
4.2.2	Disturbance detection algorithm	66
4.2.3	Pseudocode of the proposed methodology	69
4.3	Simulation Studies	70
4.3.1	Simulation testbed	71
4.3.2	Measurement latency evaluation	72
4.3.3	Observation window length	73
4.3.4	Study cases and simulation results	74
4.3.5	Comparison with the existing techniques	81
4.4	Discussion of the Results	82
4.5	Concluding Remarks	83
Chapter 5	Online Identification of Slow Coherent Generators	85
5.1	Introduction	85
5.1.1	State-of-the-art	86

5.1.2	Challenges and motivations	88
5.2	Proposed Methodology	89
5.2.1	Source of measurements	89
5.2.2	Pre-processing of measurements	90
5.2.3	Generator distance matrix	92
5.2.4	Adaptive observation window	93
5.2.5	Reverse data selectivity	94
5.2.6	Adaptive tracking of grouping changes	95
5.2.7	Time evolution of slow coherency indices	97
5.2.8	Partitioning of generators into coherent groups	97
5.2.9	Flowchart of the proposed methodology	101
5.3	Simulation Studies	103
5.3.1	Simulation testbed	103
5.3.2	Study cases and simulation results	104
5.4	Discussion of the Results	113
5.4.1	Comparison with the benchmark method	113
5.4.2	Proposed algorithm's requirements and performance	113
5.5	Concluding Remarks	116
Chapter 6 Conclusions and Further Research Directions		117
6.1	Thesis Conclusions	117
6.2	Further Research Directions	121
Nomenclature		125
	List of Abbreviations	125
	List of Symbols and Notations	129
Bibliography		131
Acknowledgements		143
Biography		145

CHAPTER 1

INTRODUCTION

The present electric power system (hereinafter referred to as power system), which represents the heart of the modern world, experiences substantial changes. For the good of our future, the energy transition drives the energy sector towards investments in clean energy technology and energy efficiency. Within this context, the conventional power generation centres, in particular fossil-fuel and nuclear power plants, are decommissioned and substituted for energy sources that are distributed (geographically dispersed and typically locally connected to a low voltage power system), sustainable (meets the needs of the present without compromising the ability of future generations to meet their own needs) and renewable (does not result in the depletion of the earth's resources), characterised by predominantly wind and solar.

The ongoing energy transition brings not only conspicuous environmental and societal benefits, but the resulting increase in power system complexity leads to unprecedented power systems' behaviour and imposes new operational challenges. The triggering factor is that there is a deficiency of crucial developments to support and prepare the power system operators for the existing and upcoming operational challenges, respectively. Especially, the limited observability of power system dynamic phenomena, limited situational awareness, and lack of coordinated protection and control schemes may lead to an inability to operate the power system in time adequately.

Given the increasing number and severity of power system outages and large blackouts, there is a pressing need not only to identify incipient technological advances to meet the operational requirements of the today and future power systems but above all, at an early stage, to design an experimental testbed suitable for analyses on how the existing power systems accommodate the emerging developments thoroughly. This thesis provides an insight into the emerging operational challenges, addresses the required developments, and presents the developed cyber-physical experimental testbed. Besides, Synchronised Measurement Technology (SMT) supported algorithms are proposed to improve the situational awareness of power systems and facilitate the development of emergency control schemes.

1.1 THESIS BACKGROUND

Ever growing world's population and technological advances are propelling the global electric power demand at an unprecedented pace. Nowadays, electric power accounts for 19 % of all consumed energy and is expected to grow up to 24 % until the year 2040 [1]. The increase in worldwide population leads to a double challenge that humanity needs to solve. The first is related to providing a sufficient amount of energy to support the living, while the second with the associated impact on the environment, in particular, climate change.

1.1.1 TRADITIONAL POWER SYSTEM OPERATION AND CONTROL

In a traditional power system, the transmission network is used as a backbone to transmit bulky volumes of electric power over large geographical distances, originally from fossil-fuel, hydro, and nuclear generation sources to distribution networks connecting end-consumers. In substations, connecting the transmission and distribution networks, the transmission network voltages are scaled down to the levels of the distribution network. The distribution network then further distributes electric power in one way directly to the end-consumers, as illustrated in the following Figure 1.1.

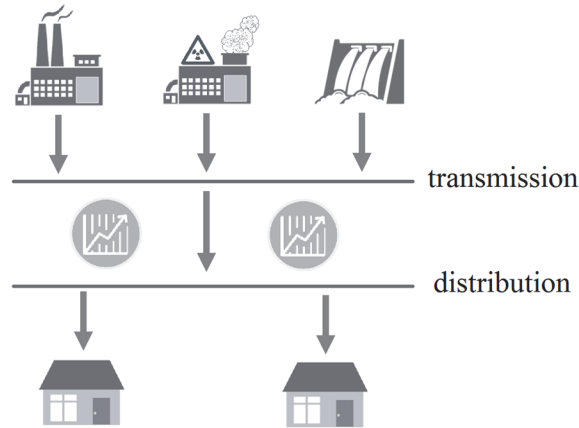


Figure 1.1: Simplified illustration of a traditional power system.

The primary function of a power system is to supply electric power with acceptable quality in a sufficient, reliable, and economically efficient manner. The following definitions are used to describe the functional aspects of a power system systematically:

- *Stability* - “the ability of an electric power system, for a given initial operating condition, to regain a state of operating equilibrium after being subjected to a physical disturbance, with most system variables bounded so that practically the entire system remains intact.” [2]

- *Reliability* - “the probability of the power system performing its function adequately, for the period of time intended, under the operating conditions intended.” [3]
- *Adequacy* - “the ability of the power system to supply the aggregated electric power and energy requirements of the customer at all times, taking into account scheduled and unscheduled outages of system components.” [2]
- *Security* - “the ability of the power system to withstand sudden disturbances such as electric short circuits or nonanticipated loss of system components.” [2]
- *Resiliency* - the ability of the power system to resist, absorb, respond to, adapt to and recover from a disturbance [4].
- *Flexibility* - the ability of the power system to deploy its resources with the aim to respond to changes that may affect the balance of supply and demand at all time, ensuring a stable and a secure operation [5], [6].

To summarise, in order to assure a sufficient level of power system reliability to deliver energy with specific quality, the power system must be most of the time flexible and secure, meaning that the power system can mitigate most unexpected supply and demand unbalances as well as abnormal system’s conditions, and regain its stable operation without violating the power system’s constraints and limitations of the hardware components [2]. To fulfil these requirements, the Transmission System Operator (TSO), a responsible authority for the operation and control of a transmission network, makes use of an Energy Management System (EMS).

A. ENERGY MANAGEMENT SYSTEM

In a power system, the EMS, encompassing a collection of computerised systems, is used to maintain the transmission network stability, meanwhile guaranteeing a reliable, secure, and economically efficient energy generation and transmission [7].

During daily operation, the transmission network can be subjected to a wide range of unexpected disturbances, observed as sudden change or sequence of changes in system parameters from its nominal values. Disturbances include but are not limited to dips, swells, momentary interruptions, and oscillatory transients [8]. Typically, disturbances are caused by different events, such as switching operations, power swings, load steps, short circuit faults, lightning, and electrical failures of power system components to name a few. In order to prevent the occurrence of disturbances or to detect, arrest and mitigate the unanticipated one, and to restore the system to its normal operation, the power system operation and control make use of diverse monitoring, protection, and control systems [9].

Nowadays, typical protection and control schemes, disseminated in remote substations, are primarily based on pre-determined and non-adaptive execution sequences that take into account only local information [10]. In the case of events, such as short circuit faults or issues with voltage and frequency, the applied protection and control schemes attempt to safeguard the power system automatically. However, any resulting power network

contingencies (loss/failure of a vital element i.e., transformer, generation unit, or transmission line) or power network congestions (operation of a power network element above its nominal values) require further manual remedial control to mitigate the instabilities and restore the power system to its normal operation. For this purpose, a Supervisory Control And Data Acquisition (SCADA) system is used.

B. SUPERVISORY CONTROL AND DATA ACQUISITION

SCADA encompasses various technologies and hardware components to enable local and remote power system monitoring and control, typically from a substation and a centralised control centre, respectively. The SCADA's data acquisition involves a collection of the substation's equipment parameter and process data. Only the most pertinent information is transferred through the supporting telecommunication infrastructure to the control centre's computerised system or Master Terminal Unit (MTU), where the necessary data analyses are carried out to assess the power system state and health. In the case when a specific analysis parameter is operating outside of the predefined boundaries, the SCADA system triggers an alarm to notify the power system operators. Figure 1.2 shows a typical control room with computerised systems and several large screens displaying the one-line diagram and status of the operated power grid components. In case of detected disturbances or when a planned network reconfiguration takes place, the power system control room operators manually perform coordinated remedial actions, often in harmonisation with the remote substation, power plant and neighbouring power system operators. For this, the SCADA's supervisory remote control is used to relay the power system operator's control decisions to the targeted devices in the remote substations and power plants, thus enabling remote network reconfiguration and redispatch of the generating units [11].



Figure 1.2: An example of a conventional SCADA-based control room, used by the power system operators to operate a power system (courtesy of IESO, Ontario).

A typical SCADA monitoring system is based on two- to ten- second measurement update rate from the hardware components, placed in a remote substation. The measurements are timestamped at the substation's main computerised system or Remote

Terminal Unit (RTU) rather than at the source, are typically not time-synchronised, and contain a small but nonzero time-skew (time differences due to telecommunication and time propagation delays, and timestamp quantisation). Besides, the limited availability of digital sensor devices in outdated hardware components often imposes a direct limitation concerning the monitoring functionality of the components. Hence, this limited power system monitoring in time and space has a direct impact on the observability of the power system dynamic phenomena. This limitation leads that the SCADA monitoring system, used in today's control centre, requires a static state-estimation to estimate the undetermined power system parameters. The resulting information is further used in a contingency analysis and static security assessment applications to estimate the quasi-real-time power system's state and detect any violations of the system operation constraints. Typically, the related static state-estimation and power-flow analyses suffer from modelling inaccuracies and parametric uncertainties as well as they introduce a processing time delay in the range of tens of seconds to tens of minutes [11]. Consequently, the limited and non-real-time situational awareness restrains preventive power system operation and control, and in case of unexpected disturbances drives the power system operators to prolong the remedial actions with restorative ones.

1.1.2 EVOLVING POWER SYSTEMS AND EMERGING OPERATIONAL CHALLENGES

In particular fossil-fuelled and coal-based energy generation for the production of electricity and heat, is currently the main source of greenhouse gas emissions contributing to the climate change globally [12], [13]. The level of carbon dioxide emissions and the resulting concentrations is now at the highest than ever in humankind's history [14]. This has a negative impact on the environment; in particular, the oceans are becoming more acidic. In turn, this leads to the mass extinction of the oceans' wild-life and plant kingdom, on which the existence of humankind depends for its nutrition and livelihood [15].

“Humanity has the ability to make development sustainable - to ensure that it meets the needs of the present without compromising the ability of future generations to meet their own needs.” [16]

To tackle the climate change and expedite the sustainable energy supply, the existing energy systems undergo a significant transformation with far-reaching implications in society, economy, and technology. The long-term strategy to tackle the anthropogenic impact on the environment is to limit global warming to 1.5 °C above preindustrial levels [13]. The main target is to reduce the worldwide greenhouse gas emissions by 40 % till the year 2030 and to below zero till the year 2100, and depletion of natural resources in the process of creating energy [13], [17].

A. ENERGY TRANSITION IN POWER SYSTEMS

“The electricity sector is witnessing its most dramatic transformation since its birth more than a century ago.” [18]

- Fatih Birol

For the sake of our own good and generations to come, the electric power landscape is changing substantially. As illustrated in Figure 1.3, the traditional power systems undergo a major transformation from vast central generation towards heterogeneous, widely dispersed, yet globally interconnected power systems with large-scale integration of Distributed Energy Generation (DEG) [18].

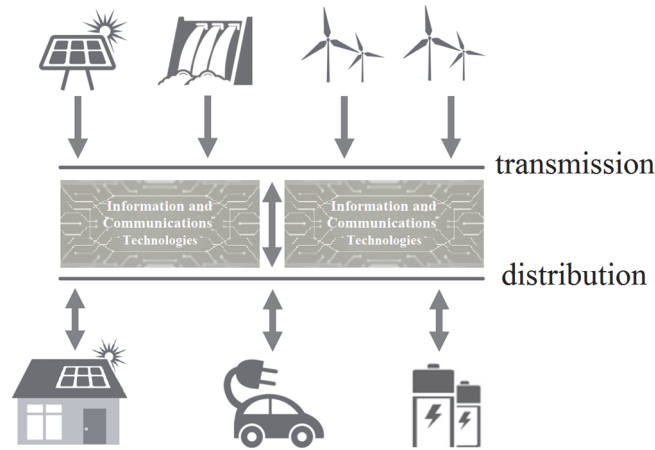


Figure 1.3: Simplified illustration of a future electric power system.

The conventional fossil-fuel and nuclear power plants are decommissioned and substituted for cost-competitive and scalable Renewable Energy Sources (RES), in particular solar, wind and tide, with the aim to reduce the greenhouse gasses released into the atmosphere. Long-term predictions suggest that RES will account for over 40 % of overall global electric power generation by the year 2040, compared to 25 % today [18]. Also, there is an increasing trend in active energy consumers with a typical small-scale RES power generation (hereinafter referred to as prosumers). The prosumers, often connected into quasi-self-sustainable communities, transform the energy market with the independent energy trade by the use of the Internet of Things (IoT) and cutting-edge blockchain technologies [19], [20]. Besides, the evolving Electric Vehicles (EV), a sustainable alternative to internal combustion engine vehicles, and emerging battery storage bring new load-profile patterns and with a bi-directional charging technology enable distributed load-balancing support [21].

B. EMERGING CHALLENGES IN POWER SYSTEM OPERATION AND CONTROL

“Today's electric power systems are continually increasing in complexity due to interconnection growth, the use of new technologies, and financial and regulatory constraints.” [22]

The ongoing energy transition brings not only conspicuous environmental and societal benefits, but a resulting increase in power system complexity imposes new challenges to the power system operation and control. Figure 1.4 illustrates the most significant changes and emerging challenges.

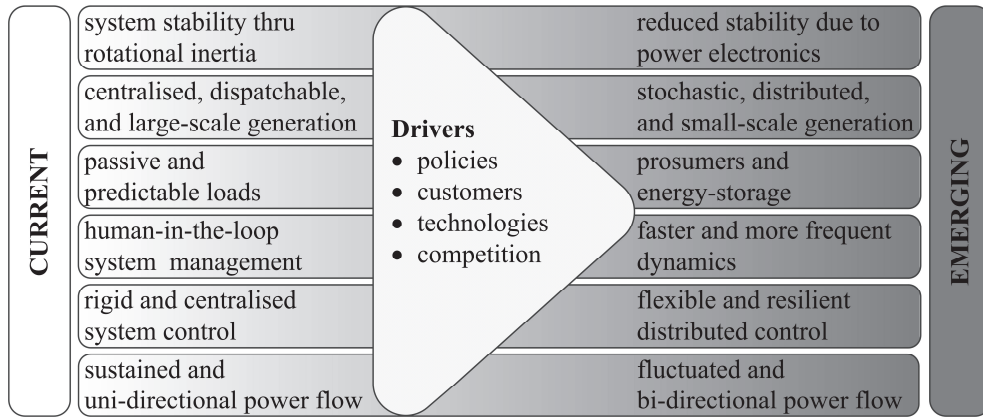


Figure 1.4: Emerging power system changes, which result in increased power system complexity and imposes new challenges to the power system operation (adapted from [23]).

Traditionally, power system operation and control rely on the fully-controllable, i.e. dispatchable, large-scale conventional synchronous power generation to meet the energy demand at each time. Due to the electromechanical coupling between a synchronous generator and the remaining power system (unity of synchronous generators and loads), the generator inertia (kinetic energy stored in the rotational mass of a rotor) acts as an instantaneous reserve, which in case of an unbalance between the generation and demand (observed as a deviation in system frequency) instantly supplies or absorbs the electric energy to arrest the change in frequency (often referred to as *inertial response*). In other words, sufficient power system inertia provides an instant frequency support in case a disturbance has an adverse impact on power system stability [22], [24].

Unlike the conventional synchronous generation, the typical DEG like non-synchronous RES, connected to the power grid via the power electronic converter technology that decouples any electromechanical interaction between the input and output, do not provide the frequency support [24]. Even the state-of-the-art converters with synthetic inertia technology may not contribute enough because of a phase-locked loop related control delay

and errors due to harmonics [25]. Clearly, with an increasing share of non-synchronous RES and simultaneous decommission of the conventional synchronous generation, the available inertial response is decreasing. The latter in parallel increases the speed and the severity of frequency fluctuations, which in turn may jeopardise the power system stability following a disturbance [2], [26], [27], [28], [29]. For example, a generator trip may cause a significant drop in the system frequency, leading to primary protection operation and cascade tripping of generators as well as load shedding [30], [31]. Also, the increase variable RES may result in the increase of power quality issues, observed in voltage profile fluctuations, reverse power flows, and harmonics. These and limited reactive power support during faults of the RES converters may result in failed or undesired protection operation leading to disconnection of large power grid sections due to selectivity issues, and has an adverse effect on the power system reliability [26], [32], [33].

Moreover, the main issue with the integration of stochastic non-controllable DEG and weather-dependent RES is their unpredictability and variability in the generated energy. This raises uncertainty related to the security of power supply and operating/spinning reserve (available but not utilised power capacity) accordingly. In parallel, this may jeopardise power system security and, in case of a severe disturbance, may negatively affect the power system stability. Also, the EVs and prosumers impose new patterns in energy demand and supply. Hence, the forecasting of operating reserve capacity is of greater challenge and any mismatch could be very cost-intensive.

The interconnection of neighbouring power systems into a large-scale power grid enables cross-border sharing of resources and market coupling to improve the power system reliability and social welfare, respectively. However, with the interconnection, the power systems are also sharing the consequences of their internally originated problems (i.e., faults, supply-demand imbalances, harmonics, and undamped oscillations), typically resulting in the volatility of frequency and power swings, and leading to inter-area oscillations. In case of significant energy import/export from/to the neighbouring power systems, a severe disturbance resulting in unplanned interconnected network splitting may significantly affect system stability.

The ever-increasing global energy consumption (more than 126 % increase from the year 1990 to the year 2018 [34]) and bulky inter-region energy transmission from generation to consumption may cause power grid congestions at peak times due to capacity limitations of the existing grid infrastructure. As a result, a combination of the reduced power system operational security during peak times and the uncertainty related to operational reserve capacity makes the power systems more vulnerable to instabilities.

Last but not least, the obsolete firmware of substation's hardware components and outdated Information and Communications Technology (ICT) subsystems of the EMS impose often overlooked cyber-security breach that may lead to denial of service, man-in-the-middle, and intrusion attacks, which can significantly affect the power system resiliency [35].

On the whole, if not thoroughly dealt with increasing challenges related to real-time operation and control of power systems, the aforementioned issues can lead to deterioration

of services, significant power quality issues, diminished lifespan of equipment, grid failures, cascading power outages, network splitting, and load shedding or in a worst-case scenario to a system-wide blackout [9]. Hence, a substantial adaptation of power system operation and control procedures and supporting systems is increasingly required to meet the existing and emerging operational challenges and safeguard the reliability of today and the future power systems, respectively.

1.2 PROBLEM DEFINITION

Typical EMS/SCADA supported control centre, used nowadays to operate the power system, was initially designed to meet the power system operation and control requirements defined in the late 1960s. However, in the last decade, the operational challenges have changed significantly as a result of the increased power system complexity (discussed in Section 1.1.2 - B).

Despite the technological advances in digitalisation, high-speed telecommunication links, and increased computational capacity [36] (further discussed in Chapter 2), the developments of EMS/SCADA functionality (advances in power system operation and control procedures based on the identified requirements) are not in line with the power system changes. Current protection, monitoring, and control systems may be insufficient to meet increasingly complex operational challenges [10].

As indicated in Figure 1.5, conventional EMS/SCADA functionality imposes an adverse control gap, seen in the time delay between the automatic primary protection operation and power system operators' manual response in the control centre.

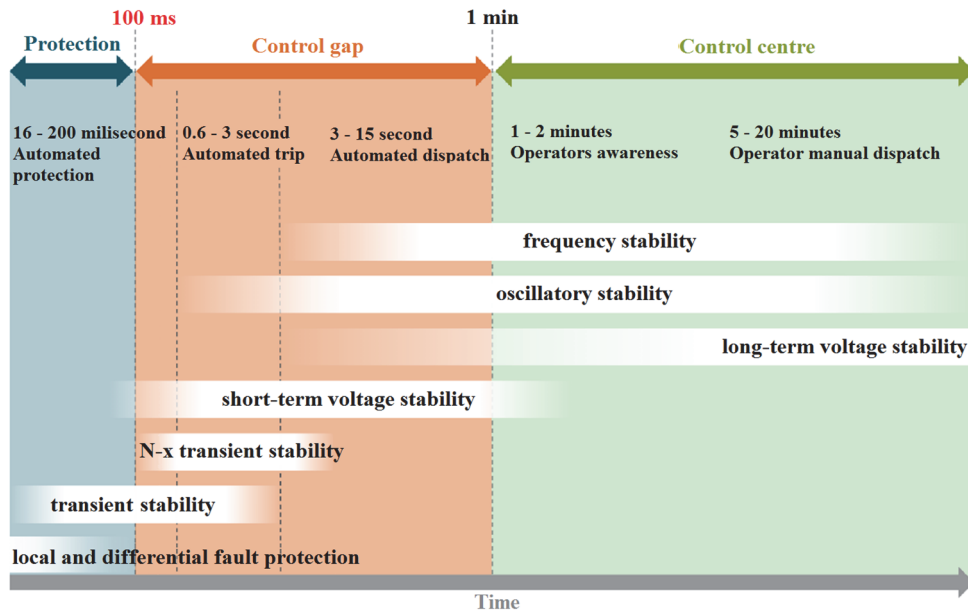


Figure 1.5: Conventional EMS system control gap (adapted from [37]).

Especially, during unexpected disturbances, the lack of real-time (ability to react to input immediately) and thorough situational awareness tools drives the power system operators to conduct mitigation decisions based on their expertise, assumptions and past operational experiences, instead of on ground truth (information provided by direct observation, such as empirical evidence). Also, the response of the power system operators is primary remedial nature due to the lack of advanced prediction and decision-support systems that would identify possible future critical states and mitigation strategies in time, thus enable preventive power system operation and control. Besides, it exists a deficiency of practical opportunities to test and verify cutting-edge technologies thoroughly under realistic conditions in an isolated and controlled environment, before being implemented into existing power systems (further discussed in Chapter 2, paragraph 2.4).

In fact, the literature [38], [39], [40], [41] suggests that the combination of severe weather conditions, increased share of DEG, human-errors, inadequate protection strategies, limited power system situational awareness, and lack of system-wide coordinated control schemes is in line with the increased level of disturbances leading to cascading power outages and catastrophic system-wide blackouts. Figure 1.6 shows the increasing number of power blackouts worldwide resulting in significant financial losses and social discomfort.

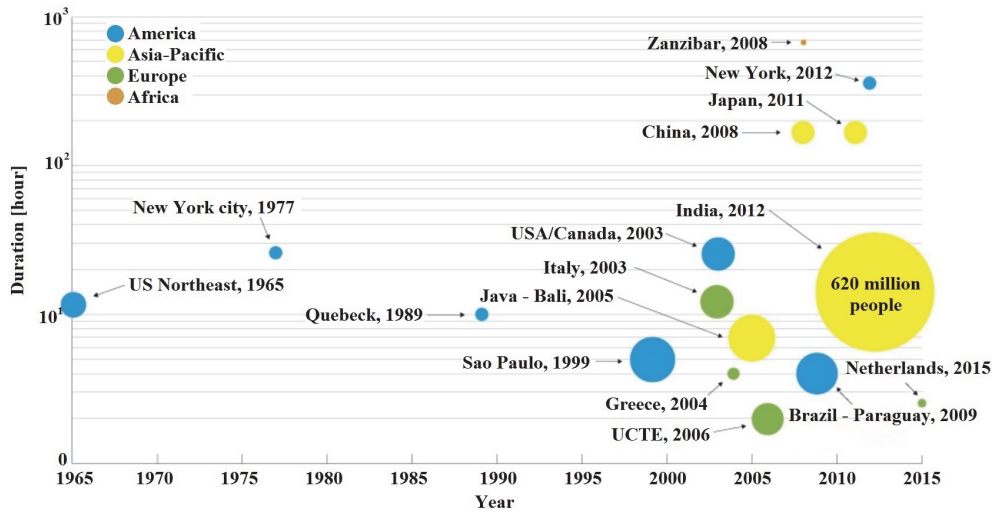


Figure 1.6: Recent worldwide power outages and blackouts are compared with the year of occurrence (x-axis), duration (y-axis), and a number of people impacted (relative size of the circle) (adapted from [42]).

In order to prevent future power disruptions, facilitate the transition towards carbon-neutral energy generation, and ensure more flexible and resilient power system operation and control, meanwhile guaranteeing a safe, reliable and economically efficient energy supply, there is a pressing need for the development of:

1. *improved monitoring and real-time situational awareness system*, to provide a comprehensive and detailed insight into the power system state and operating

boundaries, enabling an immediate disturbance detection and comprehensive event analysis in real-time;

2. *improved primary protection and advanced backup-protection system*, which would self-adapt to the changing power system state in order to avoid the unnecessary operation in case of harmless disturbances, and enable rigorous wide-area protection by taking system-wide considerations;
3. *adaptive and coordinated emergency-control system*, to in time execute a minimal number of the system-wide coordinated remedial actions to arrest and mitigate critical instabilities and bring the system to a stable state;
4. *advanced prediction and decision-support system*, to enable proactive grid operation, reduce the response time, and improve operational decisions in means of system optimisation and contingency chance reduction;
5. *real-time cyber-physical experimental testbed*, to enable the integration of physical and software components, and facilitate online testing and thorough evaluation of the emerging technologies in a closed-loop manner on digital models of real-world power grids, before being deployed in the field.

1.3 RESEARCH OBJECTIVE AND APPROACH

The research work in this thesis focuses on the most crucial early-stage improvements. In particular, to advance the first, the third and the fifth point of the list of required developments, proposed in the previous Section 1.2. Hence, the primary research objective of this thesis is:

To enhance the interconnected power system situational awareness with the aim of reinforcing power systems reliability, and to develop a cyber-physical experimental testbed for online evaluation of the emerging WAMPAC applications under realistic conditions in real-time.

In order to tackle this research challenge, the following research questions are answered in this thesis:

1. *What are the challenges and requirements for the operation, monitoring, control, and protection of large interconnected electric power systems with the high penetration of variable DEG?*
2. *Given the need to provide uninterrupted power supply, now and in the future, how to attain a near real-time situational awareness with the objective of reinforcing the reliability of power systems?*
3. *How can the performance of WAMPAC applications be thoroughly assessed and verified?*

4. *How can power system disturbances, resulting in voltage, current and frequency excursions, be online detected?*
5. *How to online identify grouping changes of slow-coherent generators in a power system with the aim to increase the effectiveness of remedial-control schemes on power system stability?*

To tackle the research objective and answer the research questions, the research work of this thesis is divided into two parts. The first part involves the development of a cyber-physical experimental testbed operating in real-time. This testbed is then utilised in the second part for the design and online evaluation of two measurement-supported algorithms, in particular for online disturbance detection and online identification of slow-coherent generators.

At the start of this research work, no SMT supported real-time power system simulation testbed was available at disposal. Thus, in the *first step*, a new cyber-physical experimental testbed is developed, used as the groundwork for further developments of this thesis. For this, an *RTDS* power system simulator and *WANem* telecommunication network emulator are used as a co-simulation in real-time. To simulate power system phenomena, the IEEE 39-bus transmission power system benchmark model and custom-designed four-terminal Modular Multilevel Converter (MMC) based High-Voltage Direct Current (HVDC) and Alternating Current (AC) transmission power system model are used. Further, the SMT-components are integrated into the testbed as software- and hardware-in-the-loop to provide realistic observability of the simulated power system phenomena for the design of the measurement-supported algorithms.

For near real-time monitoring of Phasor Measurement Unit (PMU) measured power system quantities and alarming, the *second step* involves the development of an SMT monitoring software platform.

In order to bridge the scientific gap, and to enable a simplified design, as well as to facilitate online validation of SMT supported applications under realistic conditions, the *third step* is applied to develop a *MATLAB* based Synchro-measurement Application Development Framework (SADF) software library, used further as a framework for the algorithms' design of step four and five.

To improve the power system situational awareness and backup-protection schemes the *fourth step* is applied to develop an SMT supported algorithm for online disturbance detection in AC and HVDC power grids.

Finally, the *fifth step* involves the development of an algorithm for online tracking of grouping changes of slow-coherent generators following a disturbance, intending to improve the power system further situational awareness and to increase the effectiveness of the remedial control on the system stability. This step first identifies the related challenges, which are subsequently elucidated and overcome.

1.4 THESIS OUTLINE

As indicated in Figure 1.7, the structure of this thesis reflects an integral approach, where *Chapter 2* develops the cyber-physical experimental testbed as groundwork. On top of that, *Chapter 3* further builds the SADF, which is then utilised in *Chapter 4* and *Chapter 5* for the design and validation of the algorithms for online disturbance detection and online generator coherency identification, respectively.

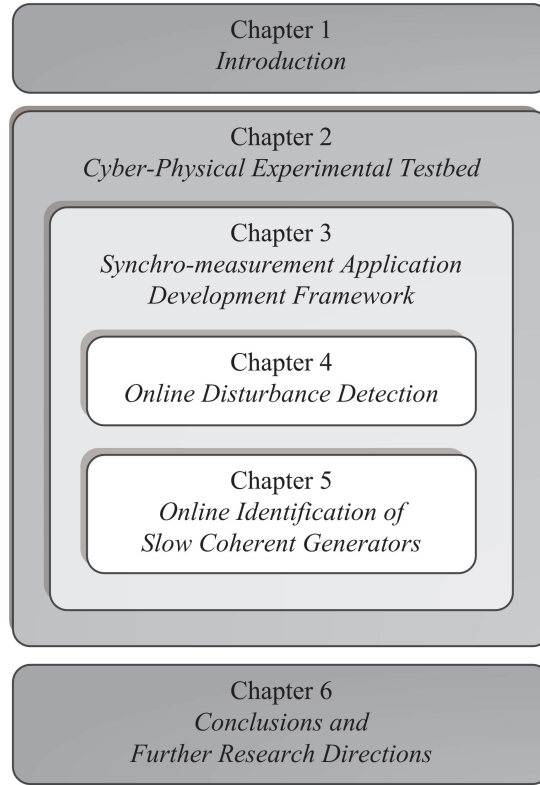


Figure 1.7: This thesis outline, indicating the integral approach of the conducted research work.

Each of the technical chapters (Chapters 2 - 5) starts with the topic-specific introduction presenting the state-of-the-art, followed by the chapter-specific scientific contribution, result and analysis sections, and ending with the conclusions of main findings and further research directions. In summary:

Chapter 2 presents the rationale behind power system monitoring with high resolution in time and space. It provides a detailed explanation of the adopted state-of-the-art SMT. This chapter further highlights WAMPAC applications and provides insight into the current research. The second half of the chapter presents the developed SMT supported

WAMPAC-ready cyber-physical experimental testbed, its conceptual architecture and the implemented hardware and software components. In this context, the developed web-based SMT monitoring platform is presented.

Chapter 3 starts with a discussion on the shortcomings of conventional software simulated bus measurements for WAMPAC application design and validation. It fills the scientific gap between the IEEE Std. C37.118.2-2011 specifications and its implementation by presenting the developed SADF software library, enabling online receiving and parsing of IEEE Std. C37.118-2005 and C37.118.2-2011 specified machine-readable messages into a human-friendly format. In this context, two methods are proposed: (i) a robust data receiver communication technique with integrated fall-back procedures, and (ii) an efficient online receiving and parsing methodology of the encapsulated machine-readable configuration and data frames. At the end of the chapter, the proposed SADF is assessed and verified against the IEEE Std. C37.118-2005 (communication part) and C37.118.2-2011 specifications by using the cyber-physical experimental testbed.

Chapter 4 starts with an analysis of state-of-the-art disturbance detection methods and presents the remaining challenges to be addressed. In the second part, a new SMT supported online algorithm for adaptive detection of disturbances in AC and HVDC power systems is presented. As demonstrated in this chapter, PMUs can be utilised to deliver time-synchronised measurements of an HVDC power grid. Finally, the chapter finishes with a detailed performance evaluation of the proposed disturbance detection algorithm using the developed cyber-physical experimental testbed and the SADF. Notably, particular attention is given to time-synchronisation of the supporting systems for an adequate determination of the disturbance detection time delay.

Chapter 5, in its first part, presents the analysis of state-of-the-art methods for the identification of grouping changes of coherent generators in an interconnected power system and identifies the remaining challenges. The second part of the chapter presents a series of advanced developed solutions, compound into the algorithm for robust and near-real-time tracking of grouping changes of slow-coherent generators during quasi-steady-state and the electromechanical transient period following a disturbance. Finally, the proposed algorithm is compared to a benchmarked method that tackles the same challenge. For validation and the comparison, the cyber-physical experimental testbed and the SADF are used.

Chapter 6 recaps the conclusions and outlines the main findings and based on the conducted research proposes further research directions.

CHAPTER 2

CYBER-PHYSICAL EXPERIMENTAL TESTBED

As elaborated in Chapter 1, the power system complexity and the number of large-scale power system blackouts have increased significantly in recent years. Motivated by these facts, there has been a notable increase in scientific research and related technological developments to advance the power system operation and planning [36]. In the first part, this chapter elaborates on the state-of-the-art SMT technology, existing WAMPAC applications, and related worldwide implementations. In the second part, this chapter presents the developed SMT supported cyber-physical experimental testbed for the design and online evaluation of WAMPAC applications and SMT components under realistic conditions in real-time.

2.1 INTRODUCTION

The recent advances in terms of diverse sensors to monitor hardware components with high resolution in time; increased functional and processing capacities of substations' high-speed microprocessor-based Intelligent Electronic Devices (IED); fast and reliable telecommunication links; and scalable software-platforms for collection and distribution of data, have created new opportunities for advances in the design, operation, and planning of a power system [10], [43], [44]. Particularly, the advent of SMT, which enabled unprecedented observability of power system phenomena, drives the research and industry towards investments in WAMPAC [45]. WAMPAC applications are favourable to ensure a more resilient, secure, and efficient operation of the power system through sophisticated utilisation of measurement data from geographically dispersed sensor devices into high-value operational and planning information.

To assure that the WAMPAC applications perform adequately during most critical power system disturbances, such as contingencies, thorough assessment and validation of the WAMPAC system is required beforehand. For this purpose, a WAMPAC-ready cyber-physical experimental testbed is built, which is used in this thesis for the design and online assessment of the remaining developments, presented in the following chapters.

2.2 SYNCHRONISED MEASUREMENT TECHNOLOGY

SMT is revolutionary by its design since it makes use of a common time source for precise sampling and timestamping of measurements at the source. This enables time-synchronised measurements (hereinafter referred to as synchro-measurements) at predefined instants in time from grid-wide remote locations. In combination with remote data acquisition, the synchro-measurements from the remote locations can be used to ensemble a precise measurement snapshot of a power system state in time. This holistic view of a power system state makes the SMT applicable for the use in advanced WAMPAC applications of an interconnected power system, particularly [46]. In contrast, the latter cannot be attained by the use of conventional SCADA monitoring only.

Historically, SMT concept was introduced in 1983 by the use of positive-sequence voltage and current phasor measurements for protection purposes [47]. This commenced the design of the first PMU prototype, built in the early 1980s, which in turn lead to the adaptation of the PMU technology by industry in 1991. At present, the IEEE Std. C37.118 based PMU technology is one of the widely adopted for SMT [48]. Figure 2.1 presents a typical IEEE Std. C37.118 based wide-area SMT system, encompassing multiple power utilities, comprises of numerous devices that are connected into a hierarchically organised network.

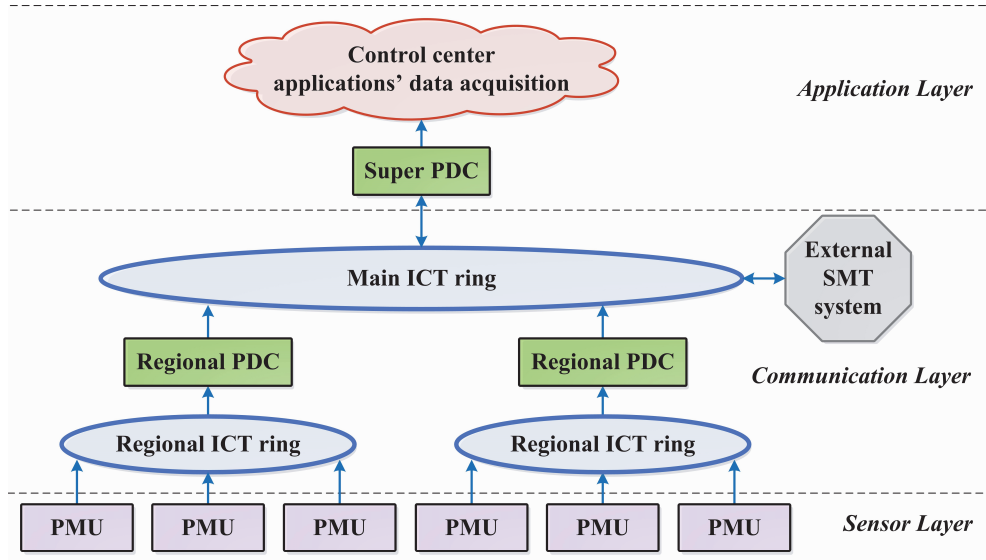


Figure 2.1: Synchronised Measurement Technology architecture.

As illustrated in Figure 2.1, the hierarchically bottom consists of geographically dispersed PMUs, typically located in power system substations, receiving feeder's voltage and current signals, provided by instrument transformers or transducers. Supported by precise time synchronisation, the PMUs send their synchro-measurements over ICT infrastructure [7] to

regional PDCs. A PDC works as a data receiver, which collects and merges synchro-measurements into a single data stream, further sent to a hierarchically higher level PDC (super PDC). Similarly, a super PDC collects and pre-processes the synchro-measurements received from underlying PMUs and/or PDCs and sends the aggregated data stream to an application data acquisition in control centre for a final analysis, and to an external SMT system of a neighbouring power utility, if applicable.

2.2.1 PHASOR MEASUREMENT UNIT

A PMU is a keystone of SMT since it serves a source of time-synchronised measurements. Unique about the PMU technology is that it estimates the time-referenced phasor, often denoted to as a synchrophasor, of a sinusoidal signal (hereinafter referred to as waveform) from the voltage and current PMU input channels [49]. According to the definition in [50]:

- a phasor is the “*complex equivalent of a sinusoidal wave quantity such that the complex modulus is the cosine wave amplitude, and the complex angle (in polar form) is the cosine wave phase angle*”, while;
- a synchrophasor is the “*phasor calculated from data samples using a standard time signal as the reference for the measurement*”.

In other words, a synchrophasor is the complex representation of a pure waveform with respect to the common time reference. For the time referencing purpose, PMU uses an internal clock, which is time-synchronised to the external time reference source, typically in Universal Time Coordinated (UTC) format. Moreover, the clock of a PMU is typically used for precise Analog-to-Digital Converter (ADC) sampling of the PMU input channels, synchrophasor estimation, and timestamping of the synchro-measurements on the PMU output.

A. SYNCHROPHASOR ESTIMATION

In a power system during steady-state, a pure waveform with a nominal system component only (50 Hz or 60 Hz) can be defined with the following static signal model [50]:

$$x(t) = A_0 \cos(2\pi f_0 t + \varphi_0) \quad (2.1)$$

where:

- A_0 is the peak amplitude of a waveform;
- f_0 is the nominal frequency;
- φ_0 is the initial phase shift at $t = 0$;
- t defines a time instant.

The equivalent synchrophasor representation of the waveform in (2.1) can be expressed as:

$$x(t) \leftrightarrow X = \frac{A_0}{\sqrt{2}} e^{j\varphi_0} = \frac{A_0}{\sqrt{2}} (\cos \varphi_0 + j \sin \varphi_0) = X_r + jX_i \quad (2.2)$$

where:

- X_r and X_i represent real and imaginary parts of the corresponding phasor X in rectangular form with the Root Mean Square (RMS) magnitude of the waveform peak;
- φ_0 is the initial phase angle offset from a reference cosine function pulsating at the nominal power system frequency (50 Hz or 60 Hz) [51].

For example, as illustrated in Figure 2.2, a waveform (mind Figure 2.2 - left) can be represented as a synchrophasor (mind Figure 2.2 - right) with the RMS magnitude of the waveform peak, where the synchrophasor phase angle is the angle between the waveform peak and the predefined moment in time, disciplined by a common time reference.

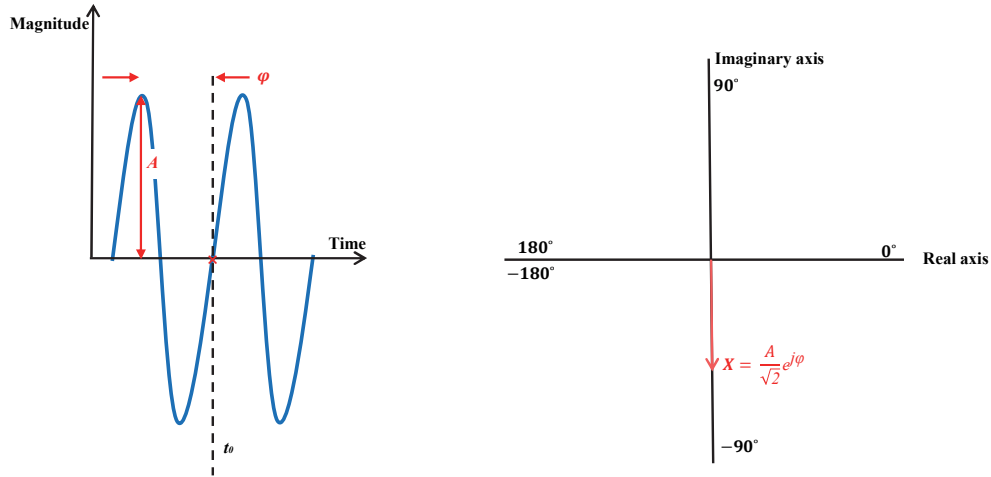


Figure 2.2: Left – waveform of interest; right - resulting synchrophasor representation. Note, the phase angle of the synchrophasor is arbitrary, as it depends upon the axis t_0 , disciplined by the common time reference, and the length of the synchrophasor is equal to the RMS value of the waveform (adapted from [49]).

Nevertheless, the above-presented synchrophasor representation is only possible for a pure waveform that is unchanging for all time. However, during the daily operation of a power system, PMUs are exposed to a broad spectrum of power system imposed phenomena, observed as variations in frequency and magnitude of a waveform due to unbalances, electromechanical oscillations, harmonics, electromagnetic transients, and other high-frequency components such as noise [52], [53], [54] to name a few. Hence, to

address these phenomena, the signal model in (2.1) is extended with the following more general dynamic signal model, defined in [51] as:

$$x(t) = A_0(t) \left(1 + \varepsilon_{A_0}(t)\right) \cdot \cos \left(2\pi f_0(t)t + \varphi_0 + \varepsilon_{\varphi_0}(t)\right) + \eta(t) + \gamma(t) + v(t) \quad (2.3)$$

where:

- $A_0(t)$ and $f_0(t)$ are the peak amplitude and frequency, respectively, of time-varying fundamental tone component;
- $\varepsilon_{A_0}(t)$ is the amplitude fluctuation in time of the fundamental tone component at t time (e.g., amplitude modulation);
- ε_{φ_0} represents the fluctuations in phase and frequency of the fundamental component at t time (e.g., phase modulation, frequency ramp);
- $\eta(t)$ models narrow-band tone components (e.g., harmonic and/or inter-harmonic components) as:

$$\eta(t) = \sum_h A_h(t) \left(1 + \varepsilon_{A_h}(t)\right) \cdot \cos \left(2\pi f_h(t)t + \varphi_h + \varepsilon_{\varphi_h}(t)\right); h = \frac{f_h}{f_0}; h \in \mathbb{R} \quad (2.4)$$

with $A_h(t)$ and $f_h(t)$ being the amplitude and frequency, respectively, of time-varying harmonic/inter-harmonic components; h is the tone order; φ_h is the initial phase; $\varepsilon_{A_h}(t)$ is the amplitude fluctuation in time of the harmonic/inter-harmonic component at t time; ε_{φ_h} represents the fluctuations in phase and frequency of the harmonic/inter-harmonic component at t time.

- $\gamma(t)$ models dynamic wide-band disturbances (e.g., decaying DC components) as:

$$\gamma(t) = A_{DC} e^{-t/\tau} \quad (2.5)$$

with A_{DC} being the initial amplitude of a DC component; and τ the time constant characterising the component;

- $v(t)$ accounts for a wide-band grid noise.

Typically, PMUs report the synchrophasors of a fundamental frequency component only. For this, it is necessary to extract the frequency component of interest and then represent it by a synchrophasor. Also in practice, the synchrophasors are considered only on a limited time span of a waveform, also known as an observation window [50]. Thus in simplified terms, to transform the time domain waveform samples of an observation window into a frequency domain synchrophasor of the fundamental frequency component, ADC sampling of the waveform on the PMU input following Discrete Fourier Transform (DFT) mathematical formulation are typically performed as [49]:

$$X = \frac{\sqrt{2}}{N} \sum_{n=0}^{N-1} x_n \left(\cos \frac{2n\pi}{N} + j \sin \frac{2n\pi}{N} \right) \quad (2.6)$$

where:

- $x[n]$ is a discrete-time series vector containing N waveform samples over the observation window interval NT_s (typically one or two periods) [51]:

$$x[n] := \{ x(t) + \rho(t), \quad t = nT_s, \quad n = [0, \dots, N-1] \in \mathbb{N} \} \quad (2.7)$$

with T_s being the sampling time of the ADC; and ρ accounts for wide-band measurement noise inherent in the data-acquisition process of a PMU.

The resulting synchrophasor X of a fundamental tone component in (2.6) has the phase angle φ equal to the angle between the time when the first sample is taken (corresponding to $n = 0$) and the peak of the input waveform [49]. Notably, for the sake of accuracy, it is important to time-align the sample moment of the first sample ($n = 0$) in the observation window with a referenced cosine function of the nominal system frequency, disciplined a common time reference.

Basically, the DFT based mathematical formulation in (2.6) can be implemented in a PMU device as the stream mixer between the waveform samples on the PMU input and in-time corresponding cosine and sine coefficients of the nominal system frequency, disciplined by the common time reference. Figure 2.3 shows the diagram of the computations needed to determine the synchrophasor of a fundamental component as an output of the tapped-delay line of a Finite Impulse Response (FIR) filter.

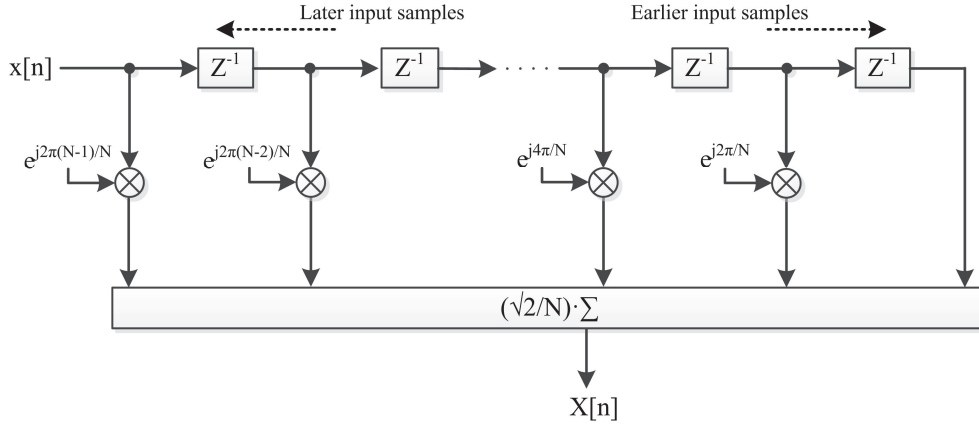


Figure 2.3: Basic implementation of a DFT based synchrophasor estimation algorithm as an FIR filter bank (adapted from [55]).

Nevertheless, the different phenomena modelled in (2.3) in combination with ADC sampling and windowing can deteriorate the accuracy of the synchrophasor estimation significantly. To suppress this adverse effect, a complex adaptation of synchrophasor estimation processes is reported in the literature [56], [57]. However, it is important to note that the PMU inherited observation window and the related synchrophasor processing, introduce an unavoidable delay in the PMU output. Particularly, the resource expensive operations connected with the complex synchrophasor estimation algorithms may even prevent the PMU from online operation due to the hardware limitations (processing speed) [58]. Therefore, a trade-off between the synchrophasor estimation algorithm's complexity, accuracy, and a PMU reporting rate is often considered.

B. OVERVIEW OF PMU STANDARDS

Over the years, common standards were developed in order to achieve interoperability among the PMU devices of different vendors [48]. Historically, the first PMU standard IEEE Std. 1344-1995 [59] was issued in 1995, defining time synchronisation and sampling requirements for the synchrophasor estimation. The standard addressed the required formats for time synchronisation and synchro-measurement data reporting based on the existing COMTRADE - IEEE Std. C37.111-1991 specification. However, this standard did not include measurement requirements and accuracy during nominal and off-nominal power system conditions.

In 2005, the first standard was superseded by IEEE Std. C37.118-2005 [60], which also addressed PMU response during off-nominal frequency conditions, and introduced a Total Vector Error (TVE) as a concept to addresses the measurement accuracy.

Next, in 2011, the IEEE Std. C37.118-2005 was split into two sub-standards as a result of joint cooperation between IEEE and IET communities. The resulting IEEE Std. C37.118.1-2011 [50] focused on the measurement accuracy and dynamic performance under power system transients, while the IEEE Std. C37.118.2-2011 [61] focused on the communication requirements for data exchange only. Additionally in 2012, as a result of the cooperation, IEC TR 61850-90-5:2012 [62] specification was issued defining synchro-measurement data transfer in IEC 61850 based systems. As compared with the previous versions, the IEEE Std. C37.118.1-2011 introduced two PMU performance classes, *P* class and *M* class, as well as their corresponding dynamic performance requirements. The *P* class PMU is targeted for protection and control applications, and features minimum filtering and measurement delay involved in the process of synchrophasor estimation to facilitate the fast response but in turn sacrifices on the accuracy. On the other hand, the *M* class PMU is mainly targeted for power system monitoring applications to achieve greater precision in case of out-of-band signals, but results in longer measurement delay and slower measurement response due to involved significant filtering and uses longer observation window. Additionally, the IEEE Std. C37.118.1-2011 specified the frequency and Rate-Of-Change-Of-Frequency (ROCOF) measurements as part of PMU output. Also, IEEE Std. C37.118.2-2011 added a new configuration frame *CFG-3* for extended PMU configuration

reporting, and defined the time quality codes in data frames to report any inconsistencies and faults with the critical PMU time synchronisation.

Lastly, in 2014, IEEE Std. C37.118.1a-2014 [63] amendment was issued with relaxed measurement performance requirements compared to IEEE Std. C37.118.1-2011 specifications.

C. BASIC PMU FUNCTIONALITY

According to the most adopted IEEE Std. C37.118.1-2011, a PMU device, as depicted in Figure 2.4 and used in this thesis, provides synchro-measurements of:

- voltage synchrophasors from analogue voltage input channels (per three-phase; positive, negative and zero symmetrical components);
- current synchrophasors from analogue current input channels (per three-phase; positive, negative and zero symmetrical components);
- system frequency of the main tone component, determined typically by using positive sequence voltage angle;
- ROCOF of the corresponding frequency;
- single point-on-wave, RMS or peak of signal sample measurements of analogue input channels (e.g., rotor speed, sampled control signal or value);
- Boolean status indicators of digital input channels (e.g., breaker position, switchgear position);

with the following user-selectable reporting rate in frames per second (fps):

nominal system frequency	50 Hz					60 Hz							
reporting rate [fps]	10	25	50	100	250	10	12	15	20	30	60	120	240
	standard defined										optional		



Figure 2.4: GE (former Alstom) MiCOM Agile P847 PMU (courtesy of GE).

Conventionally, the PMU functions are implemented into a specialised hardware platform, designed to deliver single functionality only. However, the availability of cost-

efficient multifunctional IEDs with high-processing power enabled the realisation of PMU functions as an IED embedded software package. In this case, PMUs can be implemented alongside digital fault recorders, protection relays, digital disturbance recorders, which in turn leads to new implementation challenges [64].

D. PMU AND SCADA COMPARISON

Historically, PMU technology provides unprecedented power system observability compared to existing SCADA monitoring. Notably, the relative angle information of a synchrophasor, precise timestamping at the source, and higher reporting rates lead that the synchro-measurements can be time-aligned and ensembled into a comprehensive high-resolution snapshot of the power system state in time. Table 2.1 summarises the key differences between PMU provided measurements and conventional SCADA measurements [65].

TABLE 2.1
Comparison between SCADA in PMU measurements

Attribute	SCADA	PMU
resolution	1 sample every 2 - 10 s	10 - 250 samples/s
observability	quasi-steady state, typically up to 0.133 Hz	dynamic behaviour, typically up to 25 Hz
measurements	V, I, analogue values, Boolean status	V, I, frequency, ROCOF, analogue values, Boolean status
time synchronisation	no	yes
measurement timestamp	at a substation's RTU or central MTU	at the source
relative phase angle	no	yes
focus	local monitoring	wide-area monitoring

2.2.2 TIME SYNCHRONISATION

Precise time synchronisation is one of the most critical aspects in SMT to consider since it is of fundamental importance for the synchro-measurement accuracy. For example, a time accuracy of $1 \mu\text{s}$ results in synchrophasor phase angle error of 0.02° , which is still within the TVE permitted range [66]. In case of significant time synchronisation errors, the performance of SMT supported applications may be affected, leading to devastating consequences such as power outages and blackouts. For a precise time-synchronisation in ns range, SMT can be supported by wireless or wired time propagation solutions.

The most adopted wireless-based time propagation solutions are based on Global Navigation Satellite System (GNSS), such as Global Positioning System (GPS), Galileo, GLObal Navigation Satellite System (GLONASS), and Beidou to name a few. In this case, a GNSS receiver, integrated into the PMU, determines time-based on its location and one

PPS signal received from the GNSS time reference system, which contains high-precision atomic clocks in each of the constellation satellite. The main advantage of wireless solutions is in low-cost of implementation. On the contrary, wireless solutions are prone to effortless cyber-attacks such as signal jamming (broad-band transmitter to interfere and block GNSS signal) and spoofing (false GNSS transmitter to fake location), which is an important factor to consider.

On the other hand, the wired-based terrestrial solutions are more cyber-secure by default, but typically require specialised cost-intensive equipment and network infrastructure to distribute time. Among them, the most adopted is the Inter-Range Instrumentation Group code B (IRIG-B) in combination with PPS to achieve the required level of time accuracy [67]. Typically, the IRIG-B runs over coaxial cable, while the PPS uses a fibre-optic based network. However, one of the most practical wired-based solutions is a Precise Time Protocol (PTP) version 2, specified in IEEE Std. 1588-2008 [68], which runs over an L2 Ethernet ICT network. The basic principle of the PTP includes two connected devices. The first device is typically a standalone atomic clock or a high-end GNSS disciplined receiver, named as *Master Clock* to provide local time reference. The second target device (PMU/IED) contains a *Slave Clock* that in steps synchronises to the *Master Clock*, taking the network time propagation delay into account, leading to improved accuracy. The PTP in combination with the *Power Profile*, specified in IEEE Std. C37.238-2017 [69], makes a tailored time dissemination solution for mission-critical protection, control, automation, and data communication applications. Figure 2.5 presents a GPS disciplined PTP Master Clock, adopted in this thesis. Furthermore, in recent years, an extended PTP version 3 (PTPv3), also named as White Rabbit (WR), was developed [70]. In contrasts to the native PTP, the WR runs exclusively over fibre-optic based Synchronous Ethernet (SyncE), leading to improved sub-nanosecond accuracy of picoseconds precision in time-synchronisation [71]. The latter makes WR superior compared to most adopted GPS and PTP, especially in case of sensitive PMU applications such as monitoring of angle deviations in an electrically short connected grid for example [72].

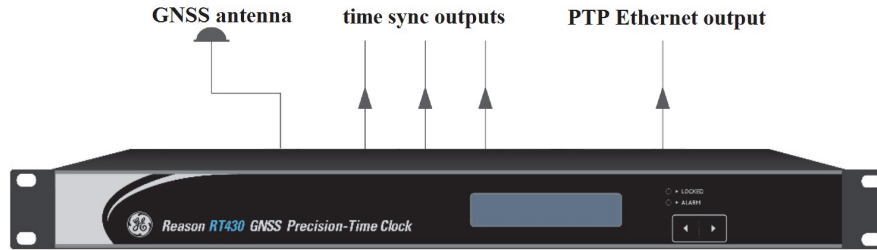


Figure 2.5: GE Reason RT430 GPS disciplined time clock with PTP, IRIG-B, and PPS outputs (courtesy of GE).

2.2.3 PHASOR DATA CONCENTRATOR

In the intermediate layer of SMT architecture (mind Figure 2.1), a PDC is used as a synchro-measurement data stream collector that receives the synchro-measurements from

numerous hierarchically lower level PMU and/or PDC data sources. It performs quality checks, time aligns and merges synchro-measurements into a single data stream based on measurement's timestamps and PDC's internal rules. The aggregated synchro-measurement data stream is then sent to the hierarchically higher-level information systems, such as super PDC or applications' data acquisition of the control centre for a final analysis. According to the most adopted IEEE Std. C37.244-2013 [73] specification, which serves as a guide for PDC design, its prime role is to:

- receive the synchro-measurements from multiple sources;
- buffer input data streams to accommodate differing receiving times;
- perform data quality and integrity validation;
- determine the latency of incoming data streams;
- convert the received data into a unison format and sample rate;
- perform simple mathematical operations and data adjustments;
- combine all the received measurements belonging to specific timestamp into a single data frame;
- forward the combined data stream to higher information systems according to the desired streaming specification, typically based on IEEE Std. C37.118.2-2011 [61];
- process the data for local visualisation, alarming and reporting;
- locally store the data for archiving.

Supported by a common time reference, PDC uses an internal processing logic for efficient data buffering and aggregation to minimise the associated processing delay (PDC waiting time) and incompleteness of the outgoing data stream (incoming synchro-measurement data loss due to telecommunication latencies for example). The PDC functions are implemented either as a software program to be run a Windows or Linux operating system (OS) based computer, or embedded into a specialised hardware platform, as illustrated in Figure 2.6.



Figure 2.6: SEL-3373 PDC, implemented as a standalone device (courtesy of SEL).

During the designing phase of an SMT based system and supporting applications, an important factor to consider is the end-to-end synchrophasor data latency, represented as a sum of the latencies imposed by the individual elements of an SMT network. The

synchrophasor data latency can significantly affect the ability of specific SMT supported applications to perform as desired, in particular fast emergency control ones [74]. In general, a PDC reporting latency can substantially contribute to the overall synchrophasor data latency, since it mainly depends on the PDC internal logic and settings with respect to the telecommunication network characteristics (delay and the jitter of individual communication paths) of incoming data streams. Figure 2.7 presents an example SMT system with corresponding data latencies decomposed in its individual contributions, where:

- PMU measurement reporting latency is “the time delay from when an event occurs on the power system to the time that it is reported in data. This latency includes many factors, such as the window over which data is gathered to make a measurement, the estimation method, measurement filtering, the PMU processing time, and where the event occurs within the reporting interval” [50];
- telecommunication network latency is “the time difference between the instant a PMU has transmitted a data frame on its physical channel and the instant the same data frame hits the PDC network interface” [75];
- PDC latency is “the time difference between the instant a time-aligned dataset is pushed to the supplied applications and the instant the first message with a given time-stamp hits the PDC. The PDC latency is composed of two contributions:
 - the PDC wait time that starts when the first message with a specific time-stamp enters the PDC and ends when the last one arrives or the associated timeout expires;
 - the PDC processing time, i.e., the amount of time needed by the PDC to complete the production of an aggregated dataset” [75].

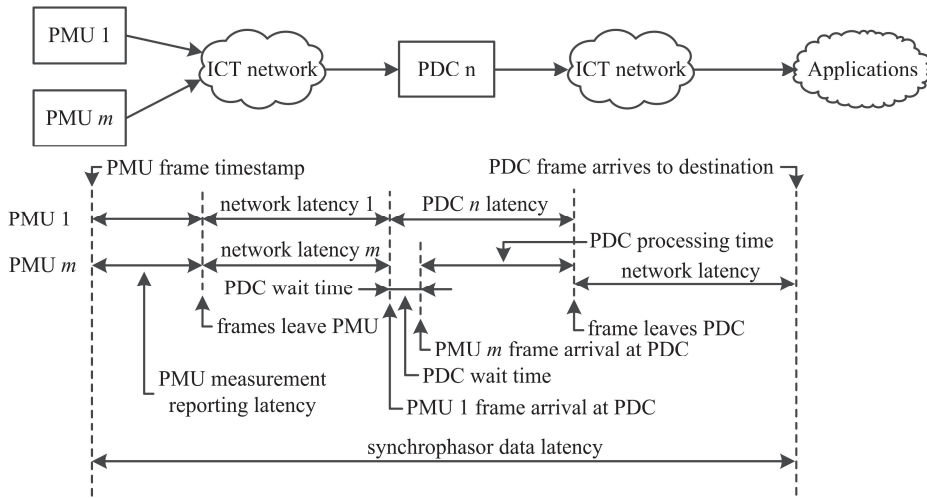


Figure 2.7: Example of a synchrophasor system with related data latencies decomposed in its individual contributions (adapted from [73]).

2.2.4 WIDE AREA TELECOMMUNICATION NETWORK

In a power system, the ICT infrastructure, connecting the remote substations and the control centre into a Wide Area Network (WAN), is an indispensable element of an SMT for remote data acquisition. During WAMPAC system design (further discussed in Section 2.3.3), the ICT infrastructure is an important aspect to consider due to its mission-critical services that supports [76], [77], [78]. Typically, for a reliable transfer of data, the ICT network utilises Quality of Service (QoS) traffic engineering mechanisms to:

- provide the required bandwidth and minimise the end-to-end packet delay (telecommunication latency);
- prevent loss of packets;
- avoid and manage potential traffic congestions;
- support traffic flow shaping;
- prioritise the traffic flows of mission-critical applications to maintain the required Service Level Agreement (SLA) parameters;
- maintain high availability of ICT services.

Currently, Internet Protocol/Multiprotocol Label Switching (IP/MPLS) and Carrier Ethernet technologies, which run over private fibre-optic-based networks to benefit of full control, are one of the most adapted due to their matureness, ability to provide a wide range of ICT services and mechanisms with a single technology, and active support of IETF, IEEE and ITU standardisation communities.

Nevertheless, the ongoing trend in power system digitalisation brings not only new benefits and opportunities for power system operation, but the resulting increase in digital solutions imposes new ICT requirements and challenges. In particular, to timely address the cyber-security risks and vulnerabilities that the digital solutions impose. [79]. For example, a cyber-attack on a telecommunication network for SMT may include an interruption attack (denial of service), a man-in-the-middle attack, a reconnaissance attack, data spoofing, and fabrication attacks such as packet and malicious code injection [80]. It is of crucial importance to enforce adequate cyber-security management from end-to-end, starting from the PMUs in substations, ICT infrastructure, data storage, all the way to the application layer, in order timely prevent cyber-attacks and mitigate cyber-treats in the earliest stage.

2.3 WIDE AREA MONITORING PROTECTION AND CONTROL

A WAMPAC refers to a framework of digital solutions, and advanced measurement supported applications to mitigate the propagation of large disturbances in an interconnected power system, particularly [45]. WAMPAC is both revolutionary and evolutionary since it leverages the information from grid-wide remote locations for the use in advanced situational awareness applications, and system-wide coordinated protection

and control schemes to improve the power system operation of today, while providing capabilities for future improvements [81], [82].

WAMPAC system encompasses elements tailored according to the requirements of preferred WAMPAC applications. Generally, it consists of geographically distributed data sources and sinks, local data acquisition and processing systems, a high-speed wide-area telecommunication network for remote data acquisition and sharing, and finally, a distributed or centralised data processing and visualisation platforms. Typically, a WAMPAC system leverages the SMT as a key building block to deliver synchro-measurements of electrical quantities and other parameters from grid-wide remote locations [45], [49], [83], [84]. It also utilises the information provided by SCADA monitoring to gain additional insight into the power system operating state and component status. Recent advances in cloud computing and data analytics enabled the design of cost-effective WAMPAC systems and related applications, respectively. For example, Figure 2.8 illustrates the conceptual scheme of an advanced digital system enabling the design of local and wide-area intelligence, disseminated between multiple IEDs locally in a substation, or between multiple substations and/or control centres.

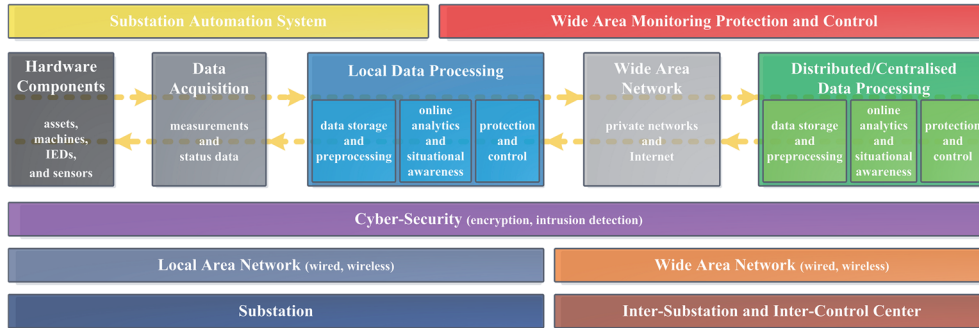


Figure 2.8: Advanced digital system main building blocks and information flow (adapted from [43]).

2.3.1 STATE-OF-THE-ART WAMPAC APPLICATIONS

The advent of SMT triggered the development of WAMPAC applications to enhance the power system operation and planning, and address the emerging challenges at the interface between TSO operators, power plant operators, large industrial consumers, DSO operators, regulatory authorities, and remaining stakeholders [85]. For this purpose, a wide spectrum of SMT supported applications has been developed, ranging from tools to improve situational awareness up to advanced fully automated system integrity protection schemes (SIPS) [65], [82], [86]. In general, the state-of-the-art WAMPAC applications can be congregated into three groups, based on the nature of the addressed challenges.

Applications belonging to the first group provide situational awareness and aim to improve the power system dynamic performance in the long run. Typical examples are: dynamic state estimation for a comprehensive power system observability and detection

of congestions in near real-time [87]; online grid vulnerability assessment such as dynamic security assessment [88] and dynamic stability assessment [89]; online oscillation monitoring [90]; dynamic thermal rating to improve grid efficiency and better manage congestions [30], [91], [92]; online tuning of hardware equipment parameters [93], [94] and Power System Stabilisers (PSSs) [78]; online inertia estimation [95]; and online tuning of the power system dynamic models [96].

The second group forms a set of pre-contingency applications for detection and mitigation of anomalies, for example: immediate disturbance detection [97], localisation [98] and classification [99]; instability detection [100], grid stress monitoring [101]; hardware performance monitoring to quickly diagnose problems [102], and online tuning of protection equipment parameters based on the present system state [94], [103].

Finally, the third group consists of applications tailored for post-contingency in order to reduce the adverse impact of the events and improve the system restoration [104]. For example, synchro-measurement supported protection schemes can be used to enhance differential protection and backup protection schemes [105], [106]; and detect and classify the line faults [107], [108]. Moreover, to mitigate severe events, improve system resiliency and security of supply, the SIPS have been developed. Their purpose is to detect critical instabilities, arrest the disturbance propagation, and restore the system to stable operation with minimal consequences [33], [109]. The most prominent SIPS applications are islanding detection [110], [111]; Intentional Controlled Islanding (ICI) [112], [113]; and adaptive under frequency load shedding [114]. Lastly, to speed up the system restoration, applications for resynchronisation [115] and post-event forensic analysis [116], [117] can be used.

2.3.2 EXISTING WAMPAC SYSTEMS WORLDWIDE

In the last two decades, catastrophic blackouts have stimulated electric power utilities worldwide to invest in WAMPAC systems [48]. In the first stage, the pilot projects mostly consisted of several deployed PMUs across the power grid for basic monitoring purposes, which in turn triggered the development of situational awareness, closed-loop-control, and protection applications. Table 2.2 presents the existing implementations of WAMPAC applications worldwide.

TABLE 2.2
Summary of WAMPAC applications in use worldwide

Region	Implemented applications
Continental Europe [48], [85], [118], [119]	<ul style="list-style-type: none"> • dynamic stability assessment • load monitoring • disturbance detection and analysis • power plant oscillation monitoring • dynamic thermal rating

	<ul style="list-style-type: none"> • intentional islanding • resynchronisation for restoration purposes • dynamic model tuning
Nordic countries [119], [120], [121]	<ul style="list-style-type: none"> • islanding detection and network splitting • automated load and generation shedding • resynchronisation assistance • oscillation monitoring and control • dynamic model tuning • disturbance detection and analysis
North America [46], [48], [119]	<ul style="list-style-type: none"> • dynamic stability assessment • improved state estimator • oscillation monitoring and control • islanding detection • resynchronisation assistance • disturbance detection and analysis
Mexico [48], [119]	<ul style="list-style-type: none"> • oscillation monitoring and control • monitoring of protection systems • post-event analysis
Brazil [48], [119]	<ul style="list-style-type: none"> • oscillation monitoring • stress monitoring • resynchronisation assistance
China [46], [48], [119]	<ul style="list-style-type: none"> • oscillation monitoring and control • dynamic state estimator • dynamic security assessment • adaptive protection • emergency control
India [46], [48], [119], [122], [123]	<ul style="list-style-type: none"> • dynamic security assessment • disturbance detection and analysis • islanding detection and network splitting • resynchronisation assistance • dynamic model tuning • stress monitoring • oscillation monitoring
Russia [48], [119]	<ul style="list-style-type: none"> • oscillation monitoring and control • system performance monitoring and analysis • dynamic model tuning

2.3.3 WAMPAC SYSTEM IMPLEMENTATION CHALLENGES

As discussed in Section 2.3, a WAMPAC system consists of predominantly digital solutions, which need to be carefully orchestrated to meet the strict application requirements for their desired outcome. Therefore, during a WAMPAC system design, the following aspects are essential to be considered since they can significantly affect the performance of mission-critical WAMPAC applications [46], [124]:

- quality of PMU related instrumentation transformers and wiring;
- response and saturation of instrumentation transformers in case of transients;
- time synchronisation accuracy and its reliability;
- PMU placement for sufficient system-wide observability;
- PMU class, measurement delay, and optimal reporting rate;
- PMU measurement accuracy and its reliability under power system dynamics;
- PMU response in case of transients;
- ICT related telecommunication delay, and packet loss, corruption, misordering, duplication, and their variability;
- PDC reliability and its processing time delay;
- application's data acquisition time delay;
- application's reliability in case of bad data;
- application's processing time delay and resulting closed-loop-control time delay;
- response time delay of actuators;
- integration of the applications into existing control rooms procedures;
- thorough validation of the application and training of the power system control room operators under nominal and off-nominal power system conditions;
- vulnerability and sensitivity of the supporting ICT systems to cyber threats and attacks.

2.4 WAMPAC-READY CYBER-PHYSICAL EXPERIMENTAL TESTBED

To assure that the WAMPAC applications perform adequately during most critical power system events, an extensive and thorough validation of the SMT components and WAMPAC applications under realistic power system conditions is required. Despite the evident benefits of WAMPAC applications for power system operation, in particular, to

strengthen the power system stability and resiliency, the existing WAMPAC applications are often used as ancillary stand-by tools with limited utilisation in existing control room procedures. One of the main reasons for this is the lack of detailed validation of WAMPAC applications on actual power system models and thorough training of power system operators, which leads to a reasonable mistrust of outside experts. To serve these purposes, a WAMPAC-ready cyber-physical experimental testbed is developed, enabling simplified design and online evaluation of closed-loop WAMPAC applications and validation of SMT components under realistic conditions.

2.4.1 MOTIVATIONS FOR THE TESTBED

The advent of SMT and fast telecommunication infrastructure enabled the development and implementation of WAMPAC applications. With this, the traditional power systems evolved into complex Cyber-Physical Systems (CPSs), encompassing a complex interaction between diverse research domains, belonging to a power system, ICT, signal processing, and control theory. For a reliable and effective operation of WAMPAC applications, a number of supporting systems (instrumentation, SMT, WAN, application's data acquisition and processing, RTU and remote actuator) need to be orchestrated. Hence, the adequate performance of a specific WAMPAC application depends on several factors, spread across multiple domains interacting in a closed-loop manner. Therefore, for the thorough validation of mission-critical WAMPAC applications, one should consider the closely related domains holistically [125].

It is clear that the real power systems cannot be used for testing and validation of mission-critical WAMPAC applications, particularly, since this may in the worst case lead to significant financial loss and societal discomfort. Hence, often as an alternative, a twist of conventional software simulation tools is used for this purpose. Typically, the main limitation of the conventional software-based simulation tools is that they specialise in one domain only and simplify or neglect the remaining domains, leading to suboptimal results [125]. To address this, the researchers couple together conventional software tools into a co-simulation environment [125]. The main challenge is to unite continuous and discrete simulation tools, such as power system and ICT simulators, respectively. In this case, demanding issues related to an exact time synchronisation and simulation time-step, initialisation, and variable data exchange need to be solved typically.

Despite the significant potential of software-based co-simulation environments, the WAMPAC implementation aspects presented in Section 2.3.3 cannot be investigated in detail due to a lack of software tools for this purpose. For this reason, the conventional purely software-based co-simulation environments are not applicable at this moment in time for the thorough validation purpose of WAMPAC applications. To bridge the gap, a CPS simulation platform can be used to seamlessly integrate hardware, software, and computational and physical components of virtual and physical processes [126].

The main goal of a CPS simulation platform is to integrate real, simulated and emulated components of a multi-domain system with a purpose to accurately recreate the phenomena

of a real-world system under investigation in a fully controlled, isolated and typically down-scaled environment. The main benefit of a CPS simulation platform compared to a conventional software-based co-simulation environment is the ability to thoroughly assess the system of interest as a whole or per specific domain in detail. This is particularly important during proof-of-concept analysis and experimental validation of different hardware and software solutions [127].

2.4.2 STATE-OF-THE-ART

Coupling of real-time digital simulators for CPS simulation has received considerable attention from research due to its unique ability to characterise the modern power system in detail. One of the distinctive features of real-time digital power system simulators is their real-time operation, meaning that the algebraic equations of a power system model are solved successively in discrete time steps, matching the real-world clock [105]. The main challenge is to generate a continuous output with small enough discrete steps to maintain the desired resolution of the output under given processing power constraints.

Several Hardware-In-the-Loop (HIL) testbeds for SMT components performance and compliance validation have been demonstrated in [128] and [129], which make use of *RTDS* power system digital simulator and voltage and current amplifiers to simulate and fed the signal of appropriate levels to the device under test, respectively. Similarly, authors in [130] and [131] make use of *LabView* simulation environment for automated testing of PMUs. Nevertheless, both simulation platforms suffer from uncertainty related to the accuracy of the actual waveform signal, fed to the PMU under test. Finally, authors in [132] presented the platform for metrological characterisation of a PMU calibrator, used for low uncertainty PMU compliance validation purposes. In [133], a testbed for automatic determination of PMU measurement latency is presented, by comparing the measurement timestamp and the time of a received PMU data frame. To tests the measurement supported applications, the authors in [134] present a cyber-physical simulation platform as a co-simulation between EPS and ICT simulation environments using *RTDS* and *Riverbed Modeler* (former *OPNET*) in combination with *Lab View PXI* for data analysis. Similarly, the authors in [135] make use of *RTDS*, simulated and real PMUs connected as HIL, to design an SMT supported testbed. The platform lacks components for ICT simulation and SMT supported application design. In [136] authors presented an *RTDS* based WAMPAC testbed, where they use real PMUs, *Riverbed Modeler*, and *OpenPDC* software for synchro-measurement aggregation. Similarly, the testbed lacks components for SMT supported application design. Finally, authors in [137] and [138] presented a *LabVIEW*-based synchrophasor software development toolkit for simplified SMT supported application design, named as *BabelFish*. The toolkit is then utilised in [139] as a part of their WAMPAC system development testbed, based on *Opal-RT eMEGAsim* real-time simulator, real and simulated PMUs, and *OpenPDC* software. Likewise, in [127], the authors used *Opal-RT's* simulator to simulate the power system and PMUs, connected with *CORE* open-source ICT simulator to *OpenPDC*. The letter testbed lacks components for SMT supported

application design. Recently, in [140], an SMT supported cyber-physical testbed based on *RTDS* is presented, which is used for cybersecurity and vulnerability assessment. Also, this testbed lacks components for SMT supported application design.

Hence, it can be summarised, that the existing testbeds often utilise *RTDS* or *LabVIEW* simulation platforms; use simulated or real PMUs; typically make use of a software-based *OpenPDC* PDC; and a commercially available *Riverbed Modeler* ICT network simulator. Yet, for online synchro-measurement data stream processing, only a limited set of tools is available, among them only the *LabVIEW* based *BableFish* can be used for online synchro-measurement parsing in user-defined WAMPAC applications.

However, at the start of this thesis research work, no SMT supported real-time power system simulation testbed was available at disposal. To serve this purpose, a WAMPAC-ready cyber-physical experimental testbed is developed, as a real-time co-simulation between an SMT supported power system model, an ICT infrastructure, and a WAMPAC application development framework.

2.4.3 COMPONENTS OF THE TESTBED

As illustrated in Figure 2.9, the developed real-time WAMPAC-ready cyber-physical experimental testbed represents a CPS simulator due to its tight coupling between simulated electric power system components, real and simulated SMT components, simulated telecommunication network characteristics, and software components for WAMPAC application design. The testbed's main functions can be summarised into the following four groups:

- *power system simulation*, for analysis of electromagnetic transient phenomena, empowering parallel digital processing for real-time operation of the targeted platform, equipped with numerous analogue and digital inputs and outputs (IO) interfaces for direct interconnection and data exchange with external devices and other systems;
- *SMT based power system observability*, by using simulated and real PMUs, and software-based PDCs that are interfaced as HIL and Software-In-the-Loop (SIL);
- *telecommunication network simulation*, empowering an ICT emulator and simulator, connected to the testbed as SIL, to resemble telecommunication characteristics of WAN;
- *WAMPAC application development framework*, empowering user-friendly programming environment for a simplified design and online validation of closed-loop WAMPAC applications.

In particular, the real-time operation and closed-loop interaction between the testbed's components enable comprehensive development and a thorough evaluation of closed-loop

applications. The remaining of this section presents the technical overview of the testbed used components.

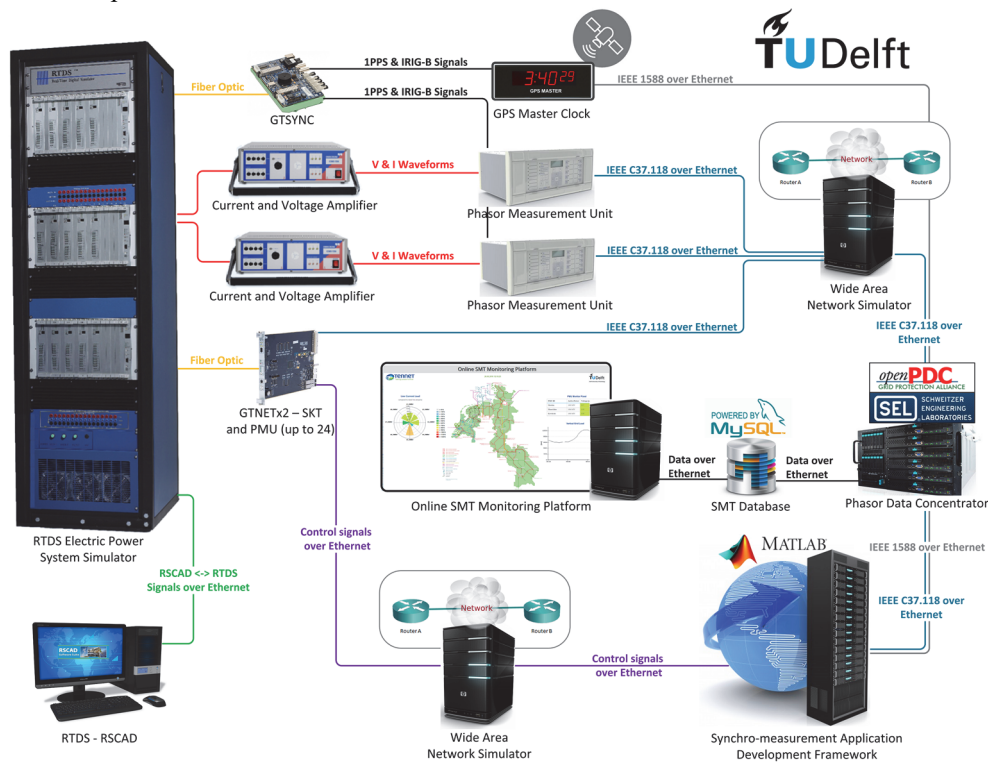


Figure 2.9: *WAMPAC-ready testbed for online validation of closed-loop applications.*

A. POWER SYSTEM SIMULATION

In order to simulate power system phenomena in real-time, an *RTDS* digital power system simulator is utilised. The *RTDS* is used for precise modelling and thorough analysis of electromagnetic transient phenomena from DC up to 3 kHz utilising a sum of specialised hardware and software components [141]. It was initially developed by Manitoba HVDC Research Centre in the 1980s for HIL testing and validation of protection equipment under realistic conditions [142]. Typically, *RTDS* produces a continuous output with a $35\ \mu\text{s}$ discrete time step, leading that the *RTDS* generated signals on its output are comparable to the signals of a real-world power system. The *RTDS* includes an *RSCAD* software tool, used for power system modelling with a Graphical User Interface (GUI) and a broad spectrum of available libraries to model power system components, substation equipment, and control logic. The latter in combination with the modular design and distinguished real-time operation makes the *RTDS* platform particularly suitable for fast prototyping and evaluation of a wide range of power system applications, and HIL performance and compliance testing of substation's hardware components like PMUs, relays, circuit breakers,

and power electronic converters for example. For this purpose, the simulated power system model quantities (voltage and current waveforms), feedback signals and control commands (protection relay status, circuit breaker trip commands) are exchanged in real-time between the *RTDS* and HIL devices under test via numerous analogue and digital IO interfaces, such as *GTAO*, *GTAI*, *GTDA* and *GTDI* for example [141]. Additionally, by using *RSCAD Runtime* software program or *GTNETx2* based standardised telecommunication protocols (UDP, TCP, Modbus, IEEE Std. C37.118, IET 61059 SV, IET 61059 GOOSE, IET 61059 MMS) it is possible to change any setpoint or power system topology remotely, and send/receive the simulation specific data to/from the other systems [141].

For this thesis related simulation of electromagnetic transient phenomena, two power system models, detailed in Chapter 4 and Chapter 5, are simulated in *RTDS* by using *RSCAD Draft* and *Runtime* software programs for modelling and real-time execution, respectively. The simulations are executed on two *PB5* based *RTDS* racks (rack-3 and rack-4) and interfaced with SMT components as HIL and SIL. Figure 2.10 presents the laboratory setup, utilised in this thesis.



Figure 2.10: Digital power system simulator interfaced with PMUs as HIL via digital to analogue converter outputs and current and voltage amplifiers.

B. SMT-BASED POWER SYSTEM OBSERVABILITY

The developed WAMPAC-ready experimental testbed (see Figure 2.8 and Figure 2.9) includes SMT components for near real-time observability of the *RTDS* simulated power system models. For this purpose, two *GE* (former *Alstom*) *MiCOM Agile P847* P-class hardware PMUs are connected to the *RTDS* via *GTAO* interfaces as HIL. Each of the PMUs

is capable of measuring two current and two voltage channels, in total providing four synchro-measurement data streams according to IEEE Std. C37.118.2-2011. Hereby, two high-precision *Omicron CMS-156* amplifiers are used to amplify the 5 V output signals from an *RTDS GTAO* card to 110 V and 5 A voltage and current signals, respectively, for direct feeding to the corresponding voltage and current channels of the PMUs. In addition, up to 48 *RTDS* embedded *P* class PMUs data streams, provided by the two *RTDS GTNETx2* cards are used simultaneously. For time alignment and aggregation of the PMU data streams, an *OpenPDC* and *SEL-5073* software-based PDCs are used. Hereby, the *OpenPDC* is used to online store the PMU provided data into a *MySQL* database, mainly for online monitoring purpose (see Section 2.4.3 - D), while the *SEL-5073* PDC is used to forward the aggregated data stream to the *MATLAB* based Synchro-measurement Application Development Framework (SADF) for online synchro-measurement data processing in user-defined WAMPAC applications.

Moreover, to provide time synchronisation between all the testbed components, a *GE RT430* GPS disciplined grandmaster clock is used, which provides time accuracy within 100 ns (peak), with the time drift less than 0.1 ppm in case an external GPS reference signal is lost. Hereby, the IRIG-B and PPS signals are fed to the hardware PMUs via coaxial and fibre-optic cables, respectively, while the PTP is distributed via L2 Ethernet-based LAN to the computers running PDCs and SADF. To time synchronise the computers, a *Greyware Domain Time II* based PTP software client and an *Oregano Systems syn1588-PCIe* based PTP hardware client are used.

C. TELECOMMUNICATION NETWORK SIMULATION

To simulate substation and system-wide telecommunication network characteristics, a *WANem* network emulator and *ns-3* ICT simulator are used as SIL. The *WANem* is used to real-time emulate specified telecommunication delay, jitter, packet loss, and data throughput for each telecommunication channel. Besides, *ns-3* network simulator can be used to investigate ICT network-related phenomena (link and node data-congestions, jitter, delay, packet drop, etc.) and to assess the cyber-security vulnerabilities (false data injection, buffer overflows, and device misconfiguration). By using the aforementioned ICT network tools, each communication channel can be characterised with its unique ICT performance characteristics that can emulate the real LAN and WAN conditions from the field.

D. WAMPAC APPLICATION DEVELOPMENT FRAMEWORK

At the start of the research work of this thesis, there existed a lack of available user-friendly tools for the rapid prototyping of WAMPAC applications. Therefore, a SADF is developed to enable simplified design and promote thorough validation of WAMPAC applications under realistic conditions. The SADF's functionality and structure are presented in detail in the next Chapter 3.

2.4.4 VALIDATION OF THE TESTBED

As a part of the WAMPAC-ready experimental testbed, a web-based online SMT monitoring platform is developed (see Figure 2.11) for the online monitoring of PMU measured power grid dynamics, simulated in *RTDS*. The monitoring platform is used for online visualisation of the PMU measurements, abnormal event detection in PMU measurements and alarming, line ampacity monitoring, and data export for offline analysis.

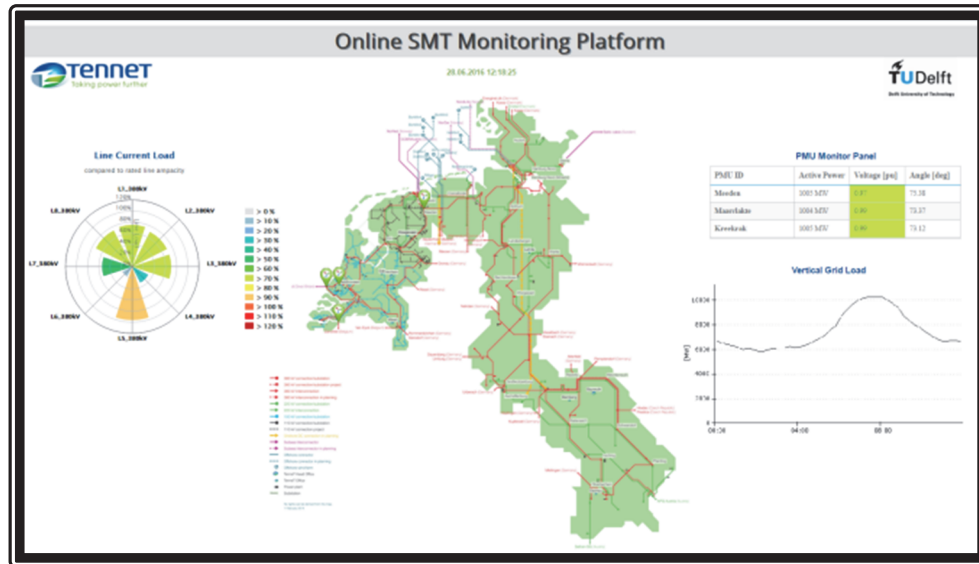


Figure 2.11: Web-based online SMT monitoring platform for real-time monitoring of EPS.

The monitoring platform is a web-based application, running on the top of an *Ubuntu* operating system (OS). It connects to the *MySQL* database and in online fashion retrieves the stored PMU measurements, continuously populated by the *OpenPDC*. The platform backend (the part of the platform that is not directly accessed by a user, typically responsible for storing and manipulating data) is built using *JavaScript* and *PHP* programming languages, while the frontend (the part of the platform that is directly accessed by a user, typically responsible for displaying of the processed data) is based on HTML markup language with *CCS* and *JQuery* support. This makes the monitoring platform cross-device (computer, tablet, smartphone) compatible and intuitive to navigate, as illustrated in Figure 2.12.



Figure 2.12: Real-time monitoring of active and reactive power.

2.5 CONCLUDING REMARKS

This chapter discussed the rationale behind the power system monitoring with high resolution in time and space. It presented the SMT, its benefits compared to the traditional SCADA system, state-of-the-art WAMPAC applications, and important implementation aspects to consider when designing WAMPAC applications. Moreover, the chapter highlighted the crucial requirement to extensively validate the emerging WAMPAC applications under realistic conditions before being implemented in the real-world power grids.

The primary objective of this chapter research work is first to stress the limitations of the conventional software-based simulators for WAMPAC application design and evaluation, and second to motivate the need to develop a realistic CPS for this purpose. The main goal of this chapter research work was to design an SMT supported testbed for the formation of realistic synchro-measurements and their direct use in user-defined applications. One of the major contributions of this chapter is the developed WAMPAC-ready cyber-physical experimental testbed.

The developed testbed enabled the online assessment and validation of SMT components and emerging closed-loop WAMPAC applications under realistic conditions in real-time. For this purpose, a combination of simulated, emulated, and real hardware and software components were used in order to attain the most realistic conditions in a fully controlled, down-scaled and isolated simulation environment. Also, the testbed can serve as

a powerful tool for training activities of power system operators on actual grid models and educational coursework.

To verify the developed testbed, a web-based SMT monitoring platform is developed. The web-based platform is suitable for online monitoring of PMU measured dynamics and is particularly useful for demonstration purposes of the testbed.

Moreover, to facilitate the simplified design and online use of synchro-measurement data in user-defined WAMPAC applications, a *MATLAB* based SADF software library was developed, which is further detailed in the next Chapter 3. In conclusion, this chapter developed the WAMPAC-ready experimental testbed that will serve as the groundwork of Chapter 3, Chapter 4 and Chapter 5 related developments.

CHAPTER 3

SYNCHRO-MEASUREMENT APPLICATION DEVELOPMENT FRAMEWORK

To enable seamless integration between an SMT supported power system and user-defined WAMPAC applications, this chapter develops *MATLAB* supported SADF software library. It provides the missing link between the IEEE Std. C37.118.2-2011 specification and its implementation. In the first part, this chapter discusses the limitations concerning the use of conventional software-based simulation tools for the development of WAMPAC applications. It continues with a presentation of the state-of-the-art tools for SMT stream parsing and processing, followed by an overview of the IEEE Std. C37.118.2-2011 specification. In the second part, this chapter presents the developed SADF library, its structure, and the proposed communication and parsing methodology. Moreover, it presents the results of SADF compliance, interoperability, and execution performance evaluation using Chapter 2 developed cyber-physical testbed. Finally, a SADF build-in example application is demonstrated and the chapter conclusions are presented.

3.1 INTRODUCTION

As discussed in Chapter 2, the IEEE Std. C37.118.2-2011 has evolved as one of the widely deployed communication protocol for synchro-measurement data exchange in an SMT supported power system. Nevertheless, there exists a lack of user-friendly tools for development and seamless integration of SMT supported WAMPAC applications. In fact, at the beginning of this research work, no *MATLAB* supported synchro-measurement parser was available. Hence, this chapter presents the developed SADF, a complete IEEE Std. C37.118.2-2011 supported implementation in *MATLAB* programming environment.

The SADF enables a simplified design, and the online validation of SMT supported WAMPAC applications. For the first time, it enables online receiving and parsing of IEEE Std. C37.118-2005 and IEEE Std. C37.118.2-2011 based machine-readable messages into a human-readable *MATLAB* format, as illustrated in Figure 3.1. This research work provides the implementation procedures of IEEE Std. C37.118-2005 (communication part) and IEEE

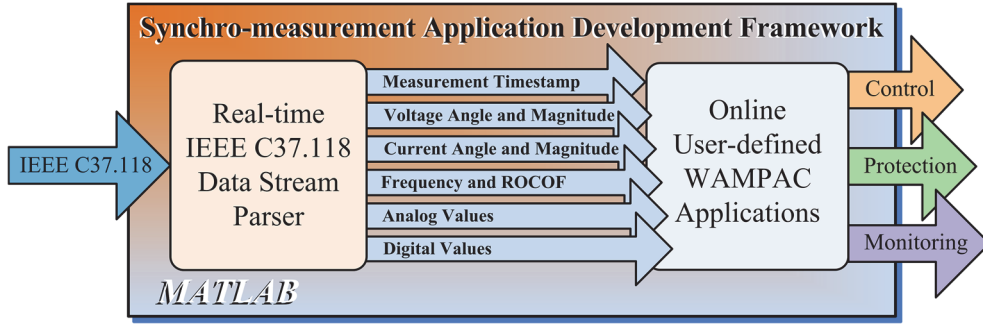


Figure 3.1: Overview of the SADF.

Std. C37.118.2-2011 specifications by proposing a robust communication technique and efficient synchro-measurement data parsing method.

In the first place, the SADF library is developed to promote the simplified design and online validation of advanced WAMPAC applications under realistic conditions. Also, the SADF library can be utilised as a part of a PMU/PDC metrological characterisation and IEEE Std. C37.118 compliance validation [143], as a tool to receive and compare the “true” synchro-measurements, produced by a reference PMU, with the synchro-measurements of a PMU under test. Combining SADF library with *MATLAB* functions for signal processing and visualisation allows mastering the design of complex WAMPAC applications.

MATLAB programming suite is a powerful engineering computing toolbox, supported by various build-in mathematical, signal processing, and visualisation functions. It is cross-OS compatible (*Windows, Mac, Unix*) and can be interfaced with programs written in *C, C++, Java, Fortran, and Python*. *MATLAB* has been a de facto programming language for research worldwide and has extended online community support [144].

3.1.1 MOTIVATIONS FOR THE SADF

The typical IEEE Std. C37.118 based data exchange is in machine-readable representation (binary format) to efficiently transfer the data between electronic devices [60], [61]. The binary format is tough to interpret for humans. Researchers often need to deal with the lack of available user-friendly tools for online synchro-measurement data acquisition to design and online validate WAMPAC applications. This is one of the reasons why many researchers prefer to work on pre-processed measurements, typically Comma Separated Value (CSV) format and stored by a PDC, primarily designed for offline analysis. However, by taking this approach, the measurements are available in the user-defined applications with processing delay concerning the write/read operations to/from a file or database. This can have a negative impact on the performance of the closed-loop WAMPAC applications, which require fast response and can consequently endanger secure power system operation. Hence, to enable seamless integration between the SMT supported power system and user-defined WAMPAC applications, the SADF is developed to enable online and direct use of synchro-measurements in the *MATLAB* programming environment.

Additionally, many of the available synchro-measurement based scientific papers make use of conventional software simulated bus measurements rather than real PMU provided synchro-measurements. It is important to note that in reality, the synchro-measurements are affected by transients [52], harmonics [54], and system-imposed high frequency components [53]; instrument transformers errors [145]; PMU analog filtering, sampling, and windowing [146], [147], [148] [149]. Therefore, the real PMU provided synchro-measurements can dramatically differ from typical bus measurements, obtained by using conventional software simulation tools. As a result, the performance of existing WAMPAC applications, published in scientific papers, may negatively differ in case actual synchro-measurements are utilised and it may in a worst-case scenario lead to a complete power system blackout. To promote extensive evaluation under realistic conditions, the developed SADF enabled the simplified design and online validation of advanced (closed-loop) WAMPAC applications.

3.1.2 STATE-OF-THE-ART

In the last two decades, the SMT solutions and WAMPAC applications have gained increased attention from research and industry. In [150] and [151], authors present the implementation of IEEE Std. C37.118-2005 (communication part) specification for PMU/PDC emulation purposes as an open-source application using *C* and *Python* programming language, respectively. However, their published work has several limitations, including: (i) lack of IEEE Std. C37.118.2-2011 support, (ii) lack of UDP connection protocol support and spontaneous communication mode, (iii) detailed performance evaluation is missing. The Grid Protection Alliance [152] developed a *Time-Series Framework* for managing of synchro-measurement data and implemented as an open-source library in *.NET*, *Java*, *C++* programming languages. Despite the big potential, the library has not been vastly utilised in research, mainly due to proficient programming required. The PMU Connection Tester and OpenPDC are currently being one of the most used open-source applications built on top of *TimeSeriesFramework* and are designed for PMU connectivity testing and aggregation of synchro-measurement streams, respectively [152]. For the first time, a *LabVIEW* based synchrophasor software development toolkit (named as *BableFish*) was developed [138] to online receive IEEE Std. C37.118.2-2011 data stream in a *LabVIEW* environment. However, their work is limited to the *LabVIEW* and can receive only TCP/IP data stream in *commanded mode* only.

3.2 OVERVIEW OF IEEE STD. C37.118.2-2011

Over the recent years the IEEE Std. C37.118 family has evolved as one of the widely deployed among SMT supported power system components. This chapter focuses on the implementation procedures regarding the IEEE Std. C37.118.2-2011 that is backwards compatible with IEEE Std. C37.118-2005 (communication part). Therefore in this chapter, only the communication part is further addressed.

3.2.1 COMMUNICATION FRAMEWORK

The IEEE Std. C37.118.2-2011 defines synchro-measurement messaging framework (application layer) requirements, including message types, use, contents and data formats. It does not put any restrictions on a utilised communication medium, and transport protocol since they are typically application dependent. Initially, the standard was designed for RS-232 serial communication, but the past implementations show the great success of fast fibre-optic based Internet Protocol (IP) telecommunication networks, utilising Transmission Control Protocol over IP (TCP/IP) and/or User Datagram Protocol (UDP).

A. TRANSMISSION CONTROL PROTOCOL

TCP/IP is a connection-oriented (one-to-one, bidirectional) data exchange protocol and is suited for applications that require high reliability of data transfer, while transmission time (latency) is relatively less critical. The TCP/IP stack guarantees that data arrives at the final destination (application layer), remains intact, and in the same order in which it was sent. As a consequence, a continuous PMU/PDC measurement data stream utilising TCP/IP may experience retransmission interruptions in case of corrupted and out-of-order received TCP/IP packets on the receiving side [153].

B. USER DATAGRAM PROTOCOL

In contrast to TCP, UDP is a simpler connectionless (one-to-one/many, unidirectional) data exchange protocol and is suited for applications that meet fast and efficient transmission of data. UDP does not guarantee the arrival of the packets to the final destination and has no inherent delivery order as all packets are independent of each other. If data ordering and recovery are required, it has to be managed by the application layer on the server and client-side [154]. In SMT, UDP is often preferred since data transmission is faster (smaller overhead size) and continuous compared to TCP/IP.

3.2.2 COMMUNICATION MODE

Synchro-measurement data exchange is server-client oriented, using either *commanded* or *spontaneous mode* of communication. In the *commanded mode* (bidirectional server-client communication), a hierarchy higher level PDC or application data acquisition (further referred to as *receiver*) initiates a connection with PMU/PDC data source device (further referred to as *sender*) and takes control of configuration and measurement data exchange. Hereby, the receiver sends specific data request commands to the sender, which afterwards replies with requested data. On the other hand, in *spontaneous mode* (unidirectional server-client communication) configuration and measurement data exchange is initiated by the sender in a continuous way without any negotiation with the receiver.

Moreover, synchro-measurement data exchange can be either *unicast* (between a sender and a receiver), *multicast* (between a sender and group of receivers, via one data stream), or *broadcast* (between a sender and all network nodes). Typically, *unicast* is utilised for one

domain network, while *multicast* is suitable for synchro-measurement data exchange between different synchro-measurement domains. *Broadcast* is utilised only in special cases since it is resources expensive.

3.2.3 FRAME STRUCTURE AND MESSAGE TYPE

The IEEE Std. C37.118.2-2011 specifies the basic structure of a frame and four types of messages for synchro-measurement configuration and data transmission. These are *data*, *configuration*, *header*, and *command*. Typically, the first three message types are sent from a sender as the response on a received command message, initiated by a receiver.

A. FRAME STRUCTURE

All four message types start and end up with the predefined header and footer respectively, forming together a frame. Header and footer contain a set of parameters, referred to as fields as illustrated in Figure 3.2.

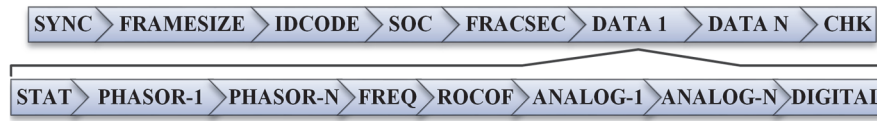


Figure 3.2: *DATA message frame structure.*

Each frame first starts with a SYNC (2-byte) field, used to identify frame type (bits 6-4), and utilised synchro-measurement standard version (bits 3-0). It continues with a FRAMESIZE (2-byte), defining total frame size in bytes. Further, an IDCODE (2-byte) field defines a unique identification number of a frame originating device or destination device in case of a command message. Next, a Second Of Century (SOC) (4-byte) and a Fraction of a Second (FRACSEC) (4-byte) fields together define measurement timestamp or transmission time for the non-DATA messages. Hence, the timestamp is given by:

$$TimeStamp = SOC + FRACSEC / TIME_BASE \quad (3.1)$$

where TIME_BASE integer determines the maximum time resolution in ticks.

Additionally, a FRACSEC contains 8-bit time quality flags to indicate the quality of time at the source plus indication of leap second status. Finally, the content of a frame (DATA 1 - N) field is encapsulated and terminated with a CHK (2-byte) field, containing Cyclic Redundancy Check (CRC) for transmission-error detecting.

B. DATA MESSAGE

DATA messages are primarily used during synchro-measurement data exchange and contain a set of measurements at the precisely determined moment in time. Each *DATA* message contains at least one encapsulated PMU measurement block (set of measurements

and control flags of a single PMU measurement stream). A PMU device can send only one (its own) encapsulated measurement block, while a PDC device typically sends multiple encapsulated measurement blocks in a single *DATA* frame from hierarchically underlying PMUs and/or PDCs. It is important to note that the *DATA* frame content cannot be interpreted without info obtained from a configuration message beforehand.

As illustrated in Figure 3.2, a single measurement block (DATA-1) includes time and measurement quality information (STAT), estimated synchrophasors (PHASOR), system frequency (FREQ), rate-of-change-of-frequency (ROCOF), analogue values (ANALOG), and digital Boolean status words (DIGITAL).

C. CONFIGURATION MESSAGE

A configuration message is used to inform the receiver about the sender related capabilities, metadata, and configuration structure of *DATA* messages being reported. Typically, it is sent during connection initialisation period and before first *DATA* is sent to permit the receiver to properly separate and interpret measurement identities of *DATA* frames. The standard defines three types of configuration frames: *CFG-1*, *CFG-2*, and *CFG-3* (optional).

A *CFG-1* denotes a PMU/PDC full reporting capability and is used in exceptional occasions. Further *CFG-2* and *CFG-3* indicate a PMU/PDC configuration structure of *DATA* frame currently being reported. It includes station identification number and name, phasor and analogue total number and channel names, measurements reported formats and scaling factors, default digital status positions, reporting rate, nominal system frequency, and configuration change number identification. Additionally, *CFG-3* introduces variable frame length, metadata related to phasor and analogue values offset, a synchrophasor estimation algorithm window length and group delay, and geographical properties of the PMU.

D. HEADER MESSAGE

A header *HDR* message is primarily used to inform one about a PMU installation location, measurement properties, filtering applied, reporting rate, and other user-defined metadata. Unique about the *HDR* message is that its content is in a human-readable *ASCII* format.

E. COMMAND MESSAGE

A command *CMD* message is used exclusively in commanded mode to send instructions from the receiver to the sender. Typically, after the sender receives the instruction, it responds with a requested action. Commands which the receiver can send to the sender are: “send *CFG-1*”, “send *CFG-2*”, “send *CFG-3*”, “send *HDR*”, “turn on *DATA*”, and “turn off *DATA*”.

3.2.4 TYPICAL DATA EXCHANGE

All message types (except *HDR*) are transmitted in machine-readable format (binary representation) to transfer data between SMT devices efficiently. Data transmission of a message frame always starts with SYNC and ends with a CHK field (see Figure 3.2). Data is transmitted using big-endian, i.e. most significant byte first.

A. SPONTANEOUS MODE

In spontaneous communication mode, the sender typically sends *DATA* messages to the receiver continuously, as illustrated in Figure 3.3 (mind the orange circle with 1). *DATA* messages are sent with a reporting rate as specified in a sender configuration settings. Additionally every minute rollover it sends a *CFG-2/CFG-3* message (mind the orange circle with 2) to inform a receiver about *DATA* message structure currently being reported.

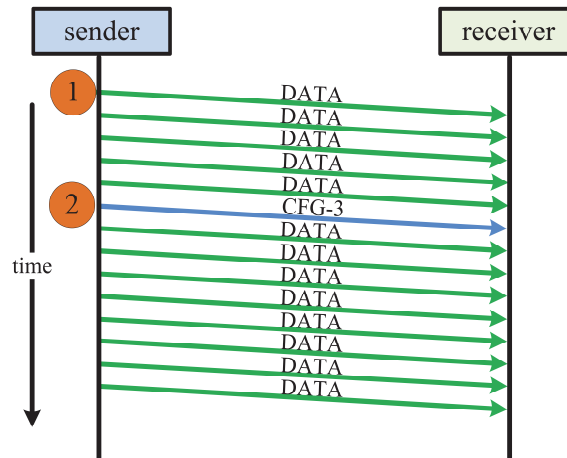


Figure 3.3: Spontaneous mode communication data exchange.

B. COMMANDED MODE

In commanded communication mode (Figure 3.4), the receiver typically starts with sending a “send *CFG-2*” or “send *CFG-3*” configuration message to the sender (mind the orange circle with 1). After a sender receives a command, it responds with a requested configuration message (mind the orange circle with 2). Further, after the receiver successfully receives the configuration message, it sends to the sender a “turn on *DATA*” (mind the orange circle with 3) command. Afterwards, the sender starts sending *DATA* frames (mind the orange circle with 4) to the receiver in continuous and equally time spaced intervals, as specified in device configuration (reporting rate). Finally, in case data exchange should be terminated, the receiver sends a “turn off *DATA*” command (mind the orange circle with 5) to the sender, which stops sending *DATA* messages immediately after receiving the command.

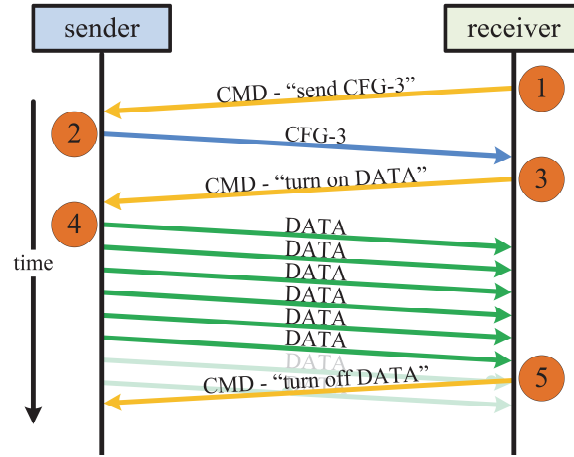


Figure 3.4: Commanded mode communication data exchange.

3.3 STRUCTURE OF SADF SOFTWARE LIBRARY

The SADF library comprises of developed scripts in *MATLAB* programming language to online receive and in real-time validate, parse, interpret, and store synchro-measurements into a human-friendly format in *MATLAB Workspace*, making it available for user-defined WAMPAC applications. Illustrated in Figure 3.5, the library includes a robust communication technique with fallback procedures for data exchange establishment and an efficient processing methodology for online parsing of the IEEE Std. C37.118-2005 (communication part) and C37.118.2-2011 specified messages.

3.3.1 CONNECTION ESTABLISHMENT FOR DATA EXCHANGE

The SADF can establish a TCP/IP or UDP unicast connection with a PMU or PDC, typically by utilising a host platform supported wired Ethernet or wireless WiFi technologies. In both cases, the *MATLAB Instrument Control Toolbox* socket interfaces in *Java* language are utilised for this purpose.

It is important to note that the proposed SADF library supports both *commanded* and *spontaneous mode* of communication. In the first case, one can select either TCP/IP or UDP, or a combination of both (TCP/IP for sending/receiving *CMD*, *HDR*, *CFG-1*, *CFG-2*, *CFG-3* frames, and UDP for sending/receiving *DATA* messages) for configuration and measurement data exchange. In the second case, UDP is supported to facilitate fast and efficient transmission of configuration and measurement data exchange, critical for fast response WAMPAC applications.

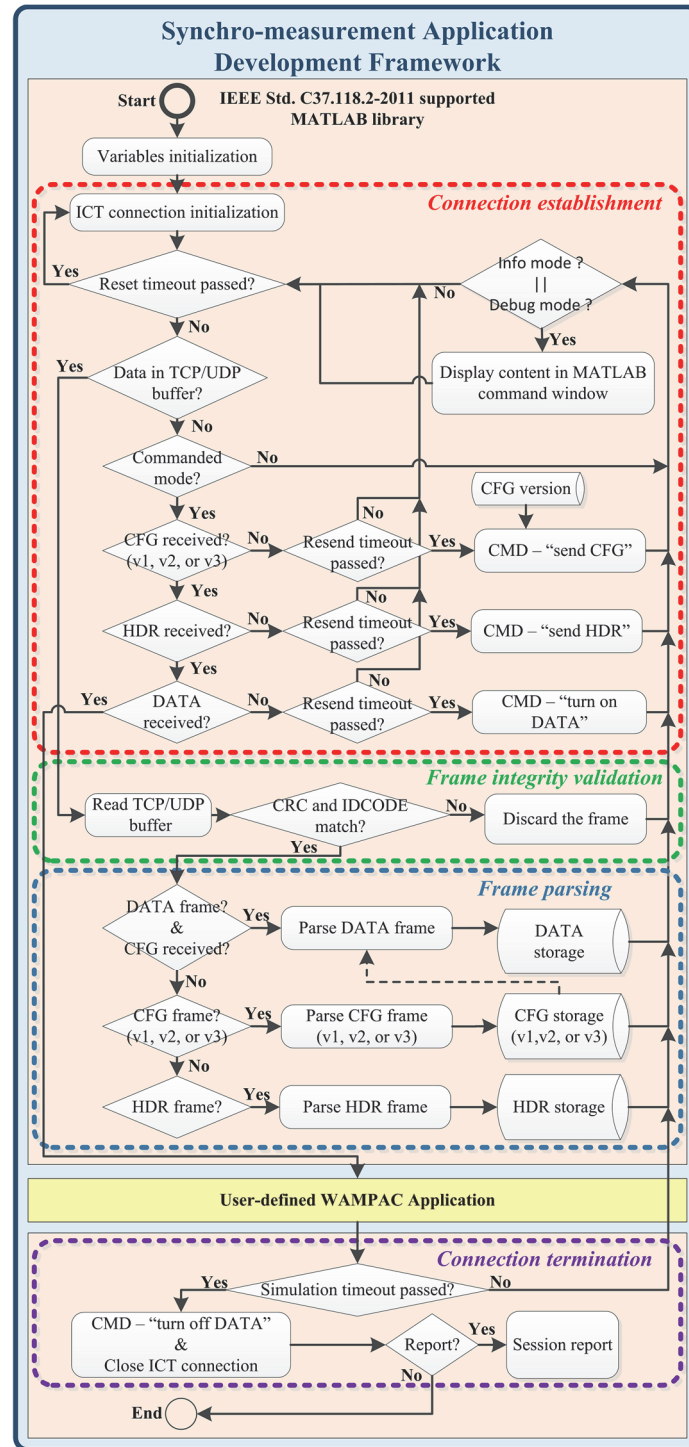


Figure 3.5: Diagram of the SADF library.

A. COMMANDED MODE

In commanded mode (see Figure 3.3), the SADF initiates a connection establishment procedure to obtain a PMU/PDC configuration and initiate measurement data transmission. This procedure is divided into multiple steps with an implemented fallback algorithm to cover situations when a PMU/PDC does not support the requested configuration message in case of ICT interruptions.

First, the SADF sequentially sends a *CMD* message request to obtain an *HDR*, following *CFG-1*, *CFG-2* or *CFG-3* messages from a PMU/PDC. It may happen that the PMU/PDC does not support the requested *CMD* message type. In this case, the PMU/PDC typically responds with a *CFG-2* message or does not respond at all. It may also happen that due to ICT interruptions, the PMU/PDC does not receive the sent *CMD* message request. Anyhow, in all the cases the specific *CMD* message is resent every two seconds and up to five times. In case the expected response from PMU/PDC is still not received, the SADF will automatically continue with the next step of the connection establishment procedure, since crucial *DATA* exchange can be still established, even without info obtained from an *HDR* or *CFG-1* message. Lastly, in case of unreceived response on sent “send *CFG-2/CFG-3*” or “turn on *DATA*” (if applicable) *CMD* message request, the ICT connection with the PMU/PDC is reestablished. Afterwards, the connection establishment procedure with the PMU/PDC is reinitiated. In this way, the SADF library does not halt in case of unexpected events.

It may also happen that the PMU/PDC starts sending *DATA* frames immediately after the establishment of an ICT connection or before the SADF requests a *DATA* exchange. In this case, a “turn off *DATA*” *CMD* message request is immediately sent to the PMU/PDC in order to terminate the existing *DATA* exchange and proceed with a standard connection establishment procedure. Any received *DATA* message is flagged and discarded since it cannot be interpreted without info obtained beforehand from a *CFG-2/CFG-3* message.

Finally, after the SADF successfully receives at least a *CFG-2/CFG-3* message, a “turn on *DATA*” *CMD* message is sent. Afterwards, online processing of received *DATA* messages is automatically initiated.

In case the data exchange between the SADF and PMU/PDC stops for any reason for more than 10 s, the ICT connection and connection establishment procedure is reestablished and reinitiated, respectively. In this way, the SADF library does not halt in case of unexpected events.

B. SPONTANEOUS MODE

In spontaneous mode, the SADF opens a user-defined UDP port and waits for a PMU/PDC to initiate frame exchange. First, the SADF waits to receive a *CFG-2/CFG-3* message, which is typically sent by the PMU/PDC each minute rollover. During this waiting period, any received *DATA* message is flagged and discarded since it cannot be interpreted without info obtained beforehand from a *CFG-2/CFG-3* message. After the successful receiving of a *CFG-2/CFG-3* frame, the online processing of *DATA* messages is automatically initiated.

3.3.2 FRAME INTEGRITY VALIDATION

The SADF performs two-step frame validation on all received frames to detect data transmission errors and verify a message frame source.

First, a CHK field value of any received message frame is compared against a newly determined CRC from a received entire frame-block. The CRC is calculated based on a CRC-CCITT error detection scheme and implemented in C programming language for processing speed increase. The CRC-CCITT is computed by following polynomial function

$$g(x) = x^{16} + x^{12} + x^5 + 1 \quad (3.2)$$

with seed value of $0xFFFF$ (-1) and no final mask [61]. In case the compared CRC values do not match, then the frame certainly contains bit-error; hence, it is flagged and discarded.

Finally, the IDCODE field of the successfully received frame is compared against the user-defined IDCODE in the SADF configuration file. In case the IDCODE values do not match, then the received frame is flagged and discarded.

3.3.3 FRAME PARSING

The SADF automatically identifies and in real-time parses the IEEE Std. C37.118-2005 and C37.118.2-2011 supported configuration and measurement messages of any reporting rate provided.

The identification of a received frame type is based on a SYNC field, unique to each message. First, a SYNC value of a received frame is compared against an identification code of *DATA*, *HDR*, *CFG-1*, *CFG-2*, *CFG-3* message. After a positive match, the message content is read using adequate parsing functions. The content of each message is stored into *MATLAB Workspace* using a structure array format by using a variable name corresponding to the message type for ease of use. Individual message content identities are stored into child structure arrays with self-explanatory names.

To get an insight into the IEEE Std. C37.118.2-2011 specified data exchange the SADF library supports three modes of operation:

- *info mode*; only basic info regarding send and received frames with the corresponding timestamp is displayed in the *MATLAB* command window.
- *debug mode*; info regarding send and received frames with detailed message frame content in a user-friendly format is displayed in *MATLAB* command window. Additionally, all the raw data exchange between sender and receiver is stored for ease of debugging purposes.
- *silent mode* (default); no info is displayed in the *MATLAB* command window. This mode is typically used during normal operation for an increase in processing speed.

Lastly, the SADF end-of-session report optionally displays in *MATLAB* command

window a summary regarding successfully received, duplicated, out-of-order, and corrupted messages, grouped by type.

A. DATA MESSAGE

In case TCP/IP is used for data transmission, the protocol itself guarantees that all message frames arrive in the same order as were sent; hence, no additional data stream post-processing is required.

On the other hand, when UDP is used, the SADF takes control over out-of-order received, duplicated, or missing data frames. In the first case, the SADF time-aligns received *DATA* messages and stores them in the right time sequence based on the message timestamp. In the case of duplicated and missing *DATA* messages, the received measurements are discarded or stored with unrepresentable (*NaN*) values, respectively.

The SADF extracts from each received *DATA* message an encapsulated PMU measurement block; time and measurement quality information, which are condensed in 8-bit FRACSEC time quality flags and 2-bytes STAT field, respectively. These include the following:

- leap second status;
- time accuracy;
- measurement data validity;
- time source synchronisation status;
- measurement device operation status;
- data sorting type;
- trigger status and reason;
- configuration change notification.

Moreover, the IEEE Std. C37.118.2-2011 defines 16-bit integer and 32-bit floating-point formats for synchro-measurement (phasors, analogue values, frequency, and ROCOF) data exchange. Most often a 16-bit integer format is used to facilitate efficient transmission, but it requires additional multiplication with a scaling factor. Phasor measurements can be transmitted in rectangular (real and imaginary components) or polar (magnitude and angle) format. Additionally, *CFG-3* message contains adjustments factors related to the magnitude or angle offset corrections (in case of phasors and analogue values) that need to be considered. To facilitate ease-of-use, the SADF automatically converts synchro-measurement data of any format into a user-friendly double format. As a result of this, phasor measurements are stored in the polar format; the magnitude is in engineering units and the angle is in degrees, all with applied correction factors (if applicable). Similar applies to the analogue values, frequency, and ROCOF measurements. In short, a *DATA* message is parsed to provide:

- timestamp of a measurement;
- phasor magnitude and phase with an applied offset;
- analogue values with an applied offset;
- digital status words;
- system frequency;
- system frequency deviation;
- ROCOF.

B. CFG MESSAGE

The SADF supports receiving of *CFG-1*, *CFG-2*, and *CFG-3* configuration message types. Since a PMU/PDC configuration settings can change over time, the SADF permits the receiving of multiple configuration messages within a single session. With this, only configuration messages containing newer structure as the already received one are stored and used for further processing of *DATA* messages. The duplicated configuration messages are flagged and discarded. For example, most informative *CFG-3* message is parsed to obtain:

- number of PMU blocks included in *DATA* frame;
- number of phasors, analogue and digital values for each PMU block included;
- PMU station, phasor, analogue channel naming;
- digital channel;
- measurement format, conversation, and offset factors;
- station geo-location properties;
- estimation algorithm window length and group delay;
- configuration change count;
- *DATA* reporting rate;
- nominal system frequency.

C. HDR MESSAGE

The SADF can receive the standard supported *HDR* message. Its content is primarily in American Standard Code for Information Interchange (ASCII) format and is typically for PMU installation and verification purposes. The SADF supports receiving of multiple *HDR* messages within one session. By using *debug mode* its content can be displayed in the *MATLAB Command Window*.

D. CMD MESSAGE

In *commanded mode*, *CMD* message content is sent (written) to the TCP/IP/UDP *Java* socket in an asynchronous mode. In this way, the *MATLAB* command line is not blocked for the duration of *Java* socket execution. Consequently, the user-defined application has more time available for its own operation (execution).

3.4 COMPLIANCE AND PERFORMANCE EVALUATION

The SADF library is primarily designed for use in SMT supported environment; therefore, the real-time operation of the SADF library is crucial. In order to evaluate the SADF library performance as well as interoperability with the IEEE Std. C37.118 compliant devices and accuracy of the provided data, Chapter 2 presented cyber-physical simulation testbed is used.

3.4.1 SIMULATION TESTBED

For SADF compliance and performance evaluation, a simple AC power system model with 50 Hz nominal system frequency is run in the RTDS to generate test signals, fed to the PMU input channels. As illustrated in Figure 3.6, a GTAO card is used to provide low-level analogue current and voltage waveforms, first fed to an OMICRON CMS-156 amplifier and further to an external GE P847 PMU. Additionally, a GTNETx2 card is used to simulate up to 24 independent PMU streams. All the PMUs are interchangeably connected to the SEL-5073 PDC or *OpenPDC*, and further over the WANem emulator to the SADF, as presented in Figure 3.6. The WANem is utilised for emulation of communication delay, and packet jitter, corruption, loss, and misordering.

The performance evaluation of the proposed *MATLAB* supported SADF library is performed on a typical personal computer (CPU: Intel Xeon E5 1620v2 - 3.70 GHz, memory: 16 GB RAM, OS: Windows 7) with installed *Wireshark* version 3.0.0 communication protocol analyser and *MATLAB* version R2017a programming environment. The *MATLAB* is executed in real-time priority.

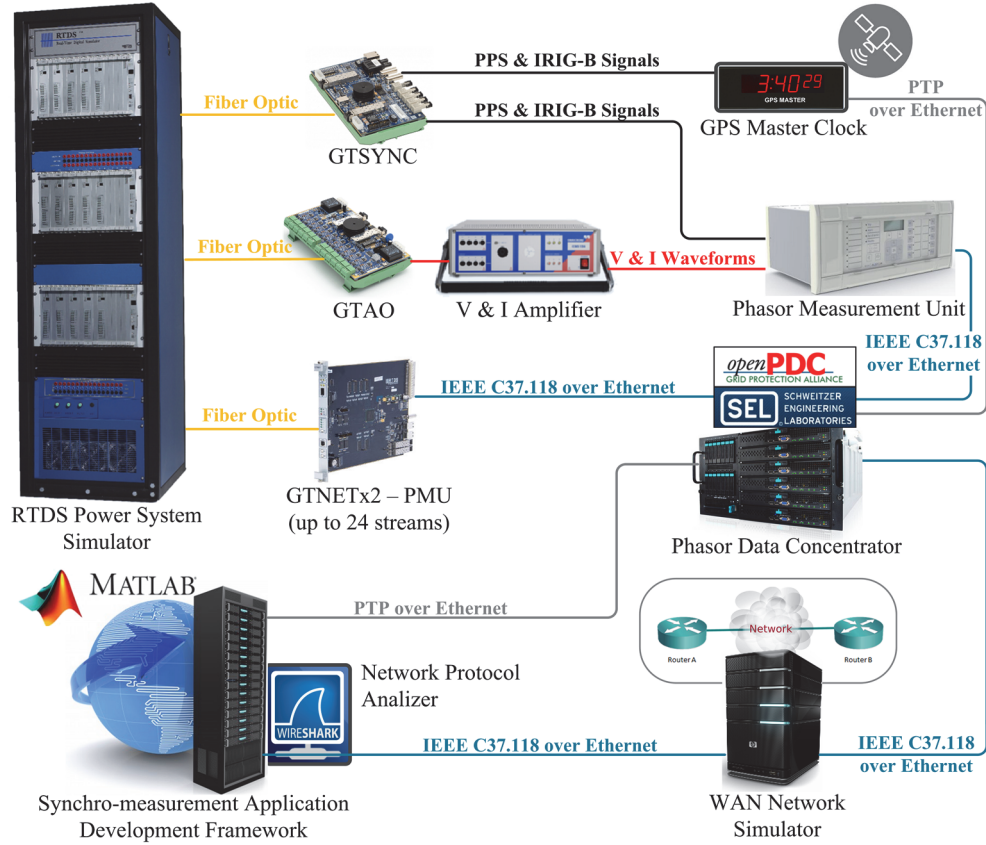


Figure 3.6: Cyber-physical simulation testbed, tailored for the evaluation purpose of the SADF.

3.4.2 COMPLIANCE VERIFICATION AGAINST IEEE STD. C37.118.2-2011

In order to develop a reliable WAMPAC application, it is prudent to confirm the SADF compliance with the IEEE Std. C37.118.2-2011 specifications and SADF interoperability between the standard supported devices as well as accuracy of provided data. First, the SADF is connected directly with the IEEE Std. C37.118.2-2011 supported external PMU to verify the typical data exchange during TCP/IP and UDP commanded mode operation. Afterwards, the SADF is interchangeably connected with both PDCs that are further connected with the external PMU and RTDS simulated PMUs. Hereby, the SADF is tested to confirm UDP, TCP/IP, and mixed TCP/IP and UDP commanded mode as well as UDP spontaneous mode of operation. Table 3.1. summarises the performed tests, obtained results, and confirms interoperability with the IEEE Std. C37.118.2-2011 standard specifications.

TABLE 3.1
Interoperability testing

SADF test	Commanded mode	Spontaneous mode
receiving of DATA	✓ / ✓	✓ / ✓
receiving of HDR	✓ / ✓	- / -
receiving of CFG-1	✓ / ✓	- / -
receiving of CFG-2	✓ / ✓	✓ / ✓
receiving of CFG-3	✓ / ✓	✓ / ✓
sending of CMD	✓ / ✓	- / -
Legend: ✓ compliant; ✗ uncompliant; - inapplicable		

Additionally, the output of the Wireshark network protocol analyser and SADF library (in *debug mode*) are compared to identify any inconsistencies in configuration and synchro-measurement data exchange, as indicated in Table 3.2. In this way, the SADF compliance and interoperability with the IEEE Std C37.118-2005 (only communication part) and IEEE Std. C37.118.2-2011 compliant devices are confirmed.

TABLE 3.2:
Comparison between the Wireshark and SADF (debug mode) output

SADF output	Wireshark output
2019-07-17 16:50:10.381 RCV - IEEE C37.118.2 DATA	IEEE C37.118 Synchrophasor Protocol, Data Frame [correct]
Synchronization word (hex): "AA01"	Synchronization word: 0xaa01
Framesize: 98 Bytes	Framesize: 98
PMU/PDC ID number: 1	PMU/DC ID number: 1
Timestamp: 2019-07-17 14:50:10.040	SOC time stamp: Jul 17, 2019 14:50:10.000000000 UTC
Time quality flags:	Time quality flags
Time quality indicator: "Normal operation, clock locked to UTC traceable source"	.0. = Leap second direction: False
Number of PMU blocks included in the frame: 1	..0. = Leap second occurred: False
Station #1: "PMU1 "	...0 = Leap second pending: False
PMU ID number: 1 0000 = Time Quality indicator code: Normal operation, clock locked (0x0)
Quality flags:	Fraction of second (raw): 671089
Good measurement data, no errors	Measurement data, using frame number 2952 as configuration frame
Time synchronization: "locked to UTC traceable time source"	Station: "PMU1 "
Data sorting: "by timestamp"	Flags
Time quality: "not used"	0... = Data valid: Data is valid
Time source: "locked or unlocked less than 10 s"	..0. = PMU error: No error
Trigger reason: "manual"	..0. = Time synchronized: Clock is synchronized
Phasors (2)	...0 = Data sorting: By timestamp
Phasor #1: name: "PHASOR CH 1:V1 ", magnitude: 219045.2344 V, angle: -89.6764 deg 0... = Trigger detected: No trigger
Phasor #2: name: "PHASOR CH 2:I1 ", magnitude: 642.3479 A, angle: -88.5973 deg0. = Configuration changed: No
System frequency: 50.05 Hz00 = Unlocked time: Time locked, best quality (0x0)
System frequency deviation: 0.050001 Hz 0000 = Trigger reason: Manual (0x0)
Rate-of-change-of-frequency (ROCOF): 0.20335 Hz/s	Phasors (2)
Analog values (2)	Phasor #1: "PHASOR CH 1:V1 ", 219045.23V/_-89.67°
Analog #1: name: "ANALOG CH 0 ", value: 38310.4922	Phasor #2: "PHASOR CH 2:A1 ", 642.34A/_-88.59°
Analog #2: name: "ANALOG CH 1 ", value: 0	Frequency deviation from nominal: 50mHz (actual frequency: 50.050Hz)
Digitals (1)	Rate of change of frequency: 0.203Hz/s
Digital #1: name: "DIGITAL CH 0 ", status-flag: UNSET	Analog values (2)
Digital #2: name: "DIGITAL CH 1 ", status-flag: UNSET	Analog value #1: "ANALOG CH 0 ", 38310.49
Digital #3: name: "DIGITAL CH 2 ", status-flag: UNSET	Analog value #2: "ANALOG CH 1 ", 0
Digital #4: name: "DIGITAL CH 3 ", status-flag: UNSET	Digital status words (1)
Digital #5: name: "DIGITAL CH 4 ", status-flag: UNSET	Digital status word #1: 0x0000
Digital #6: name: "DIGITAL CH 5 ", status-flag: UNSET	Checksum: CACA [correct]
Digital #7: name: "DIGITAL CH 6 ", status-flag: UNSET	
Digital #8: name: "DIGITAL CH 7 ", status-flag: UNSET	
Digital #9: name: "DIGITAL CH 8 ", status-flag: UNSET	
Digital #10: name: "DIGITAL CH 9 ", status-flag: UNSET	
Digital #11: name: "DIGITAL CH 10 ", status-flag: UNSET	
Digital #12: name: "DIGITAL CH 11 ", status-flag: UNSET	
Digital #13: name: "DIGITAL CH 12 ", status-flag: UNSET	
Digital #14: name: "DIGITAL CH 13 ", status-flag: UNSET	
Digital #15: name: "DIGITAL CH 14 ", status-flag: UNSET	
Digital #16: name: "DIGITAL CH 15 ", status-flag: UNSET	
Checksum (hex): "CACA" [correct]	

3.4.3 SADF PROCESSING PERFORMANCE EVALUATION

Synchro-measurement latency in SMT supported system refers to a time delay between the PMU measurement timestamp and the instant when a PMU measurement data is available in an end-user application [73]. It depends on different intermediate factors, such as PMU synchro-measurement estimation and processing, ICT capabilities, PDC processing performance, and application data acquisition [61]. The synchro-measurement latency is a crucial factor to consider since it may affect the SMT system's ability to deliver synchro-measurements fast enough to meet the WAMPAC application requirements [73]. Since the synchro-measurement data latency is a variable system property and it depends on the used PMUs, PDCs, and supporting ICT network capabilities and utilisation, hence only the latency related to SADF is further investigated. For the purpose of the analysis, the *MATLAB* process in the Windows OS based host PC is executed in real-time priority to enable as near-real-time operation as possible.

As illustrated in Figure 3.7, the SADF latency is a sum of individual delays, introduced by *MATLAB* and SADF implemented functions to read individual message frames from *Java*-based TCP/IP or UDP buffer, parse its content, and store it into *MATLAB Workspace* for further use in user-defined applications. It is important to note that *MATLAB Instrument Control Toolbox* (version 3.11), used to establish a TCP/UDP connection with a PMU/PDC, introduces additional delay, caused by the insufficient *Java* TCP/UDP socket implementation, in particular with the update (refresh rate) of the *Java* TCP/UDP buffer. By comparing the timestamp of a received PMU message on the Ethernet socket (via *Wireshark*) and the moment the message is available in *MATLAB* for reading and parsing, the undesirable *Java* TCP/UDP socket refresh delay is estimated to be in a range of ~ 1 to 20 ms. However, this delay is not taken into account during the analysis of the SADF latency but affects the overall synchro-measurement latency in user-defined applications.

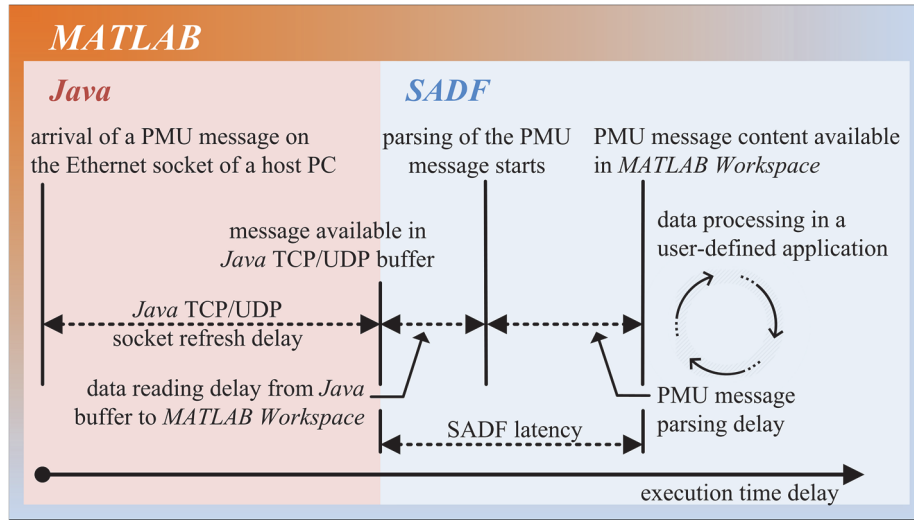


Figure 3.7: SADF associated execution delays to process a PMU/PDC message.

For the SADF latency analysis, the processing time of different PMU configuration settings has been evaluated based on [50], Annex C, Table C.1] and the most commonly used configuration scenarios. Table 3.3. presents the median processing time per *DATA*, *CFG-2*, and *CFG-3* frame of a total of 100 received messages of the same type and size.

TABLE 3.3
Performance evaluation

PMU/PDC configuration	Processing time [ms] length [bytes]		
	DATA	CFG-2	CFG-3
1 block, 2 phasors, 1 freq, 1 ROCOF, floating point	0.77 42	1.64 94	1.88 152
1 block, 2 phasors, 1 freq, 1 ROCOF, integer	0.78 30	1.62 94	1.87 152
1 block, 12 phasors, 1 freq, 1 ROCOF, integer	1.09 70	2.11 294	2.63 442
1 block, 12 phasors, 2 analog, 2 digital, 1 freq, 1 ROCOF, integer	1.12 78	2.54 854	2.88 1044
2 blocks, 24 phasors, 4 analog, 4 digital, 2 freq, 2 ROCOF, integer	1.53 140	3.51 1684	/
4 blocks, 48 phasors, 8 analog, 8 digital, 4 freq, 4 ROCOF, integer	2.41 264	5.53 3344	/
24 blocks, 48 phasors, 24 freq, 24 ROCOF, integer	3.62 640	7.29 1704	/

Based on the obtained results it can be summarised that the SADF processing time in parallel increases with the length of the messages. The message measurement format (floating point or integer) has a direct impact on frame size and practically negligible effect on the required processing time. Based on the performed evaluation, it takes 0.77 ms to process a received *DATA* frame (1 block, 2 phasors, 1 freq, 1 ROCOF, floating-point). In this case, a maximum *DATA* receiving rate that the SADF library is capable of processing is theoretically limited to ~ 1300 fps. However, the SADF library is confirmed to successfully receive 250 fps *DATA* frame rate (1 block, 12 phasors, 2 analogues, 2 digitals, 1 freq, 1 ROCOF, integer), which is the maximum data reporting rate of the GTNETx2 based PMUs. Table 3.3 presented results also include delay introduced by the data reading from *Java*-based TCP/IP or UDP buffer of *MATLAB Instrument Control Toolbox* to the *MATLAB Workspace* for SADF parsing. To illustrate, the average time to read a single *DATA* or *CFG-2/CFG-3* message from *Java*-based TCP/IP or UDP buffer to *MATLAB Workspace* takes 0.31 or 0.78 ms on average, respectively. Due to the PDCs limitations, the evaluation of the time required to process a *CFG-3* frame in case of multiple PMU blocks included in the configuration is not performed. Due to the lack of suitable open-source tools, the performance benchmarking of the proposed SADF library with the existing tools is not possible. The available open-source implementations are either specific software-dependent (*LabVIEW* for example), lack of the IEEE Std. C37.118.2-2011 support, or are primarily not designed for synchro-measurement data acquisition purposes.

Finally, the analysis of the SADF library confirms the following:

- the SADF library is compliant with the IEEE Std. C37.118.2-2011 specifications and backwards-compatible with the IEEE Std. C37.118-2005 specifications;

- the integrated fall-back procedures prevent halting the data exchange due to unexpected events or IEEE Std. C37.118.2-2011 noncompliant devices under test, resulting in SADF robust and reliable operation;
- the user-friendly *MATLAB* based SADF implementation results in acceptable execution time, making it suitable for research applications particularly. Although, implementation in *C* or similar high-performance oriented programming language would make the SADF applicable in high-demanding industrial environments.

3.4.4 EXAMPLE APPLICATION: ONLINE VOLTAGE MAGNITUDE MONITORING

The primary purpose of the proposed SADF is to enable simplified design and facilitate the extensive online validation of emerging WAMPAC applications under realistic conditions. As a proof-of-the-concept, a simple online voltage magnitude monitoring (Figure 3.8) is implemented in *MATLAB* that displays the received synchrophasors in an online fashion as soon as they are received. Herby, the visual output of the application is automatically updated every instant a new PMU measurement becomes available. This application is available as a part of the open-source SADF library to demonstrate the required procedures for the online use of synchro-measurements in user-defined WAMPAC applications.

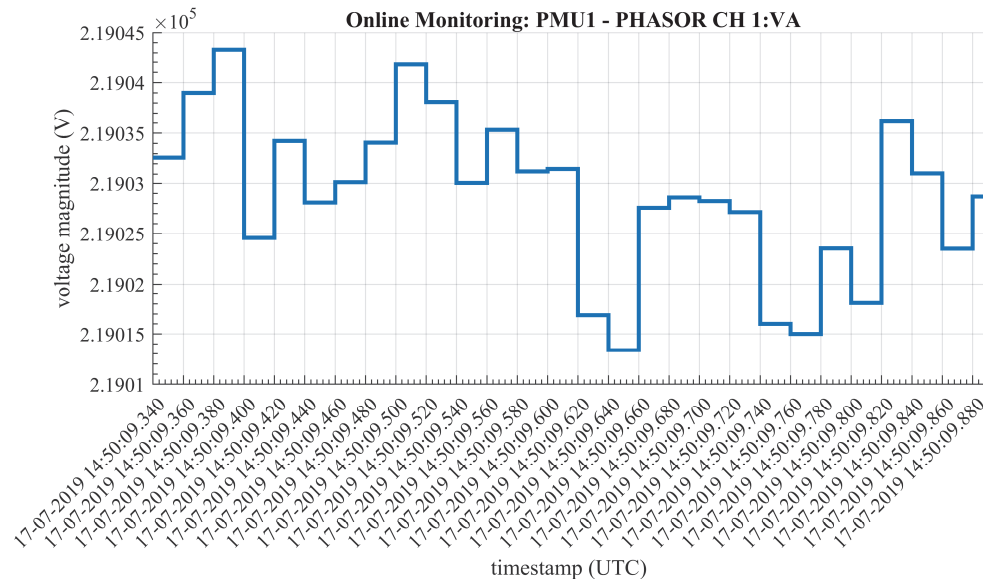


Figure 3.8: Example application: Online voltage magnitude monitoring of station PMU1, channel PHASOR CH 1:V1, with 50 fps measurement reporting rate.

3.5 CONCLUDING REMARKS

This chapter is motivated by the need for seamless and online use of actual synchro-measurements for WAMPAC application design and validation. It elaborated on the state-of-the-art tools for this purpose and briefly presented the most adopted IEEE Std. C37.118.2-2011 specifications. Despite the evident interest of the research community for SMT-supported WAMPAC applications, there existed a lack of available user-friendly tools for the application design and validation. One of its major contributions is the missing link between the IEEE Std. C37.118.2-2011 specification and its implementation. This chapter proposed the robust data receiver communication technique with integrated fall-back procedures and the efficient online receiving and parsing methodology of the encapsulated machine-readable configuration and data frames. The outcome of this work is the *MATLAB* supported SADF software library, which for the first time enabled online parsing and direct-use of IEEE Std. C37.118.2-2011 synchro-measurements in user-friendly *MATLAB* programming environment. The SADF features real-time operation and simplified use of the synchro-measurements. Combining this library with *MATLAB* signal processing and visualisation functions enabled mastering the design and online validation of closed-loop WAMPAC applications. Also, the library can be utilised as a part of a PMU/PDC metrological characterisation and IEEE Std. C37.118 compliance validation. Finally, the SADF library is available as open-source on *GitHub* (a web-based version-control and collaboration platform for software developers) repository [155].

The proposed SADF is integrated with the cyber-physical simulation testbed as SIL and utilised for the development and evaluation of online disturbance detection and online coherent generator grouping identification applications, presented in Chapter 4 and Chapter 5, respectively.

CHAPTER 4

ONLINE DISTURBANCE DETECTION

In a power system operation, situational awareness tools are indispensable elements to provide a comprehensive insight into the power system state in real-time. In this context, online disturbance detection is used to immediately detect disturbances in order to summon actions to fortify the stability and improve the reliability of the power system in time. This chapter presents an SMT supported online disturbance detection algorithm, suitable for adaptive detection of disturbances in AC and HVDC power grids. The chapter starts with an analysis of the state-of-the-art disturbance detection methods and presents the identified challenges to be addressed. Thereafter, the methodology of the proposed disturbance detection algorithm is presented. Hereby, the PMU supported data acquisition of an HVDC system is discussed, followed by a presentation of the developed algorithm for disturbance start- and end-instant identification. Finally, the chapter presents a detailed performance evaluation of the proposed algorithm under different use-cases by using Chapter 2 developed cyber-physical testbed and Chapter 3 developed SADP. The chapter concludes with a discussion on the findings.

4.1 INTRODUCTION

Adequate disturbance detection has become an essential part of power system operation and protection. It refers to the detection of voltage and current excursion caused by a wide variety of power system phenomena [156]. An important requirement for disturbance detection techniques is to provide online, fast, and reliable detection of disturbances that potentially endanger the safe operation of power systems.

4.1.1 STATE-OF-THE-ART

A significant amount of work has been done to locally detect and monitor the grid operating state by leveraging the information extracted from raw samples of signals of interest [157], [158]. The existing disturbance detection methods can be generally classified into two groups.

The first group consists of digital signal processing techniques, where the Wavelet Transform (WT) [159], [160], [161], [162] Fourier transform [163], [164] and S-transform [165], [166] based methods are dominating. However, these methods require either a high

measurement sampling rate or a long observation time interval associated with complex mathematical operations, thus making them less appropriate for real-time operation. However, WT based techniques perform well in identifying singularities in the decomposed signal components, although the precise time localisation of a transient can be ensured, the WT techniques are in general computationally costly, noise sensitive, and their performance depends on the utilised mother wavelet [167], [168], [169].

On the other hand, the statistical techniques [170], [171], [172] are often less complex and computationally more efficient. However, many of the presented methods are prone to false-trigger events due to the fixed threshold used to identify a disturbance. Hence, the remaining challenge is to dynamically tune the disturbance identification threshold based on the present system state and measurement variance.

With the advent of SMT, there was a parallel development of backup protection schemes utilising the advantages of PMU-provided measurements in AC power grids [33]. Authors in [173] make use of the characteristic ellipsoid method and a decision tree technique to monitor dynamic system behaviour, identify system events and their location. Although the results are promising, the heavy computational burden makes the algorithm not suitable for real-time operation. In [174], the authors perform principal component analysis to predict the measurement trend and detect abnormalities resulting from unexpected sudden changes. Likewise, a centralised disturbance detection scheme was recently presented, based on the grid parameter estimation technique [175]. The impact of data drop and ICT delay on disturbance detection was also discussed. However, both corresponding papers fail to detail the disturbance identification threshold value and related procedure. Also, to the best of knowledge, none of the literature available papers makes use of PMUs to deliver synchro-measurement of an HVDC power grid that can be, as presented in Section 4.2.1, utilised for disturbance detection purpose.

4.1.2 CHALLENGES AND MOTIVATIONS

An important requirement for disturbance detection techniques is to provide online, fast, and reliable detection of disturbances. This leads that a disturbance detection method should be:

- computationally efficient to enable online operation in real-time;
- capable of fast response to detect a disturbance in time;
- adaptive in means of adaptive thresholds for the reliable and robust detection of disturbances;
- applicable in AC and HVDC power grids;

The following Section 4.2 addresses these challenges and presents the developed solutions.

4.2 PROPOSED METHODOLOGY

This section develops an online SMT supported adaptive disturbance detection algorithm, suitable for the detection of excursions in voltage, current and frequency PMU measurements. The emphasis of the proposed algorithm is on fast response and low computational burden, making it suitable for online operation.

The proposed algorithm is based on a Median Absolute Deviation (MAD) sample dispersion method, which is a robust statistical measure of univariate dataset variability. The uniqueness of the algorithm is the ability to adapt to measurement variance, leading to improved robustness in case of measurement noise and small-load fluctuations. The algorithm is shown to be capable of detecting disturbances in AC and HVDC grids that are seen as sudden deviations (short-duration dips, swells, interruptions) in PMU measurements. Disturbances include but are not limited to short circuit faults, line trips and reclosing actions, and considerable loss of generation or load. Each identified disturbance is characterised with the disturbance occurrence and the disturbance clearance measurement sample.

4.2.1 DATA ACQUISITION IN AC AND HVDC

In this work, instantaneous positive sequence voltage magnitude and HVDC voltage magnitude synchro-measurements are exploited for disturbance detection of an AC and HVDC power grid, respectively. In this way, only one source of measurements (positive sequence voltage) can be used to detect single-phase and multi-phase disturbances in an AC power grid.

It is assumed that in a power system, including AC and HVDC grids, only N buses of interest are observed by a PMU device. Each PMU measurement channel $i \in \{1, 2, \dots, N\}$ reports discrete time-interval synchro-measurements of interest x with 50 fps reporting interval. With M being the total number of samples to be processed, the sample vector is defined as $X_i = [x_{i,M}, \dots, x_{i,2}, x_{i,1}] \in \mathbb{R}^M$, where $x_{i,l}$ denotes the most recent synchro-measurement (sample) of PMU measurement channel i . The observation window W , containing M -most recent samples from N buses, is presented by the following ensembled matrix:

$$W[X] = \begin{bmatrix} X_1 \\ X_2 \\ \vdots \\ X_N \end{bmatrix} = \begin{bmatrix} x_{1,M} & \cdots & x_{1,2} & x_{1,1} \\ x_{2,M} & \cdots & x_{2,2} & x_{2,1} \\ \vdots & \ddots & \vdots & \vdots \\ x_{N,M} & \cdots & x_{N,2} & x_{N,1} \end{bmatrix} \in \mathbb{R}^{N \times M} \quad (4.1)$$

In order to extend the applicability of the proposed algorithm and enable PMU supported disturbance detection in an HVDC grid, the IEEE Std. C37.118.2-2011 messages are exploited as a medium for transferring of time-synchronised HVDC measurements. For this purpose, the HVDC signals of voltage magnitude of appropriate levels are fed to the multi-functional analogue input channels of a PMU device. Hereby, the HVDC voltage

signal magnitudes are sampled and transferred as “single point-on-wave” values in user-selectable 16-bit integer or IEEE floating-point format [61]. In the case of a GTNETx2 based PMU, the sampling of an input signal is done after synchrophasor estimation (windowing), leading to a time difference between the timestamp of a synchrophasor and the analogue sampling. Hence, to compensate, it is prudent to delay the HVDC input signals (τ_{analog}) for the duration equal to the half of the synchrophasor estimation window length to account the synchrophasor group delay as [61]:

$$\tau_{analog} = \frac{N}{2Fs f_0} \quad (4.2)$$

where:

- N denotes the PMU windowing filter order;
- Fs is the PMU synchrophasor sampling rate (samples/cycle);
- f_0 is the nominal system frequency of an AC grid.

In this way, the PMU sampling of an HVDC voltage signal is time-aligned with the synchrophasor timestamp, leading that the GTNETx2 based PMU reports the AC and HVDC synchro-measurements belonging to the same measurement timestamp.

4.2.2 DISTURBANCE DETECTION ALGORITHM

MAD is utilised as a robust sample dispersion measure to locate the outlier samples of X_i sample vector [176]. MAD is similar to the well-known *standard deviation*, however, it is more appropriate (robust) for the screening of dataset outliers due to used *median* instead of *mean* statistic measure. $MAD_{i,k}$ is defined as a *median* of the absolute deviations from each $x_{i,k}$ sample and the *median* of the whole X_i sample vector, as:

$$MAD_{i,k} = \text{median}(|x_{i,k} - \text{median}(X_i)|) \quad (4.3)$$

The combination of sample median and MAD builds a robust method for screening of X_i sample vector outliers, as:

$$X_mad_{i,k} = (x_{i,k} - \text{median}(X_i)) / MAD_{i,k} \quad (4.4)$$

where $X_mad_{i,k}$ represents the MAD-denominated matrix of samples, defined as deviations of each $x_{i,k}$ sample from the median of the whole X_i sample vector, and divided by the corresponding $MAD_{i,k}$ sample value. The higher the $X_mad_{i,k}$ value, the more outlying that value is from the whole X_i sample vector. In this way, the $X_mad_{i,k}$ sample value serves to identify the corresponding $x_{i,k}$ outlier, and $X_mad_{i,k}$ sample polarity (\pm) to identify the $x_{i,k}$ outlier direction.

It is important to note that the proposed algorithm is executed sequentially for each or $X_{i,:}$ sample vector (N in total) with a moving window approach. In this way, the algorithm updates the observation window W and executes the proposed algorithm procedures each time a new PMU measurement becomes available.

The proposed online disturbance detection algorithm consists of two operational modes. The first mode is used to identify a disturbance occurrence instance. The disturbance-affected $x_{i,k}$ sample (outlier) is flagged when the corresponding $X_mad_{i,k}$ surpasses the dynamically determined threshold. This mode operates online and reports a detected disturbance “immediately” after its occurrence. As soon as the disturbance is identified, the algorithm switches into the second operation mode to identify a disturbance clearance instance. Similarly, the disturbance clearance is identified after the $X_mad_{i,k}$ samples stabilise below the dynamically determined threshold. In the case of line switching actions, and generator or load loss, it may happen that the disturbance affects the power grid permanently. To accommodate these cases, the second operation mode of the proposed algorithm is time-limited and automatically switches into the first mode after a predefined timeout. In this case, the disturbance clearance is reported for the moment after measurements reach a new stable point. Although the algorithm is executed in online fashion, the disturbance clearance moment is reported with a delay due to the algorithm’s waiting timeout for a possible disturbance clearance moment.

A. DISTURBANCE OCCURRENCE IDENTIFICATION

In the first mode, a disturbance is detected when the most recent $x_{i,M}$ sample is flagged as an outlier compared to the rest of $X_{i,:}$ vector samples. Hence, for the disturbance occurrence identification, it is prudent to take into account only the $X_mad_{i,M}$ most recent sample value of each observation window and save it into a dynamically erected $mad_r_{i,t}$ matrix for further use, where index t is used to identify the most recent instance, as:

$$mad_r_{i,t} = X_mad_{i,M} = (x_{i,M} - \text{median}(X_{i,:}))/MAD_{i,M} \quad (4.5)$$

In this way, $mad_r_{i,:}$ matrix is erected, which consists of the most recent sample $X_mad_{i,M}$ of each observation window (over time) of each monitored bus- i . In a similar way, the first (least recent) $X_mad_{i,1}$ sample is saved into a dynamically erected $mad_l_{i,t}$ vector for the further use as:

$$mad_l_{i,t} = X_mad_{i,1} = (x_{i,1} - \text{median}(X_{i,:}))/MAD_{i,1} \quad (4.6)$$

In order to determine whether the most recent window sample $x_{i,M}$ is affected by the disturbance and flagged as an outlier, an adaptive threshold is applied. The $tr_start_{i,t}$ threshold is twofold and consists of a dynamically determined cut-off value based on the *mean* value of the most recent 25 samples (half of the observation window length) of

$mad_l_{i,:}$ vector samples, multiplied by a user-determined $factor$ parameter to control the algorithm's resistance to measurement variance in case of noise and small load fluctuations (4.7). The $tr_start_{i,t}$ threshold value is dynamically determined for each observation channel i separately. Moreover, the $tr_start_{i,t}$ threshold is lower-bounded with the user-determined $limit$ parameter in order to control the algorithm's sensitivity to a disturbance, as:

$$tr_start_{i,t} = \max \left\{ \begin{array}{l} (mean|mad_l_{i,t-M} \dots mad_l_{i,t-(M/2)}|) factor \\ limit \end{array} \right\} \quad (4.7)$$

Based on the performed simulations, the $factor$ value of 15 and $limit$ value of 15 work generally well for suppressing the undesired disturbance identification in case of measurement noise and small load fluctuations, respectively. Notably, these parameters should be user-adjusted in case of severe sample variance under normal operating conditions.

When the following condition is satisfied, a disturbance is identified and $D_start_{i,t}$ disturbance detection start trigger is set:

$$D_start_{i,t} = \begin{cases} 1, & |mad_r_{i,t-1} - mad_r_{i,t}| \geq tr_start_{i,t} \vee |mad_r_{i,t}| \geq tr_start_{i,t} \\ 0, & else \end{cases} \quad (4.8)$$

As seen from (4.8), the most recent $mad_r_{i,t}$ sample value is compared to $tr_start_{i,t}$, which is determined by using the past $mad_l_{i,:}$ sample values. Hereby, the algorithm detects a disturbance when the difference between the two most recent $mad_r_{i,:}$ samples surpasses the dynamically defined $tr_start_{i,t}$ threshold value, or when the $mad_r_{i,t}$ most recent sample value surpasses the $tr_start_{i,t}$ threshold. In this way, the algorithm detects a disturbance that is observed as severe amplitude jumps and also amplitude differences between the two most recent measurements compared to the variance of remaining dataset measurements. After a disturbance on bus- i is identified (4.8) and reported, the proposed algorithm switches to the second operation mode in order to start with the disturbance clearance identification procedure of corresponding bus- i only.

B. DISTURBANCE CLEARANCE IDENTIFICATION

Disturbance clearance identification can be seen as a mirrored procedure of the disturbance occurrence identification. In a similar way, a disturbance clearance moment is identified as soon as the $mad_l_{i,:}$ vector samples fall below $tr_end_{i,t}$ dynamically determined threshold as:

$$tr_end_{i,t} = \max \left\{ \begin{array}{l} (mean|mad_r_{i,t-(M/2)} \dots mad_r_{i,t}|) factor \\ limit \end{array} \right\} \quad (4.9)$$

where $limit$ and $factor$ parameters are the same as in the case of (4.7). If the following condition is satisfied the $D_end_{i,t}$ disturbance detection end trigger is set:

$$D_{end_{i,t}} = \begin{cases} 1, & |mad_{l_{i,t}-1} - mad_{l_{i,t}}| \geq tr_{end_{i,t}} \vee |mad_{l_{i,t}}| \geq tr_{end_{i,t}} \\ 0, & else \end{cases} \quad (4.10)$$

Notably, the proposed algorithm searches for the disturbance clearance instant for a time period of 5 window lengths from the instant it switched to the second mode. Afterwards, the algorithm reports the identified disturbance end measurement sample and switches back to the first mode in order to restart with the disturbance detection identification procedure of corresponding channel i .

4.2.3 PSEUDOCODE OF THE PROPOSED METHODOLOGY

The following Pseudocode 4.1 drafts the proposed disturbance detection algorithm procedure. The *MATLAB* implementation of the proposed algorithm is available on the *GitHub* open-source repository [177].

PSEUDOCODE 4.1

Online disturbance detection

```

1: ## initialisation
2: t = 1; //initialise window index
3: D_start_holdi = false; //clear disturbance flag
4: populate W; //populate the window with 50 recent measurements (4.1)
5: ## online processing
6: while 1
7:   for i = 1...N //sequential processing for each monitored channel i
8:     madri,t; //determine (4.5)
9:     madli,t; //determine (4.6)
10:    if t > M //collect enough data for determination of (4.7),(4.9)
11:      ## disturbance start scan - Mode 1
12:      tr_starti,t; //determine threshold (4.7)
13:      if D_starti,t == 1  $\wedge$  D_start_holdi,t == false //check for disturbance occurrence (4.8)
14:        ## ALERT, disturbance detected
15:        D_start_holdi = true; //set disturbance flag
16:        D_start_windowi = t; //disturbance window index
17:        return D_start_samplei = xi,M; //report disturbance start sample
18:      elseif D_start_holdi == true //disturbance detected?
19:        ## disturbance end scan - Mode 2
20:        tr_endi,t; //determine threshold (4.9)
21:        if D_endi,t == 1  $\wedge$  t < D_start_windowi + 5 M //scanning for 5 window lengths (4.10)
22:          D_end_samplei = xi,M; //disturbance end sample
23:        else //disturbance end scan finished
24:          ## ALERT, disturbance cleared
25:          return D_end_samplei; //report disturbance end sample
26:          D_start_holdi = false; //clear disturbance flag
27:        end
28:      end
29:    end
30:  end
31:  t = t + 1; //increase window index
32:  update W; //update with 1 next recent measurement and shift by 1 (4.1)
33: end

```

4.3 SIMULATION STUDIES

This section presents the validation results of the proposed disturbance detection algorithm under different scenarios. First, the section presents the simulation testbed and the power system model used for this purpose. Furthermore, it elaborates on the measurement latency and on the observation window length. Second, it presents the results of the analysis under different simulated use-cases and elaborates on the findings. Finally, the results of benchmarking with existing techniques are presented.

4.3.1 SIMULATION TESTBED

In order to demonstrate the performance capabilities of the proposed disturbance detection algorithm, Chapter 2 presented cyber-physical simulation testbed is used and adjusted for the simulation requirements of this chapter.

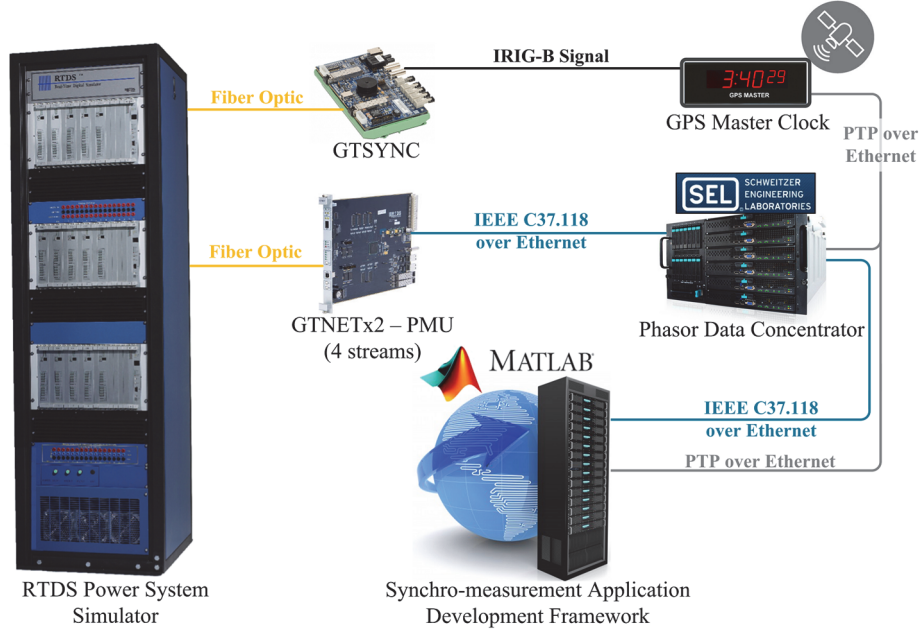


Figure 4.1: Real-time testbed with online disturbance detection algorithm implemented as software-in-the-loop.

For the simulation of power system phenomena, a four-terminal MMC technology-based HVDC and AC power system model, as illustrated in Figure 4.2, is designed. The 50 Hz nominal system frequency model contains 201-level MMC converters of Type-4 with the setpoints listed in Table 3.1. The model contains a circulating current suppression controller to contract voltage imbalance issues in sub-modules of each arm. The voltage level of the HVDC network is controlled to operate at ± 200 kV, while the winding ratios of interface transformers Tr1/Tr2 and Tr3/Tr4 are 220/380 kV and 220/145 kV, respectively.

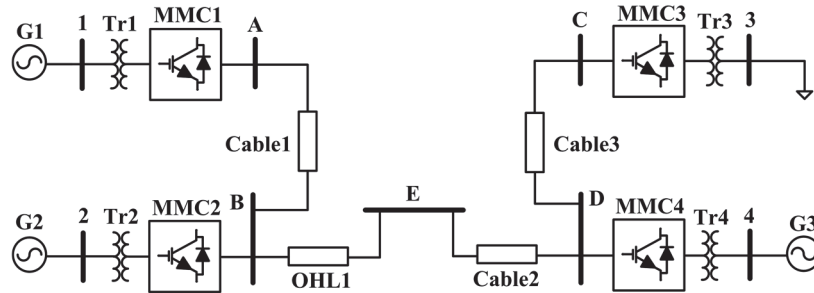


Figure 4.2: Four-terminal MMC AC and HVDC power system model.

TABLE 4.1
System control mode and setpoints

AC system		HVDC system	
Bus	RMS voltage	Converter	Control mode and setting points
1	380 kV	MMC1	$P/V_{dc}; P_{ref} = 400 \text{ MW}, V_{dc_ref} = \pm 200 \text{ kV}, \text{droop} = 0.2$
			$Q; Q_{ref} = 0 \text{ MVAR}$
2		MMC2	$P/V_{dc}; P_{ref} = -800 \text{ MW}, V_{dc_ref} = \pm 200 \text{ kV}, \text{droop} = 0.2$
			$Q; Q_{ref} = 0 \text{ MVAR}$
3	145 kV	MMC3	Island mode; $V_{ac_ref} = 145 \text{ kV}$, frequency = 50 Hz
4		MMC4	$P; P_{ref} = 500 \text{ MW}$
			$Q; Q_{ref} = 0 \text{ MVAR}$

To provide observability of the RTDS simulated power system model, a GTNETx2 based PMUs of class P with 50 *fps* reporting rate are used. The four PMUs in total are installed on the AC side of the MMCs (bus-1 to bus-4 in Figure 4.2) and interconnected with the voltage signals from HVDC side (bus-A to bus-D in Figure 4.2) in order to deliver AC and HVDC synchro-measurements, respectively. The SEL-5073 PDC is used to time-align the synchro-measurements, sent further to the computer running SADF, where the proposed disturbance detection algorithm is executed in an online fashion. All the testbed components are precisely time-synchronised to the GE RT430 grandmaster clock. For this, IRIG-B is used to time synchronise the RTDS running the simulation, and PTP for time synchronisation of the PDC and SADF. In order to determine the time instant of a disturbance (fault) occurrence and its disturbance detection using the proposed algorithm, two analogue input channels of the PMU installed on bus-1 are used to deliver timestamps (in Unix format) of the actual occurrence and clearance of a fault for precise determination of the disturbance detection delay associated with the specific use case. Finally, the proposed algorithm is implemented in *MATLAB* by using Chapter 3 developed SADF and integrated with the testbed, as illustrated in Figure 4.1.

4.3.2 MEASUREMENT LATENCY EVALUATION

Measurement latency is an unavoidable and adverse property of every SMT supported power system. It is the sum of the delays caused by the PMU synchro-measurement processing, telecommunication, PDC time-aligning and application data acquisition. Since measurement latency can significantly affect the performance of the SMT supported WAMPAC applications, in particular closed-loop control and protection, it is a crucial aspect to consider. To evaluate the measurement latency which directly affects the disturbance detection latency of the proposed algorithm, the individual contributions to the total latency needs to be assessed. In case of the used testbed, the τ_{total} total measurement latency corresponds to the sum of the delays imposed by the:

$$\tau_{total} = \tau_{PMU} + \tau_{PMU-PDC} + \tau_{PDC} + \tau_{PDC-SADF} + \tau_{SADF(Java)} + \tau_{SADF(parse)} \quad (4.11)$$

where:

- τ_{PMU} is PMU windowing and processing delay (the time difference between the timestamp of a PMU message and the instant the message is seen the Ethernet interface);
- $\tau_{PMU-PDC}$ is ICT delay between PMU and PDC;
- τ_{PDC} is PDC processing delay;
- $\tau_{PDC-SADF}$ is ICT delay between PDC and SADF;
- $\tau_{SADF(Java)}$ is the response time of *Java* I/O - TCP/IP socket implementation (*MATLAB* Instrument Control Toolbox version 3.11);
- $\tau_{SADF(parse)}$ is SADF parsing time of IEEE Std. C37.118.2-2011 messages.

To evaluate the delays of the individual testbed components, the following software tools are used: the PDC build-in delay monitor, *Ping*, *Wireshark*, and *MATLAB* profiling. Table 4.2 lists the obtained approximate time delays of the testbed components.

TABLE 4.2
Testbed delays

Delay source	Time range [ms]
τ_{PMU}	~ 21
$\tau_{PMU-PDC}$	~ 0.4
τ_{PDC}	~ 0.6
$\tau_{PDC-SADF}$	~ 0.4
$\tau_{SADF(Java)}$	between ~ 1 and less than 20
$\tau_{SADF(parse)}$	~ 0.7 per PMU block

It is important to note that the time delay between a disturbance occurrence and its detection by the proposed algorithm differs compared to τ_{total} . The time delay is mainly affected by the instant of a disturbance occurrence with respect to the PMU windowing and measurement reporting (further discussed in the next Section 4.4.3 - A) as well as the SADF related *Java* update rate of the TCP/IP socket implementation.

4.3.3 OBSERVATION WINDOW LENGTH

When designing a measurement supported application, an observation window length is a crucial factor to consider. An increase in an observation window length typically leads to a proportional increase in the processing power required, which at some point limits the application's ability to process the measurements fast enough for online and real-time operation. However, the observation window length of a specific application is typically

application dependent and requires a thorough assessment in order to assure a sufficient level of power system observability for adequate application's performance.

Nevertheless, based on numerous preformed simulations (not part of this thesis) it can be concluded that the sensitivity of the proposed disturbance detection algorithm to slow magnitude changes (due to low-frequency oscillations for example) increases with the increasing observation window length. However, when sufficient observability in means of window length is provided (10 to 20 s of measurements), the algorithm becomes resilient to significant magnitude changes due to low-frequency oscillations. While on the other hand, the shorter observation window makes the proposed algorithm more sensitive to relatively small and temporal amplitude changes in the measurements.

Assuming an application of backup protection, where a severe disturbance should be detected as quickly as possible in order to perform a remediate action, the length of an observation window W (4.1) of the proposed algorithm is limited to $M = 50$, which is equal to one second of PMU synchro-measurements with 50 f_{ps} reporting rate. The proposed disturbance detection algorithm is operated in online fashion; being executed every instant (approximately every 20 ms) the observation window W is updated with the new set of synchro-measurements belonging to the most recent PMU measurement interval.

4.3.4 STUDY CASES AND SIMULATION RESULTS

The proposed algorithm is validated on voltage sag disturbances caused by different faults and a generator trip. In case of AC grid faults, a self-cleared three-phase line-to-ground (3-LG) and a single line-to-ground (1-LG) short circuit faults on bus-1 and bus-3 are performed, while in case of HVDC faults a pole-to-pole (PP) and pole-to-ground (PG) short circuit faults on bus-B and bus-D are performed. Each of the fault cases contains an additional three scenarios with varying short circuit resistance R_f and clearing fault times. Table 4.3 summarises the preformed cases and related scenarios. As presented in Table 4.3, the disturbance is successfully detected on the faulted bus in all the cases.

TABLE 4.3
Study cases

Grid	Scenario Case	1: $R_f = 0.001 \Omega$			2: $R_f = 10 \Omega$			3: $R_f = 100 \Omega$		
		fault duration [ms]			fault duration [ms]			fault duration [ms]		
		1	80	200	1	80	200	1	80	200
AC	A: 3-LG@bus-1	✓	✓	✓	✓	✓	✓	✓	✓	✓
	B: 1-LG@bus-3	✓	✓	✓	✓	✓	✓	✓	✓	✓
HVDC	C: PG@bus-B	✓	✓	✓	✓	✓	✓	✓	✓	✓
	D: PP@bus-D	✓	✓	✓	✓	✓	✓	✓	✓	✓

For the purpose of analysis and demonstration, only the following most distinguished use cases are studied in detail.

A. CASE A, SCENARIO 1

Figure 4.3 and Figure 4.4 present the disturbance on AC and HVDC power grid, respectively, initiated by a 3-LG fault with 0.001Ω resistance on bus-1, and self-cleared after 80 ms . The fault occurrence and clearance time are indicated with the red and black stem respectively. The blue line represents the voltage magnitude, while the black line represents the combined $mad_{r_{i,t}}$ and $mad_{t_{i,t}}$ before and after disturbance, respectively. Similarly, the red line represents the combined $tr_{start_{i,t}}$ and $tr_{end_{i,t}}$ threshold, before and after disturbance, respectively. The measurement sample at which the proposed algorithm identifies the disturbance is marked with the green stem, while the disturbance clearance measurement sample is marked with the orange stem. The instant when the disturbance is detected is marked with the blue stem. For the sake of simplified interpretation, the actual PMU measurement timestamp ('HH:MM:SS.FFF dd.mm.yyyy' format) has been modified into simulation time, starting with 0 ms for the 6th measurement sample before the disturbance identification (green stem).

The disturbance imposed by the single-phase line-to-ground fault on bus-1 is successfully detected on all monitored buses. The disturbance is first detected on bus-1 with a 21.75 ms delay, caused by data acquisition and processing. On the other buses, the disturbance occurrence instant is detected with 53.76 ms delay due to disturbance propagation and the way it affected the PMU sampling (windowing) with respect to measurement reporting. The disturbance clearance instant (orange stem) for each bus i is identified as soon as the $mad_{l_{i,:}}$ vector samples fall below $tr_{end_{i,t}}$ dynamically determined threshold (10).

Due to the nature of PMU sampling, windowing, and measurement timestamping, the disturbance-affected PMU measurement sample (green stem in Figure 4.3 - top) seems to report the disturbance, caused by the fault before the fault actually occurred (red stem in Figure 4.3 - top). This has practical merits since the PMUs estimate synchrophasors with a 2-cycle window length, with a measurement timestamp corresponding to the time of an observation window centre. Therefore, when the fault-affected waveform samples are present in the second half of the PMU synchrophasor estimation window, they also affect the corresponding resulting synchrophasor measurement with the measurement timestamp before the fault actually occurred. For an illustration of this effect, Figure 4.5 graphically presents the situation, when the PMU reports the disturbance affected measurements with the timestamp before disturbance actually occurred.

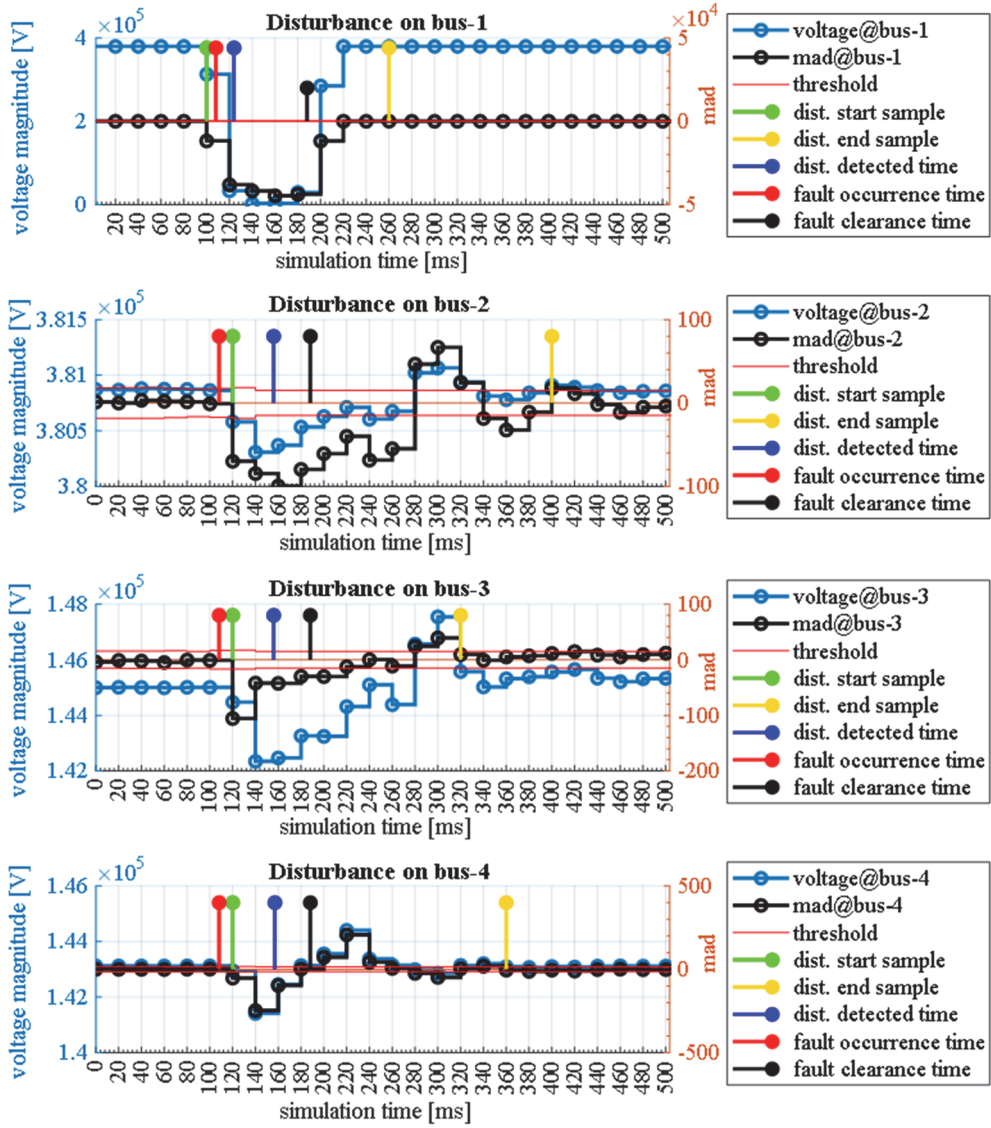


Figure 4.3: A three-phase line-to-ground fault on bus-1 and self-cleared after 80 ms, observed as a disturbance on the AC busses.

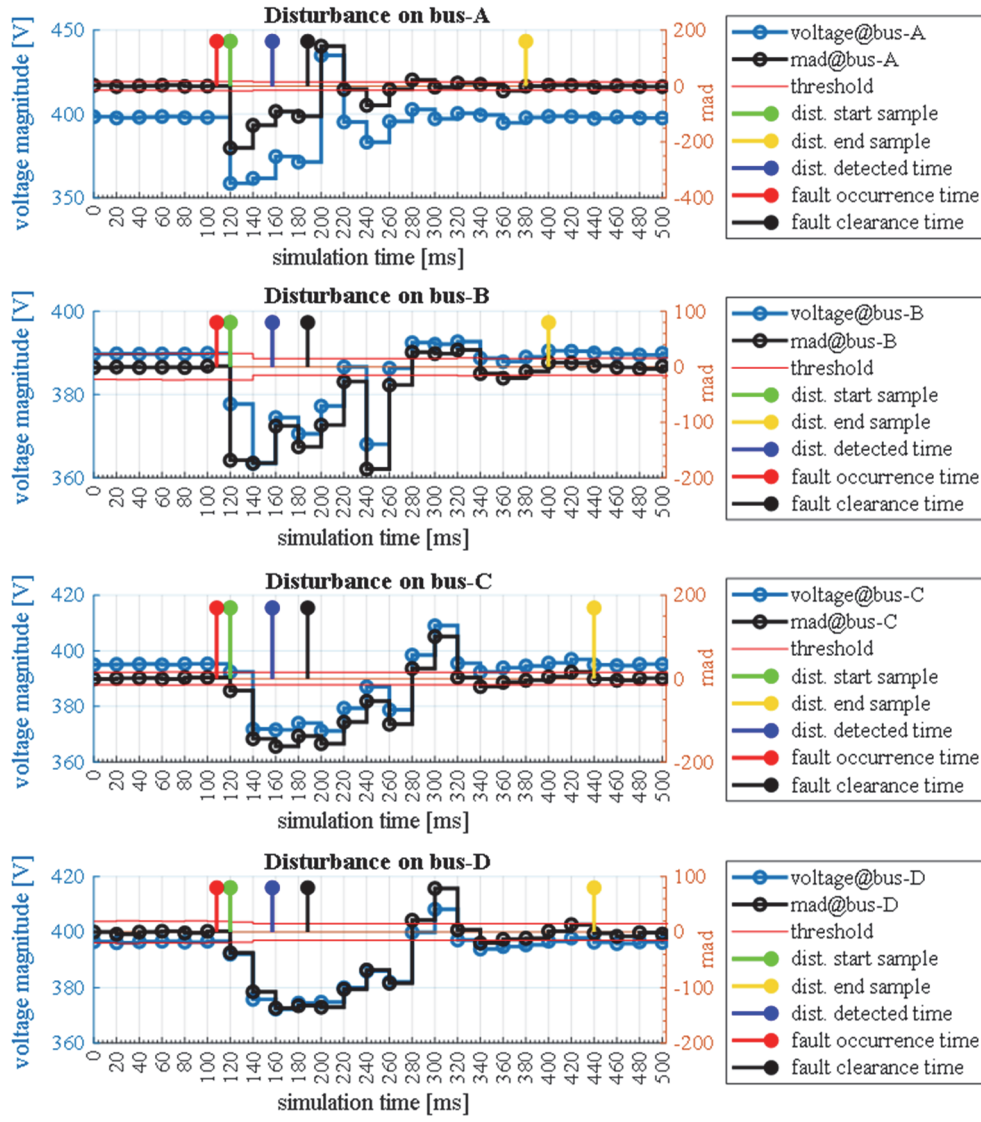


Figure 4.4: A three-phase line-to-ground fault on bus-1 and self-cleared after 80 ms, observed as a disturbance on the HVDC busses.

As seen in Figure 4.5, the two-cycle PMU observation windows, used to estimate the corresponding synchrophasors with the measurement timestamp equal to the observation window centre, includes samples of a waveform signal of interest. *PMU window 0* and *PMU window 1* includes only the samples, belonging to the pre-disturbance, while *PMU window 4* and *PMU window 5* include only the post-disturbance waveform samples. Notably, *PMU window 2* includes samples, belonging to the pre- and post-disturbance (mind the orange coloured area). As seen from the figure, only the last part of the second half of the observation window is affected by the disturbance. Hence, the waveform samples belonging to the disturbance affect the corresponding synchrophasor with the measurement timestamp equal to the observation window centre. This leads that a PMU reports a disturbance affected synchrophasor with the T_2 measurement timestamp before the disturbance actually occurred. A similar effect can also be seen in Figure 4.3 - top (mind the green and red steam). In the case of HVDC in Figure 4.4 - top, this effect is not observed, since the PMU HVDC input signals are delayed in order to time-align their sampling with the measurement timestamp. This leads that the PMU reported HVDC voltage measurement for this particular case is not affected by the disturbance, which is an expected outcome.

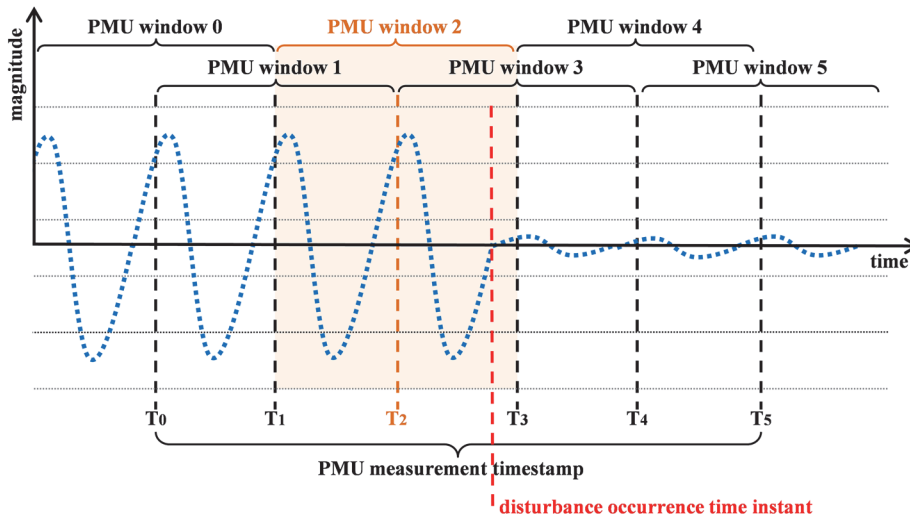


Figure 4.5: Waveform samples (blue) of pre- and post-disturbance, which affect the synchrophasor belonging to the PMU observation window 2 (orange). This leads that the PMU reports the disturbance affected measurement with a timestamp belonging to the time before the disturbance actually occurs (mind red and orange stem).

B. CASE B, SCENARIO 3

Figure 4.6 presents a 1-LG fault with $100\ \Omega$ resistance, initiated on bus-3 and self-cleared after $200\ ms$. The disturbance is identified (blue stem) on bus-3 with $12.26\ ms$ delay after the fault occurrence (red stem). On bus-C the disturbance is identified during the next measurement interval.

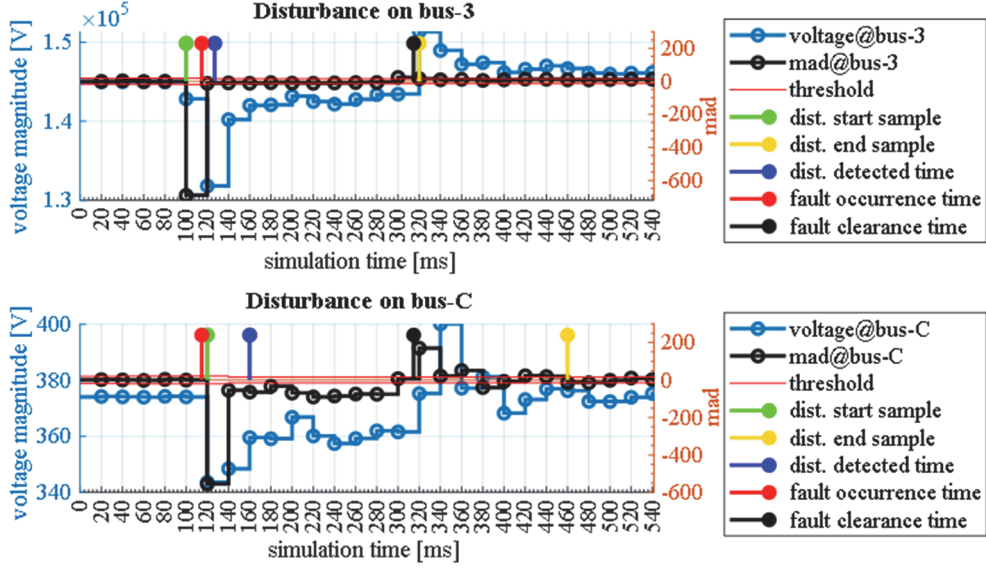


Figure 4.6: A single-phase line-to-ground fault, initiated on bus-3 and self-cleared after $200\ ms$.

C. CASE C, SCENARIO 1

Figure 4.7 presents a PG fault with $0.001\ \Omega$ resistance initiated on bus-B and self-cleared after $1\ ms$. The disturbance caused by the fault is detected (blue stem) $27.21\ ms$ after the fault occurrence (red stem) by the PMUs on bus-2 and bus-B. As illustrated in Figure 4.7, the dynamic threshold (8) to detect the disturbance start sample (9) has automatically adjusted to the past system conditions (7). Similarly, the dynamic threshold (10) to detect disturbance end sample (11) has automatically adjusted to the most recent system conditions (6), characterised by the measurement data variance.

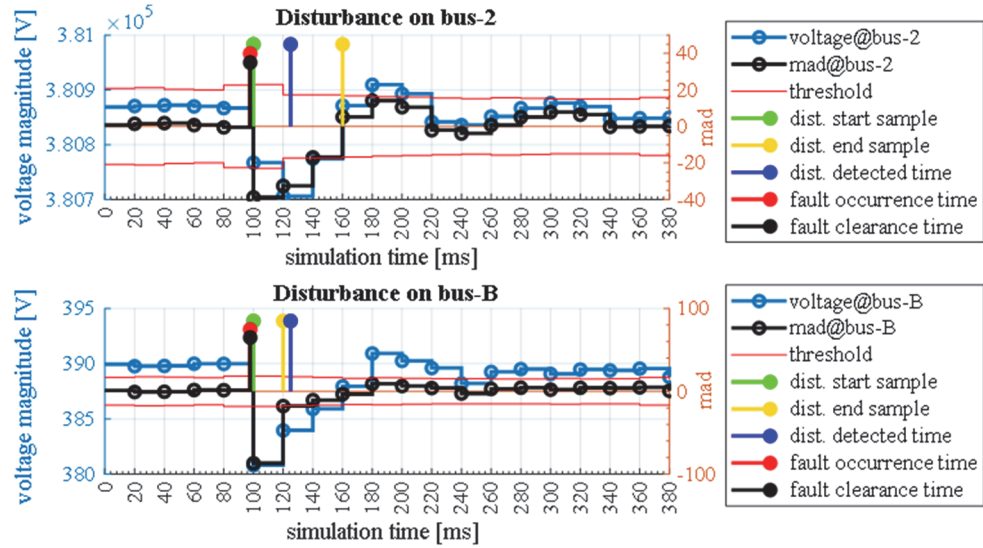


Figure 4.7: A pole-to-ground fault on bus-B and self-cleared after 1 ms.

D. GENERATION LOSS

The next simulation case shows the detection of disturbance caused by the permanent disconnection of the 500 MW generator machine installed at bus-4. The disturbance, caused by the opening of the circuit breaker, installed between bus-4 and Tr4, is presented in Figure 4.8. The disturbance end sample is identified when the measurement samples stabilised below the dynamically defined threshold.

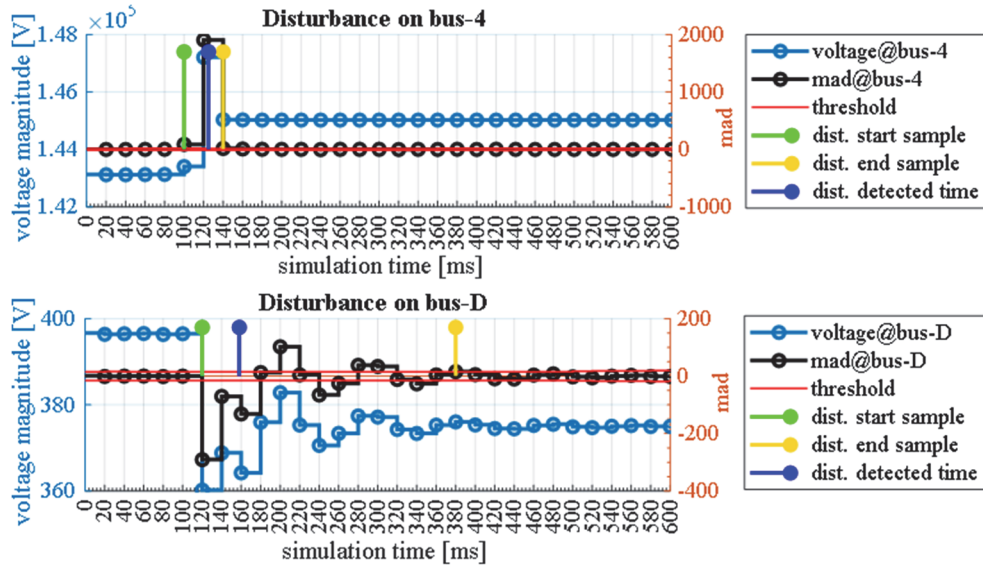


Figure 4.8: A disturbance caused by the permanent trip of a generator, connected to bus-4.

4.3.5 COMPARISON WITH THE EXISTING TECHNIQUES

The performance of the proposed algorithm is compared with the most commonly used WT techniques for disturbance identification. For this, Discrete Wavelet Transform (DWT) and Stationary Wavelet Transform (SWT) methods with the *Haar* mother wavelet are implemented using SADP. Hereby, only the execution time to determine (6) and (7) of the proposed method and first level signal decomposition of SWT and DWT is compared. Figure 4.9 presents the disturbance, initiated by a self-cleared (80 ms) 3-phase to ground fault on bus-1. The figure presents the response of the above methods on the disturbance. In the case of DWT, the detail coefficients are down-sampled by the factor of two compared to the original signal. This has practical merits due to the time-invariant properties of DWT, which should be taken into account. However, this effect is not present in the case of SWT due to the zero-padding of high-pass filter coefficients.

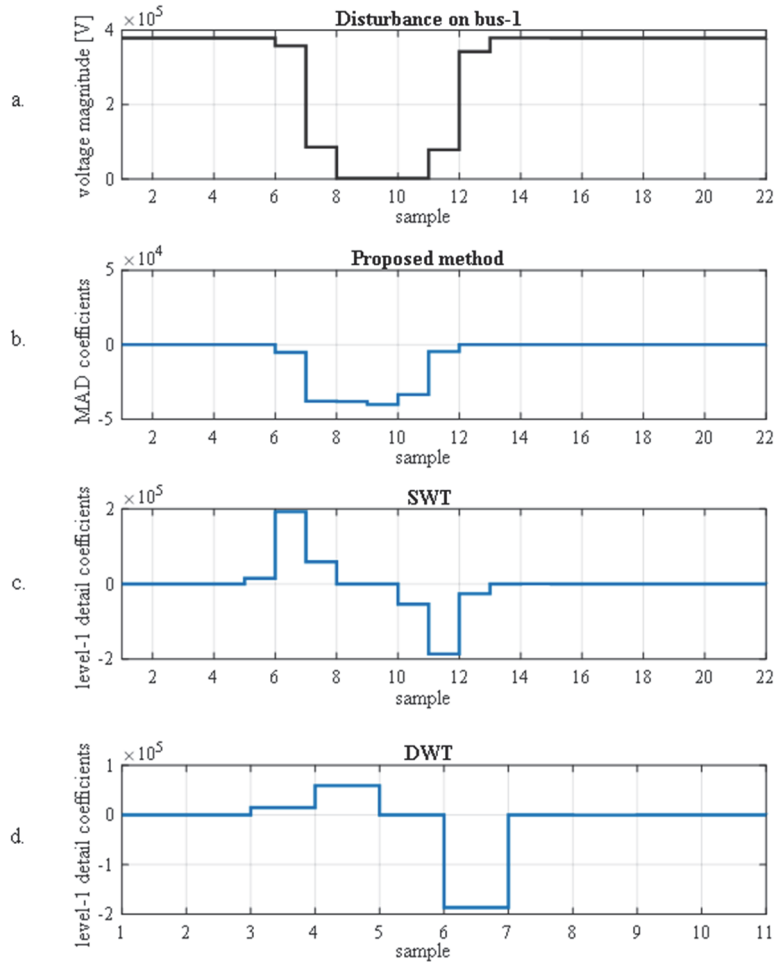


Figure 4.9: Comparison of the proposed (b.), SWT (c.) and DWT (d.) methods on a voltage sag disturbance (a).

Moreover, the median execution time of each method to process an observation window (vector) containing 50 samples is presented in Table 4.3.

TABLE 4.3
Execution time

Method	Median execution time [ms]
<i>MAD</i>	0.02
<i>SWT</i>	0.50
<i>DWT</i>	0.35

As seen from Figure 4.9, the MAD coefficients are more closely related to the shape of the disturbance, compared to SWT and DWT. In the case of SWT, a small transition can be observed at $t = 5\text{ s}$, which has no direct connection to the raw measurements and can be seen as a side effect (anomaly) of SWT processing of the abrupt transition that follows. Based on the obtained results of the analysis, the proposed method outperforms SWT and DWT in execution speed for the factor of 25 and 17.5, respectively. This is a significant improvement compared to the SWT and DWT, which comes to light when there is a need to process a high number of measurement channels.

4.4 DISCUSSION OF THE RESULTS

The above-presented results demonstrate the effectiveness of the proposed algorithm for the disturbance detection caused by the variety of short circuit faults, the generation disconnection, and the line trip. Based on the simulations performed on a desktop computer, the disturbance detection algorithm outperforms the WT based techniques in terms of execution time. This is an important property in case of a large number of monitored buses. Similar to WT-based techniques, the proposed method can be used for disturbance polarity detection, which is often used as a pre-step of protection schemes. As demonstrated, PMUs can be successfully utilised for the delivery of time-synchronised HVDC grid measurements. It is important to note that latency between the disturbance occurrence and its detection varies with respect to the fault occurrence moment (relative to the centre of PMU observation window), PMU synchrophasor estimation algorithm (its window length and complexity), measurement reporting rate, ICT data transmission latencies, and delays introduced by PDC and SADF data processing. Particularly, the τ_{Java} delay, introduced by *MATLAB (Java)*, could be minimised/omitted when the parsing of IEEE Std. C37.118 measurements and proposed algorithm are implemented in *C* or similar high-performance programming language.

Based on the performed simulations and analysis, the developed algorithm features execution speed improvement compared to SWT and DWT for the factor of 25 and 17.5, respectively. It takes 0.02 ms to process the observation window of 100 measurement points, making the algorithm suitable for the processing of multiple PMU data streams

simultaneously. Simulations confirmed that the algorithm is capable of detecting 1-LG and 3-LG faults in AC grid, and PP and PG faults in HVDC grid, including a high-resistance 100 Ohm fault with 1 ms duration;

It is important to note that latency between the disturbance occurrence and its detection varied with respect to the fault occurrence moment (relative to the centre of PMU observation window), PMU synchrophasor estimation algorithm (measurement delay), measurement reporting rate, ICT data transmission latencies, and delays introduced by PDC and SADF data processing. Notably, the *Java* delay introduced by *MATLAB* could be minimised/omitted when the parsing of IEEE Std. C37.118 measurements and proposed algorithm are implemented in *C* or similar high-performance programming language.

4.5 CONCLUDING REMARKS

This chapter proposed the computationally efficient and robust algorithm for an SMT supported online disturbance detection. The algorithm is shown to be suitable for the detection of magnitude excursions in PMU bus voltage measurements of AC and HVDC grids, caused by a wide variety of faults in AC and HVDC, including a high resistance fault with 1 ms duration. However, the algorithm can also be used to detect excursions in other signals, such as PMU current and frequency measurements. Although the PMUs are primarily designed for AC grid applications, the practical simulations confirmed their applicability to deliver voltage and current measurements of HVDC grids. The performed simulations confirmed that the proposed algorithm can identify a measurement sample belonging to the occurrence and the clearance of a disturbance. Moreover, the adaptive threshold, driven by the measurement variance, makes the algorithm robust to load fluctuations and noise. Considering the modern small fibre-optic telecommunication latencies, the proposed algorithm has practical merits in advanced backup protection schemes, when primary protection fails to operate, or as a standalone situational awareness application.

In this work, bad data detection on PMU measurements was not performed, despite that it can lead to false identification of the proposed algorithm. Further research is needed to preform bad data detection and removal while keeping in mind that this leads to unavoidable delays related to pre-processing of measurements. The proposed disturbance detection algorithm can be adopted for the purpose of outlier detection, to preform bad data cleaning on received PMU data before being used for the disturbance detection purpose. Furthermore, the observation window length was determined based on preformed simulations with a goal to detect voltage sag disturbances, caused by the use-cases, reliably. However, the observation window length of the proposed algorithm is dependent on the intended use and should be user-adjusted to detect desired changes in magnitude measurements.

CHAPTER 5

ONLINE IDENTIFICATION OF SLOW COHERENT GENERATORS

In a power system, slow coherency can be applied to identify groups of the generating units, the rotors of which are swinging together against each other at approximately the same oscillatory frequencies of inter-area modes. This information serves as a prerequisite-step of several emergency control schemes to identify power system control areas and improve transient stability. This chapter presents a novel SMT supported algorithm for an online and near real-time tracking of grouping changes of the slow coherent generators in a power system. In the first part, the chapter elaborates on state-of-the-art methods and identifies the remaining challenges. In the second part, the chapter elaborates on the challenges and presents the developed solutions, compound into a novel algorithm. Finally, the chapter presents a detailed performance evaluation of the proposed algorithm and comparison with the benchmark method under different use-cases. For this, Chapter 2 developed cyber-physical testbed and Chapter 3 developed SADF are used. The chapter concludes with a discussion on the findings.

5.1 INTRODUCTION

Typically, in a large-scale interconnected power system, interarea oscillations may occur due to the electromechanical interactions between the synchronous generators. These inherited phenomena are unique to every power system and cause fluctuations in system frequency, bus voltages, tie-lines (long transmission lines) power flows, hardware damage, and financial loss [178]. However, if not minor in magnitude or damped, these inter-area oscillations can lead to stability issues, leading to the power grid separation and in the worst case to widespread outages during large power grid utilisations [179].

Moreover, the inter-area oscillations associated with groups of generators or power plants are termed inter-area modes, which usually excite between large generation and load centres that are typically weakly connected via tie-lines [179]. The inter-area modes include groups of slow coherent generators swinging against each other [180].

The slow coherent generator groups, i.e., generators swinging together at oscillatory frequencies of inter-area modes (0.1 to 0.8 Hz), have a relatively strong electromechanical

coupling [180], [181], [182]. This phenomenon is adopted in emergency control applications to identify control areas and improve the transient stability of the power system. For example, the generator slow coherency is often a required constraint in the case of an ICI [112], [113], [182] and wide-area oscillation damping [183]. Besides, slow coherency information is used for dynamic equivalencing and aggregation, in particular, to reduce the size and complexity of a power system model under investigation [181], [184].

Moreover, the slow coherent generators have a high tendency to operate synchronously, even after being exposed to the severe network perturbation following a disturbance such as a fault [181]. Nevertheless, the generators may change their coherent groups as a response to the modified system state following a significant disturbance such as topology change, generator trip, or large load step [113]. Moreover, as suggested in [185], the power system continuously evolves (mind the energy transition), leading that the frequency and damping of existing inter-area oscillations may change or even excite new ones. Therefore, the ability to online track the slow coherent behaviour of synchronous generators of a disturbed interconnected power system in real-time is a relevant challenge. This chapter overcomes the challenge by proposing a novel online algorithm, suitable for near real-time tracking of grouping changes of slow coherent generators during quasi-steady-state and the electromechanical transient period following a disturbance.

5.1.1 STATE-OF-THE-ART

A significant amount of work has been done in the research community to identify coherent generators. *Singh et al.* discuss the commonly used coherency methods for aggregation of generators [186]. These methods firstly assess generator coupling indices being further used for the clustering of coherent generators into groups.

The classical approach to identify the groups of slow coherent generators belongs to model-based methods [112], [181]. Typically, these methods perform the eigensubspace analysis of a linearized power system model to determine the electromechanical modes and their mode shapes of each generator [181]. The resulting analysis is valid only for a particular equilibrium point and suffers from the modelling inaccuracies and parametric uncertainties. While being able to provide valuable information about the general dynamic structure of the power system, the slow coherency theory does not consider the transient system dynamics. However, during the power system contingency operation, the swings of generators with respect to each other are influenced not only by the structure of the system but also by the type and location of the disturbance, generator internal electrical dynamics, controller's response, and other system nonlinearities [185], [187]. Any significant change in the power system operating state, such as a topology change, large load step, or generator trip, might cause the weakly slow coherent generators to change their grouping association [188]. This makes the model-based methods not suitable for online use in actual power systems [189]. Therefore, the ability to track the slow coherent behaviour of generators in a profoundly disturbed power network in real-time is a relevant problem that cannot be directly solved by the model-based methods.

In order to overcome the above-mentioned deficiencies, measurement-based methods have been developed. Their main advantage is the inherent ability to adapt, and online identify the grouping changes of slow coherent generators following a contingency, as well as in independence from the system parameter data. Those methods can be coarsely sub-classified into mode estimation analysis and time-series similarity-based techniques.

The methods belonging to the first sub-class estimate the system modes or frequency spectrum and partition the coherent generators into groups by using k-means, fuzzy and agglomerative hierarchical clustering algorithm [190], [191], [192], [193], [194]. While being able to extract information about the inter-area oscillations, these techniques often suffer from the mode estimation related inaccuracies, and high processing power required to process the relatively long observation window. Therefore, mode estimation methods are most suitable for offline analysis.

On the other hand, the time-series similarity-based methods identify generator coherency based on the similarities of the extracted features (indices), typically with less processing power required [186], [187], [188]. Generally, these methods are most suitable for online operation but suffer from the inability to operate only on the frequency content of interest (inter-area oscillations). A data mining-based technique [195] has been presented to identify the unstable system operation and identify coherent generators based on the supervised offline training of binary classifiers. Despite the fast and high accuracy of estimates, this method suffers from an inherent requirement to perform a substantial number of model-based supervised training simulations making this method suitable only for a limited set of disturbances and well-detailed power system models. Recently, a spectral clustering-based method was presented, which makes use of generator rotor angle and speed measurements to assess the weighted multi-indices dissimilarity distance [196]. The optimal number of coherent groups is determined by comparing the average silhouette value of different clustering combinations (number of groups), and finally selecting the clustering configuration with the highest average silhouette value among all evaluated cases. However, limited availability of rotor angle and speed measurements makes the implementation at this moment not applicable in real-world power systems. The method in [197] makes use of kernel principal component analysis and affinity propagation (AP) clustering technique to reduce dimensions of the multi-indices distances and to determine the optimal number of coherent groups automatically, respectively. However, the method requires centre-of-inertia centred generator rotor angles and speeds; and due to the basic preference parameter method for the AP clustering tends to partition independent (outlier) generators to the nearest group, leading to suboptimal results. Authors in [187] presented a dynamic coherency identification method suitable for online tracking of coherent generator grouping changes based on the PMU measured frequency-deviation from the generator terminals. This method also partitions the non-generator buses together with the corresponding coherent generator groups. The authors further extend the method in [198] to consider also the transient behaviour of wind power plants. The work, presented in [187], tackles the same challenge as the proposed algorithm of this chapter, in particular to online identify grouping changes of coherent generators following a disturbance for the purpose of

ICI. Therefore, the method presented in [187] (referred further as the benchmark method) is used in this chapter for comparative analysis.

5.1.2 CHALLENGES AND MOTIVATIONS

The available measurement-based generator coherency identification methods, in particular, the benchmark method:

- do not pre-process the measurements to retain only the inter-area oscillation frequencies of interest;
- require relatively long and nonadaptive observation window for estimation;
- do not perform observation window data selectivity in case of interfering pre- and post-event coherency indices;
- and are validated upon simulated bus measurements or machine signals in non-real-time fashion by using conventional software tools.

These deficiencies may lead to:

- erroneous results, particularly when:
 - measurements contain higher frequency components;
 - an observation window contains measurements belonging to two or more coherency configuration;
 - actual PMU measurements are used as data input;
- impose large estimation delay due to long and nonadaptive (fixed in length) observation window used;
- poor resolution of estimates after critical contingencies when generator coherency may change, also due to long and non-adaptive observation window used;
- and the inability of the methods to operate in real-time due to the high-computational burden associated with the high-complexity of the implementation.

This chapter addresses the above-mentioned deficiencies and proposes an SMT supported online generator slow coherency identification algorithm, suitable for near real-time tracking of grouping changes of slow coherent generators in an interconnected power system.

5.2 PROPOSED METHODOLOGY

In the previous Section 5.1, a formal introduction to the generator slow coherency identification is provided. However, the practical implementation of the generator slow coherency identification algorithm, suitable for online use in real-world power systems, has revealed several new and unresolved challenges (mind Section 5.1.2). Hence, this section elaborates on the identified challenges and presents proposed solutions, compound into an algorithm.

Briefly, the proposed algorithm performs PMU measurements conditioning for the rigorous identification of slow coherency indices. It adaptively determines the minimal number of samples to be processed in an observation window and performs data selectivity on the observation window to prevent the mixing of interfering coherency indices. Finally, based on the determined generator distance matrices adaptively tracks grouping changes of slow coherent generators and determines a finite number of coherent groups for an improved AP clustering.

5.2.1 SOURCE OF MEASUREMENTS

Generally, the generator rotor angle provides the most direct information about the rotor dynamics and related generator coherency [180]. However, PMU devices do not report rotor angle measurements, and even rotor angle estimations based on PMU voltage angle measurements may produce inaccurate results. As suggested in [181], [187], [199] a PMU, installed at the generator terminal bus, can send frequency measurements of positive sequence voltage containing vague information of the rotor associated dynamics. Hence, a PMU device can be used to monitor inter-area oscillations of interest of the particular generator in a power system (further discussed in Section 5.2.2).

It is assumed that in an electric power system consisting of N generators, each generator terminal bus is equipped with a PMU device. Each PMU device $i \in \{1, 2, \dots, N\}$ reports discrete time-interval samples of frequency x with 60 frames per second reporting interval (hereinafter referred to as *fps*). With M being the total number of samples to be processed, the sample vector is defined as $X_i = [x_{i,M}, \dots, x_{i,2}, x_{i,1}] \in \mathbb{R}^M$, where $x_{i,l}$ denotes the most recent frequency measurement of PMU i . The observation window W , containing M -most recent samples of frequency from N generator terminal buses, is presented by the following ensembled matrix:

$$W[X] = \begin{bmatrix} X_1 \\ X_2 \\ \vdots \\ X_N \end{bmatrix} = \begin{bmatrix} x_{1,M} & \cdots & x_{1,2} & x_{1,1} \\ x_{2,M} & \cdots & x_{2,2} & x_{2,1} \\ \vdots & \ddots & \vdots & \vdots \\ x_{N,M} & \cdots & x_{N,2} & x_{N,1} \end{bmatrix} \in \mathbb{R}^{N \times M} \quad (5.1)$$

5.2.2 PRE-PROCESSING OF MEASUREMENTS

Generator slow coherency is defined upon inter-area oscillation modes typically between 0.1 to 0.8 Hz, which are associated with the rotor swings between a group of generators or plants [181], [180]. Any higher frequency components present in the PMU measurements, as a consequence of excited local plant oscillations, may result in erroneous generator slow coherency identification [200]. Moreover, actual PMU measurements are affected by transients, and the system imposed high-frequency components such as measurement noise [97]. Therefore, for generator slow coherency identification, it is prudent to pre-process the measurements with a digital low-pass filter in order to retain only the inter-area oscillation frequencies of interest. Despite the evident interest of the research community for measurement-based generator coherency identification, only a small number of papers [194], [201] address the issue of high-frequency components present in the measurements. In this chapter, only the most critical low-pass filtering and down-sampling are addressed.

A. DIGITAL LOW-PASS FILTERING OF MEASUREMENTS

Digital filtering is extensively adopted in many diverse applications to perform the frequency-dependent alteration of an original signal. It can be used for noise reduction and frequency band extraction. In general, digital filters can be classified into two subcategories, named as Finite-duration Impulse Response (FIR) and Infinite-duration Impulse Response (IIR) filters [202]. The advantage of FIR filters over IIR filters is in their stable and linear phase response operation with an introduced constant delay for the whole frequency spectrum. On the contrary, IIR filters often require a much higher filter order than FIR filters to achieve a comparable level of performance and can be realised more efficiently by using hardware, which in case of online operation in real-world power systems a critical factor to consider.

In this research work, digital low-pass filtering of measurements is performed to retain only the inter-area modes of interest. This step enables vigorous grouping of slow coherent generators during the quasi-steady-state and the electromechanical transient period following a disturbance. For this, a low-pass FIR filter is adapted due to its filtering superiorities [53]. The design of a low-pass FIR filter with a narrow frequency band between 0 to 0.8 Hz and a sharp cut-off slope requires a relatively high filter order (length) to suppress higher frequency components sufficiently. It is important to note that digital filtering introduces delay since the filter output samples are shifted in time compared to the input. Hence, the objective is to design a low-pass FIR filter with satisfactory performance (attenuation of undesired higher frequency components) and minimum filter length. To determine the digital filter parameters, the *MATLAB* Signal Processing Toolbox is used. Table 5.1 and Figure 5.1 present the used filter design parameters and the response, respectively.

TABLE 5.1
FIR filter parameters

<i>design algorithm:</i>	Equiripple	<i>passband ripple:</i>	1 dB
<i>filter length:</i>	126 samples	<i>stopband edge:</i>	2 Hz
<i>filter delay:</i>	63 samples	<i>passband edge:</i>	0.5 Hz
<i>response:</i>	low-pass	<i>stopband attenuation:</i>	80 dB

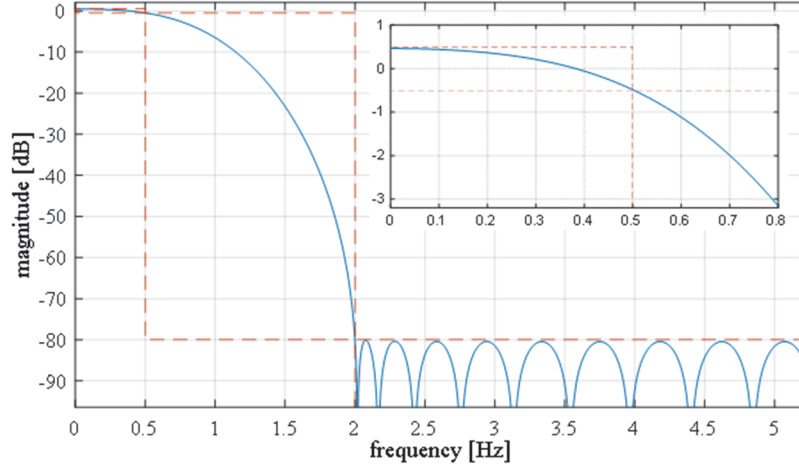


Figure 5.1: Magnitude response of the digital low-pass FIR filter for 60 fps PMU reporting rate.

As observed in Table 5.1 and Figure 5.1, the filter includes a relatively high stopband edge. This is intentionally mastered in order to minimise the required filter length and associated filtering delay, meanwhile, maintain adequate low-pass filtering performance for slow coherency estimation.

Notably, during the filter initialisation period, the filter stages are loaded with zeros, which causes transients in the filter output until the filter stages are fully loaded with actual measurements. Thus, during the filter initialisation period, it is prudent to discard the number of output samples equal to the filter length.

B. DOWN-SAMPLING OF MEASUREMENTS

As suggested in [201], a typical 50/60 fps PMU reporting rate provides measurements significantly faster compared to the electromechanical modes of interest resulting in redundant information. Indeed, the preformed simulations (not part of this thesis) confirm that the proposed algorithm performance is not affected in case of available 10, 15, 30, and 60 fps PMU reporting rate. However, it is important to note, that the parameters of the low-pass FIR filter to pre-process the measurements on the pre-step depend on the used PMU fps reporting rate and should be adjusted accordingly. Hence, the proposed algorithm is designed in a way that can adapt to the available PMU fps reporting rate automatically.

5.2.3 GENERATOR DISTANCE MATRIX

For generator coherency identification, a distance matrix $DM \in \mathbb{R}^{N \times N}$ is used to define relations between the pairs of generators, where DM_{mn} denotes the dissimilarity between the m^{th} and n^{th} generator. To determine the DM , as presented in [203], a wide variety of distance measures can be used, in particular, to assess the generators' slow coherency indices.

In this research work, a revised generator dissimilarity measure method of the benchmark method is proposed to assess the coherency indices in greater detail. This is realised as a weighted combination of the normalised *cosine* and *Minkowski* p -metric based distance matrices. *Cosine* distance measure determines an angular displacement, whereas the *Minkowski* distance measure determines a modified Euclidean norm between a set of sample vectors X , embedded in M -dimensional vector space [204]. The $dcos_{mn}[X]$ between two sample vectors X with M -dimensional points of generator m and n is defined as:

$$dcos_{mn}[X] := 1 - \frac{\sum_{k=1}^M X_{m,k} X_{n,k}}{\sqrt{\sum_{k=1}^M X_{m,k}^2} \sqrt{\sum_{k=1}^M X_{n,k}^2}} \in \mathbb{R} \quad (5.2)$$

and ranges from 0 to 2, where 0 indicates perfect angular alignment. Similarly, the $dmik_{mn}[X]$ of order $b = 1/2$ between two sample vectors X with M -dimensional points of generator m and n is defined as:

$$dmik_{mn}[X] := \left(\sum_{k=1}^M |X_{m,k} - X_{n,k}|^b \right)^{1/b} \in \mathbb{R} \quad (5.3)$$

and ranges from 0 to ∞ , where 0 indicates perfect magnitude match. The proposed distance matrix method represents a weighted combination of the normalised cosine $DM_{cos}[X] \in \mathbb{R}^{N \times N}$ and Minkowski $DM_{mik}[X] \in \mathbb{R}^{N \times N}$ symmetric distance matrixes to assess the orientation and strength of generators electromechanical coupling, respectively. To reduce the required memory and computational power, both distance matrices, named as $DM \in \mathbb{R}^{N \times N}$, are converted into a row distance vectors $DV \in \mathbb{R}^{I \times L}$ of length $L = (N-1)N/2$, where between the generator pair distances are arranged as:

$$DV = [DM_{1,2}, \dots, DM_{1,N}, DM_{2,3}, \dots, DM_{2,N}, \dots, DM_{N-1,N}] \in \mathbb{R}^L \quad (5.4)$$

To ensemble both distance vectors into a single vector, a unit vector normalisation is performed beforehand as:

$$DVN := \frac{DV}{\sqrt{\sum_{k=1}^L DV^2}} \in \mathbb{R}^L \quad (5.5)$$

Finally, the generator distance-vector $DVG \in \mathbb{R}^L$ to be further used resembles the *Euclidean norm* of the weighted individual dissimilarities, where the vectors' elements are represented as scalars in 2-dimensional Euclidean space by the equation:

$$DVG[t] := \sqrt{w_1\{DVNcos[X]\}^2 + w_2\{DVNmik[X]\}^2} \in \mathbb{R}^L \quad (5.6)$$

where $w_1 = 1$, $w_2 = 0.5$ represent the heuristically determined contributions of individual measures; and $t \in \{1, 2, 3, \dots\}$ resembles the time index as a point in time of a given variable. In this way, the angular displacement (cosine distance) impacts the results more significantly, although the identification of areas with a different frequency (Minkovski distance) is still possible.

5

5.2.4 ADAPTIVE OBSERVATION WINDOW

The existing generator coherency identification methods expect a long (10 - 20 s) and a non-adaptive (fixed in length) observation window. While this approach mostly works well during quasi-steady-state, it lacks fast response and resolution during the critical electromechanical transient period following a contingency. Generally, the stronger the power system is perturbed, the more conspicuous the present generator coherency is. In other words, one could online adjust the observation window length based on the present system state. Hence, in this research work, the observation window length M is automatically adjusted for each coherency identification instance. In general, the shorter the observation window, the more sensitive is the algorithm to temporary coherency changes. However, a too-short window may lead to irrational results due to the lack of observability. Also, the window length decrease is proportionally related to the decrease in estimation latency and required computational power.

The proposed adaptive observation window length method is based on a stability criterion, driven by the angular deviation of two most recent successive generator distance vectors (5.6) in L -dimensional vector space, as illustrated in Figure 5.5 - bottom. The following procedure determines the minimum number of samples to be processed for rigorous coherency identification:

a. Initialisation: set the window length to $M = fps$ to provide minimum observability, fix the observation window starting position (remains fixed till *Exit*) to the first incoming measurement sample being low-pass filtered, populate the observation window with M consecutive samples, determine the normalised generator distance-vector $DVG[t]$ (5.2) - (5.6), and save $DVG[t]$ for further use.

b. Increase the window length as $M = M + I$, and populate the observation window with a next-measurement-interval sample. Again, determine the $DVG[t]$ and save it for further use.

c. Determine the *cosine* angular difference $\Delta DVG[t]$ between the two most recent consecutive DVG vectors in L -dimensional vector space by using equations (5.2) and (5.7) and save it for later use.

$$\Delta DVG[t] := \cos^{-1}\{d\cos_{t-1,t}(DVG)\} \quad (5.7)$$

d. Exit condition: if the median of $(fps/5+1)$ most recent angular deviations ΔDVG (5.7) drops below the heuristically determined threshold $stab_tresh = 3/fps$, as:

$$median\{\Delta DVG[t - (fps/5)] \dots \Delta DVG[t]\} \leq stab_tresh \quad (5.8)$$

then the current window length adjustment procedure finishes (see Figure 5.5 - bottom) and continues with the reverse data selectivity method, presented in Section 5.2.5. In this case, the next observation window for the next coherency identification instance starts with the next incoming sample of step *a*. Otherwise, the procedure continues with step *b* and so forth.

Notably, $stab_tresh$ plays a vital role in determining the observation window length. The performed simulations suggest that it can typically range between $0.01 \leq stab_tresh \leq 0.1$, where a smaller value leads to a shorter observation window (higher resolution of estimates; more sensitive to temporal changes), whereas a higher value indicates a longer observation window (lower resolution of estimates; more robust to temporal changes). In our case, the $stab_tresh$ is controlled by the PMU reporting rate automatically.

5.2.5 REVERSE DATA SELECTIVITY

During the electromechanical transient period following a significant disturbance, such as a line trip, the generator coherency may change. This can be observed in the change of coherency indices (see Section 5.2.7). In this case, the observation window containing interfering pre- and post-event coherency indices, extracted from measurements, may result in erroneous coherency identification. Especially during the critical post-event period, it is prudent to perform data selectivity on the given observation window to prevent the mixing of the interfering indices and retain only the observation window measurements belonging to the post-event. The following steps significantly improve the critical coherency results immediately after an event:

e. Initialisation: flip the order of elements of the observation window W , named as $W_{flipped}$. This enables processing of $W_{flipped}$ elements in a reverse direction to retain only the post-event samples; set the minimum observation window length $M_{flipped} = fps$.

f. In steps for each increase in $M_{flipped}$ repeat Section 5.2.4 steps *a*, *b*, *c* (mind to use (5.2) - (5.7) with $W_{flipped}[1:M_{flipped}]$).

g. *Exit* condition: a severe change in coherency indices is detected if the following selectivity threshold condition (mind the red line in Figure 5.8 - bottom) is satisfied:

$$\Delta DVG_{flipped}[t] \geq 60 M_{flipped}^{-(fps/300 + 0.6)} \quad (5.9)$$

Afterwards, a local minima search is performed on the $\Delta DVG_{flipped}$ of the given observation window, to identify the instant when the $\Delta DVG_{flipped}$ elements start to deviate, indicating a change in coherency indices. This step tends to find the last dip $\Delta DVG_{flipped}[local_min]$ (for example, mind the blue circle in Figure 5.8 - bottom). The procedure continues with Section 5.2.6, where the DVG to be further used is equal to the $DVG_{flipped}[local_min]$.

h. In case the condition in step *g* is not satisfied, indicating sustained coherency indices within the given observation window, then the DVG to be used in Section 5.2.6 is identical to the last determined $DVG[t]$ of Section 5.2.4.

5.2.6 ADAPTIVE TRACKING OF GROUPING CHANGES

Generator slow coherency is a quasi-permanent system property under a sustained power system state. During a severe disturbance, such as the topology change, the generator slow coherency may change as a response of the generators on the new operating state. To enable adaptive tracking of grouping changes of slow coherent generators, two operation modes are proposed. A *permanent mode* is activated during the quasi-steady-state, while a *transient mode* is activated during the electromechanical transient period following a significant disturbance. In both cases the first-order exponential low-pass filter is adopted to enable robust coherency identification, being prone to temporally changes in a power system state, caused by transients due to small load changes, for example.

A. PERMANENT TRACKING MODE

Typically, during quasi-steady-state, the generator coherency does not change significantly. However, it may happen that due to temporal small system perturbations the weakly coherent generators separate and form new groups. To enable robust generator coherency identification meanwhile being still able to adapt to the grouping changes, the $DVGA[t]$ (5.10) vector to be used as an input for the AP clustering (mind Section 5.2.8) resembles the proportional contribution of the most recent $DVG[t]$ (5.6) and $DVGA[t - 1]$, defined in the previous coherency estimation instance, as:

$$DVGA[t] := \alpha DVGA[t - 1] + (1 - \alpha) DVG[t] \quad (5.10)$$

where heuristically determined $\alpha = 0.7$ controls contributions of the previously determined coherency indices $DVGA[t - 1]$.

Generally, α can range between 0 and 1, where a higher value of α puts more weight on the past coherency indices leading to more robust results, while on the contrary, a smaller value of α leads to increased adaptiveness of the algorithm to the most recent coherency indices of $DVG[t]$.

B. TRANSIENT TRACKING MODE

On the other hand, to enable more responsive tracking of grouping changes of slow coherent generators during the critical electromechanical transient period, when the slow coherency may change, the $DVGA[t]$ to be used is next step (mind Section 5.2.8) is defined as (5.10), where $\alpha = 0.4$ enables better adaptiveness of the algorithm and results to the present coherency configuration.

C. THE TRANSITION BETWEEN THE TRACKING MODES

The transition between the tracking modes is based on a cosine angular difference of the two most recent $DVGA$ vectors defined as:

$$\Delta DVGA[t] := \cos^{-1}\{d\cos_{t-1,t}(DVGA)\} \quad (5.11)$$

A significant increase in $\Delta DVGA[t]$ indicates a significant change in the generator coherency indices, while minor changes indicate sustained conditions (mind blue and red steams in Figure 5.7).

To switch from *permanent* to *transient mode* or vice versa, the following criterion applies:

$$mode[t] = \begin{cases} transient, & \Delta DVGA[t] \geq tran_tresh \\ permanent, & median\{\Delta DVGA[t-3] \dots \Delta DVGA[t]\} \leq perm_tresh \end{cases} \quad (5.12)$$

where heuristically determined $tran_tresh = 20$ and $perm_tresh = 10$. In order to enable a smooth transition from *transient* to *permanent mode* (5.12) at least four most recent $\Delta DVGA$ need to be determined during the *transient mode* operation.

Generally, when a change in the coherency occurs, the value of $\Delta DVGA[t]$ will increase over the $tran_tresh$, leading to *transient mode* activation. Contrary, during sustained conditions, the medium value of the four most recent $\Delta DVGA[t]$ should drop below the $perm_tresh$. Notably, in the case of a profoundly disturbed power system, leading to continuous *transient mode* activation, one might need to increase the value of α , $tran_tresh$, and $perm_tresh$ to decrease the algorithm's sensitivity.

It is important to note that during the algorithm initialisation period (*transient mode* by default) and when the transition from *permanent* to *transient mode* occurs (5.12) the first $\Delta DVGA[t]$ (5.10) to be used further in the partitioning (mind Section 5.2.8) is equal to most recent $DVG[t]$ by setting $\alpha = 0$ in (5.10). In this way, the partitioning algorithm considers only the most recent coherency indices (5.6) and neglects any past contributions. This

enables full adaptiveness of the proposed algorithm on the new conditions following a significant event.

5.2.7 TIME EVOLUTION OF SLOW COHERENCY INDICES

In a multi-dimensional dataset, a Principal Component Analysis (PCA) dimensionality reduction method identifies Principal Components (PCs) or directions with the most substantial variance in the dataset variables (dimensions) [188]. In this chapter, the PCA is performed on the $Y \in \mathbb{R}^{L \times N}$ dataset of N total number of past $DVGA \in \mathbb{R}^L$ vectors (5.10) to analyse the evolution of generator slow coherency indices over time. In other words, it is possible to visually demonstrate the changes in generator slow coherency indices of a power system, observed as variations in the first (dominant) PC with N dimensions (hereinafter referred to as PC1). To define the PC1 vector values, the following mathematical formulation is applied [205]:

$$w_{(1)} = \arg \max \left\{ \frac{w^T Y^T Y w}{w^T w} \right\} \in \mathbb{R}^L \quad (5.13)$$

which finds a solution when w is the corresponding eigenvector of the covariance matrix of Y with a maximum eigenvalue. Hence, the PC1 of the transformed dataset Y can be defined as [205]:

$$PC1 = w_{(1)} Y \in \mathbb{R}^N \quad (5.14)$$

For illustration, the black coloured line in Figure 5.7 presents the PC1 of 37 $DVGA \in \mathbb{R}^L$ vectors of the preformed simulation with 45 dimensions in total, where the vertical changes in the black line resemble the shift in Y datasets (and related slow coherency indices) in the most dominant direction over time. In the case of Figure 5.7 and corresponding performed simulations, the PC1 exhibits 61.9 % of the total dataset variance.

5.2.8 PARTITIONING OF GENERATORS INTO COHERENT GROUPS

In generator coherency identification, a clustering technique is used to partition a set of N generators as nodes $k \in \{1, 2, \dots, N\}$ into $C = \{c_1, c_2, \dots, c_K\}$ clusters (K total number of groups), based on a distance matrix, so that $G = \bigcup_{i=1}^K c_i$ and $c_i \cap c_j = \emptyset$, for $i \neq j$ [203]. The main challenge is to partition the generators into robust (over time) and an optimal number of clusters. This research work extends the unsupervised AP clustering technique to partition coherent generators into groups [197].

A. AP CLUSTERING

The AP clustering is an exemplar-based technique, which based on the similarity matrix adopts the max-product algorithm on a factor graph to identify a set of nodes as clusters'

centre (exemplars), and partition the remaining nodes into the corresponding clusters [206], [207]. The AP clustering is based on the message-passing approach between nodes, which in iterative steps maximises the following unconstrained optimisation problem:

$$\max F(C, S) := \sum_{i=1}^N S(i, c_i) + \sum_{k=1}^N \delta_j(c) \quad \forall i, k \leq N \quad (5.15)$$

where $S(i, c_i)$ denotes the negative dissimilarity matrix between node i and its potential exemplar c_i , and δ_j is a coherence constraint to guarantee the exemplar-consistency and eliminate incorrect results, defined as:

$$\delta_j(C) = \begin{cases} -\infty, & \text{if } c_j \neq j, \text{ but } \exists c_i = j \\ 0, & \text{otherwise} \end{cases} \quad (5.16)$$

To identify K exemplars as cluster centres and partition the remaining nodes into corresponding C clusters, the AP takes the negative distance matrix as an input $S = -DM \in \mathbb{R}^{N \times N}$ and recursively updates the responsibility matrix:

$$R(i, k) = S(i, k) - \max\{A(i, j) + S(i, j)\} \in \mathbb{R}^{N \times N} \quad (5.17)$$

where $j \in \{1, 2, \dots, n\}$ but $j \neq k$, representing the accumulated evidence of node k to be the exemplar for node i , and the availability matrix:

$$A(i, k) = \min\{0, R(k, k) + \sum\{\max(0, R(j, k))\}\} \quad (5.18)$$

where $j \in \{1, 2, \dots, n\}$, but $j \neq i$ and $j \neq k$, representing the accumulated evidence of node k to be the exemplar for node i . Detailed iteration formulas can be found in references [206], [207]. Finally, the resulting clusters C can be obtained by:

$$c_i[t] = \arg \max_k \{A(i, k) + R(i, k)\} \quad (5.19)$$

B. AP PREFERENCES PARAMETER

The initialisation of AP preference parameter $p = \{p_k\}$, in $S(k, k) = p_k$ plays an important role in AP to facilitate node k to be elected as an exemplar, control the total number of identified clusters, and avoid trivial solution as every node chooses itself as its exemplar. Frey et al. suggests p being the median of the input similarity matrix [206]. In many cases, this approach leads to suboptimal clustering results, since it tends to cluster the outlier

nodes (often implied as independent exemplars) to the centrally oriented exemplars [197], [207].

In order to overcome this problem, a novel *AP preferences parameter* adaptive method is proposed for the identification of exemplary nodes. The proposed method identifies outlier generators as independent clusters, automatically determines a finite number of groups, and reduces the number of iteration steps of AP clustering to converge. It is based on the distribution of values of $DVGA[t]$ distance vector to identify cluster exemplars and related cluster sub-nodes. In short, the method first, presumes all nodes as being potential exemplars. Second, based on the similarity matrix of $DVGA[t]$ searches for centrally oriented nodes and marks them as exemplars. Third, based on the combination of the mean and the median absolute value of $DVGA[t]$ distance vector in multiple steps identifies the cluster sub-nodes and rejects them for being exemplars. Finally, the method returns the defined preference vector p with identified exemplar nodes as:

$$p_k = \begin{cases} 0, & \text{exemplar} \\ -\infty, & \text{subnode} \end{cases} \quad (5.20)$$

The following Pseudocode 5.1 illustrates the implementation procedure of the proposed AP preference adjustment method.

PSEUDOCODE 5.1

Determination of AP preference p parameter

```

1: input:  $DVGA[t]$ , output:  $p$ 
2:  $ex = \{ex_k\} = 1, k \in \{1, 2, \dots, N\}$  //init: nodes as exemplars
3:  $pn = \{pn_k\} = 0, k \in \{1, 2, \dots, N\}$  //init: processed nodes
4:  $dc = (\text{mean}(DVGA) + \text{mad}(DVGA)) \cdot \beta$  //distance to cut based on DVGA value distribution
5:  $ca = \text{sort}(DVGA)$  //sort in ascending order
6:  $DMGA = \text{squareform}(DVGA)$  //convert to  $N \times N$  matrix
7: for  $i = 1$  to  $\text{size}(ca)$  //for each distance of DVGA
8:    $\{m, n\} = \text{find}\{DMGA == ca(i)\}$  //find node matrix indexes
9:   if  $pn(n) == 0 \wedge ex(n) == 1 \wedge \text{median}\{DMGA(:, n)\} \leq \text{median}\{DMGA(:, m)\}$ 
10:      $ce = n$  //node n as potential exemplar
11:      $cs = m$  //node m as potential sub-node
12:      $go = \text{true}$  //flag to continue
13:   elseif  $pn(m) == 0 \wedge ex(m) == 1$ 
14:      $ce = m$  //node m as potential exemplar
15:      $cs = n$  //node n as potential sub-node
16:      $go = \text{true}$  //flag - continue
17:   else
18:      $go = \text{false}$  //flag - nothing identified
19:   endif
20:   if  $go$  //continue with procedure?
21:      $pn(ce) = 1$  //mark node as exemplar & processed
22:      $s = \text{find}[\{DMGA(:, ce) \leq dc\} \notin pn]$  //find nodes as sub-nodes that are not already processed
23:     if  $\text{size}(s) > 0$  //cluster sub-nodes identified
24:        $ex(s) = 0$  //reject sub-nodes as exemplars
25:        $pn(s) = 1$  //mark sub-nodes as processed
26:       for  $x = 1$  to  $\text{size}(s)$  //for each sub-node
27:          $r = \text{find}[\{DMGA(:, s(x)) \leq dc\} \notin pn]$  //find more sub-nodes that are not already processed
28:         if  $\text{size}(r) > 0$  //sub-nodes of cluster sub-nodes
29:            $ex(r) = 0$  //reject sub-nodes as exemplars
30:            $pn(r) = 1$  //mark sub-nodes as processed
31:         endif
32:       endfor
33:     else
34:        $pn(cs) = 1$  //mark node as processed
35:     endif
36:   endif
37: endfor
38:  $p = ex - 1$  //mark as exemplar
39:  $p(p == -1) = -\text{Inf}$  //mark as subnode

```

Notably, one can influence the granularity of identified groups by changing the parameter β value (mind the fourth line in Pseudocode 5.1). Generally, a higher value of β reflects in a smaller number of groups (stiffer grouping), while a smaller value results in a higher number of groups. Based on the performed simulations, the $\beta = 0.2$ results in the most rational number of identified groups.

5.2.9 FLOWCHART OF THE PROPOSED METHODOLOGY

In summary, the proposed algorithm, firstly, pre-processes the incoming PMU frequency measurements with a low-pass filter; secondly, by using the improved generator distance measure it adaptively determines the minimum number of observation window samples; thirdly, it searches for the interfering coherency indices and retains only the observation window samples containing the most recent coherency indices; fourthly, performs adaptive tracking of grouping changes of slow coherent generators based on the identified coherency indices; finally, adaptively identifies a finite number of groups and partitions the coherent generators accordingly. Figure 5.2 presents the corresponding flowchart of the proposed algorithm.

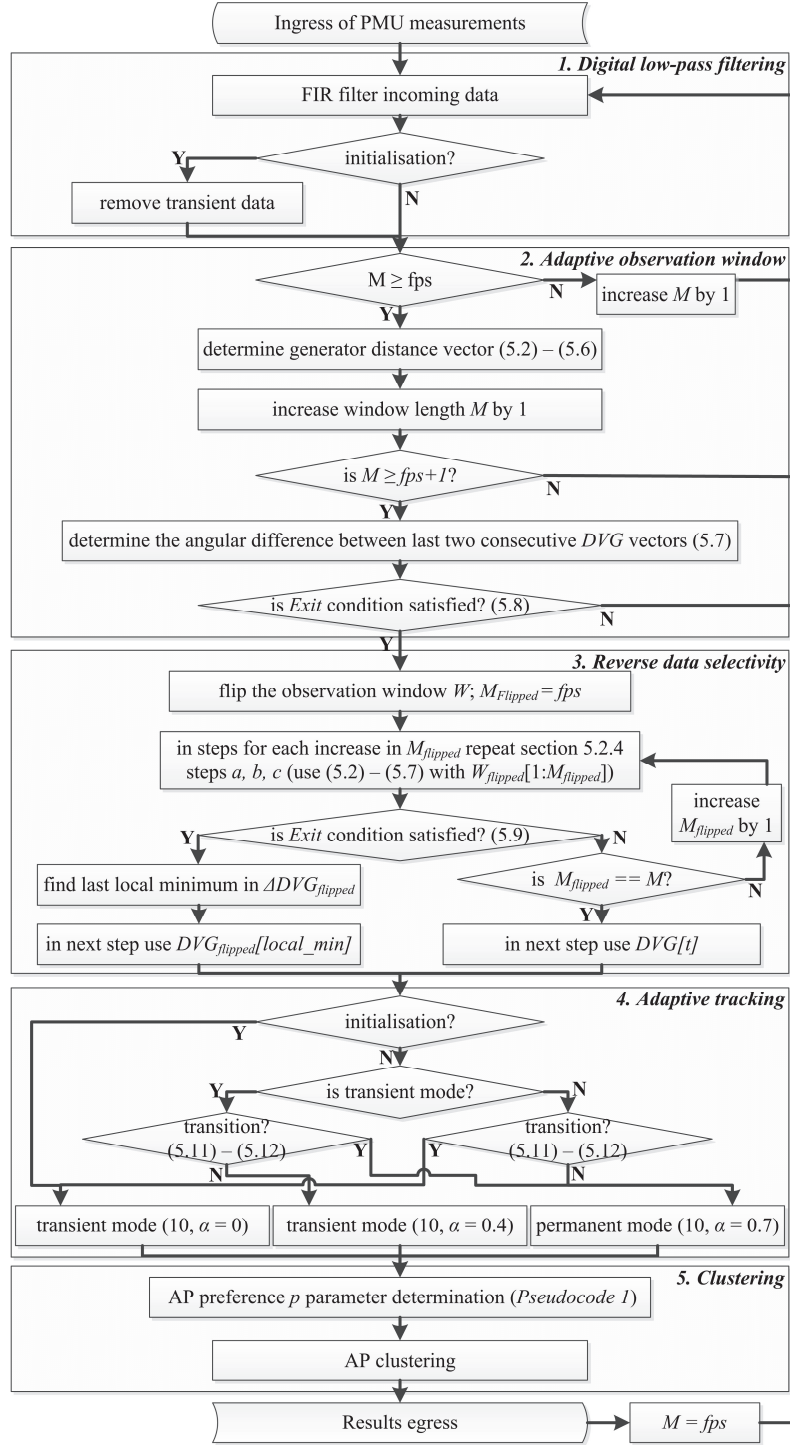


Figure 5.2: Flowchart of the proposed online algorithm.

5.3 SIMULATION STUDIES

This section presents the validated results of the proposed generator coherency identification algorithm and the benchmark method under different use-cases. Firstly, the section presents the simulation testbed and the power system model used for this purpose. Secondly, it presents the results of the comparison and elaborates on the findings. Finally, a detailed performance assessment of the proposed method is conducted.

5.3.1 SIMULATION TESTBED

In order to demonstrate the proposed algorithm capabilities, Chapter 2 presented cyber-physical testbed is utilised. For this purpose, the IEEE 39-bus benchmark model, also known as a reduced 10-machine New-England transmission power system, is simulated in the RTDS power system digital simulator [208]. As illustrated in Figure 5.3, the model comprises of ten synchronous machine generators, wherein the generator $G1$ represents the aggregation of the remaining New England system connected to *bus-39*, being supplied with a fixed field voltage (exciter) and mechanical torque. All the loads in the model are dynamic to maintain the given active (P) and reactive (Q) set points by using a variable conductance. The detailed specifications of the model components are available in [208].

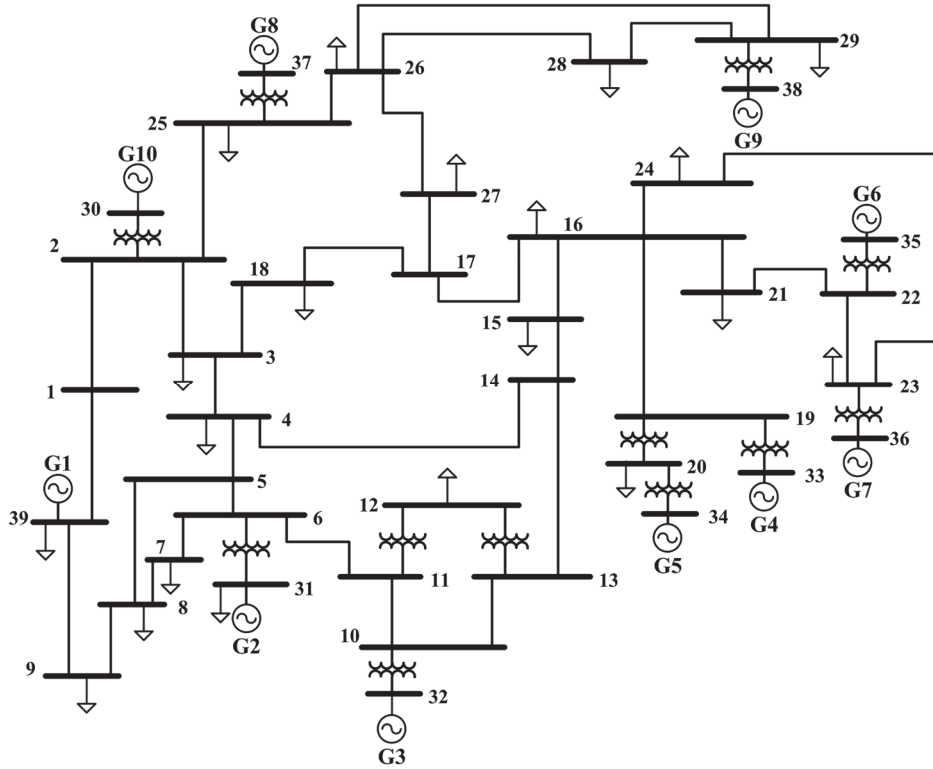


Figure 5.3: IEEE 39-bus benchmark power system model (adapted from [208]).

To provide SMT observability of the power system model, the GTNETx2 based PMUs are installed on the generator terminal buses. The PMUs are of class P with a 60 *fps* reporting rate and send their measurements to the SEL-5073 PDC for aggregation and time-alignment. The aggregated PMU measurements are further sent to a computer running the SADP (presented in Chapter 3), where the proposed coherency identification algorithm and the benchmark method are implemented and executed in parallel as an online *MATLAB* program in real-time. To provide accurate time synchronisation between all testbed components, the GE RT430 grandmaster GPS clock is used for IRIG-B and IEEE 1588 Precise Time Protocol based time dissemination. Figure 5.4 illustrates the applied components of the simulation testbed of this chapter.

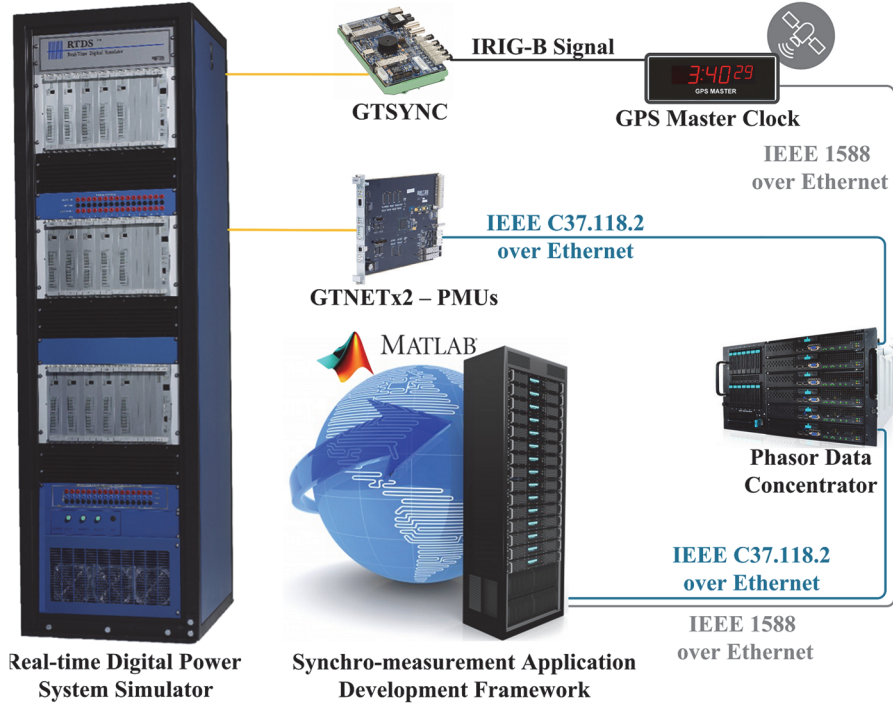


Figure 5.4: SMT supported real-time cyber-physical simulation testbed.

5.3.2 STUDY CASES AND SIMULATION RESULTS

This section presents the clustering performance of the proposed algorithm and the benchmark method on the IEEE 39-bus system [208], wherein the generator *G1* represents the aggregation of the remaining New England system, being connected to *Bus-39*. For the sake of clarity, the algorithm performance is demonstrated on a limited set of excited modes. For this purpose, the generator *G1* mechanical torque is being modulated every 200 *ms* with a random perturbation within $\pm 1\%$ of the nominal value [189].

For result comparison, the benchmark method parameters $\gamma = \gamma_r = 0.9999$ are tuned to achieve the most rational results. However, the benchmark method paper fails to detail the observation window length. To bridge the gap, both methods are evaluated side-by-side, where the observation window length is online determined by the proposed method. The only differences are that the benchmark method makes use of raw frequency deviation measurements [187].

In all the following result figures, the white area marks measurements (raw or processed) that are being used for the analysis; the grey area marks the raw measurements effected by the filtering delay, if applicable; and the red area marks the measurements being discarded due to detected interfering coherency indices of the reverse data selectivity method, if applicable.

Unfortunately, the number of presented graphical results is intentionally limited. Nevertheless, readers are encouraged to run the offline simulation available on *Code Ocean* open-source platform [209] to acquire in total 37 successive graphical results of the following simulated three use-cases, constructing in total 86.6 s of simulation and 5197 PMU frequency measurements per generator. It is important to note that the presented results are obtained by executing the following three use-cases successively without interruption of the simulation. Table 5.2 presents the clustering results of the comparison for each of 37 coherency identification instances in total, where time in the brackets of the table's first column resembles the simulation time equal to the observation window centre of each instance. Moreover, the clustering results in bold indicate an exact result match of the proposed algorithm and the benchmark method.

A. QUASI-STEADY-STATE OPERATION

During quasi-steady-state operation (see Figure 5.5 and Figure 5.6 - top, displaying results of the 7th instance in Table 5.2) the proposed algorithm identifies three groups of coherent generators as $c_1 = \{G1\}$, $c_2 = \{G2, G3, G8, G10\}$, and $c_3 = \{G4, G5, G6, G7, G9\}$ continuously (mind the orange area in Table 5.2 between 1st and 8th instance). Moreover, in Figure 5.7 the PC1 on the past *DVGAs* shows no significant deviations (mind the black coloured line from 1 to 8 in x-axis), indicating sustained generator slow coherency configuration. This behaviour is expected and it is in accordance with the slow coherency theory [181].

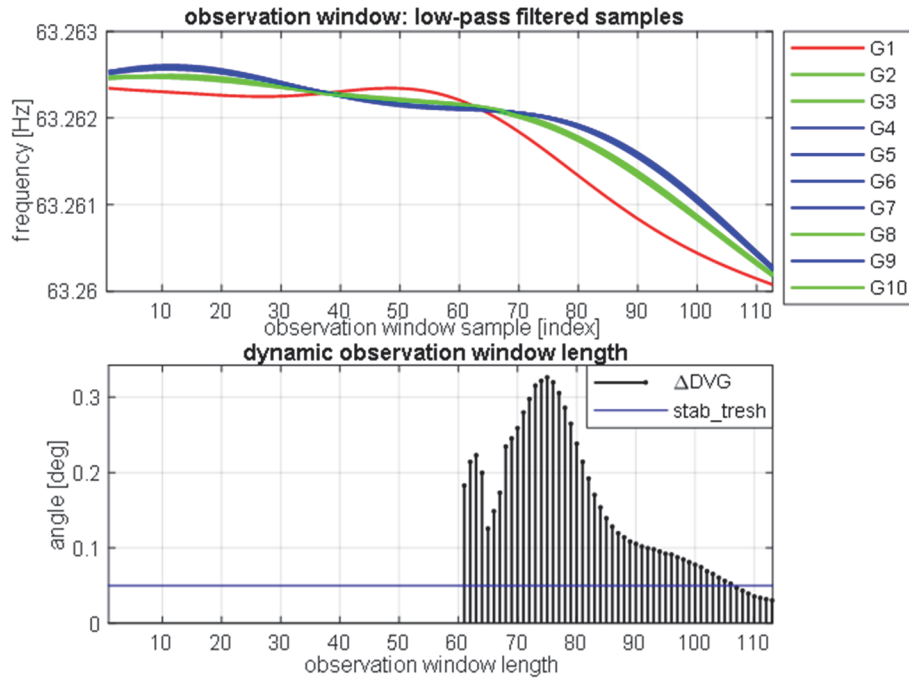


Figure 5.5: Visualised procedure to determine the observation window length (bottom); and corresponding low-pass filtered frequency measurements, coloured according to the identified groups of coherent generators (top).

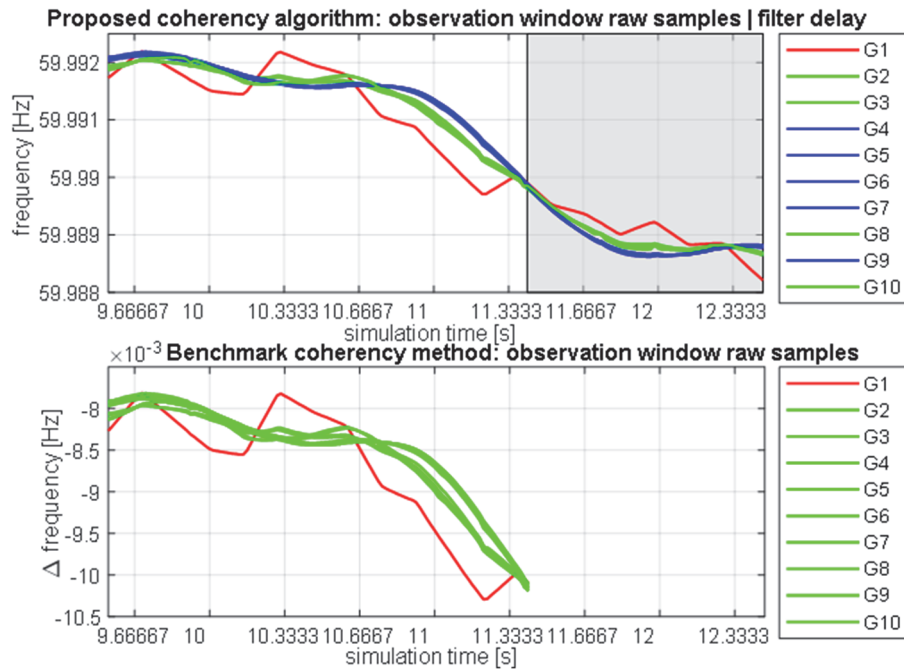


Figure 5.6: Quasi-steady-state; the proposed algorithm identifies three groups (top); while the benchmark method identifies two groups (bottom).

On the other hand, as observed in Table 5.2, the benchmark method identifies the same three groups as the proposed method and additionally two coherent groups as $c_1 = \{G1\}$, $c_2 = \{G2, G3, G4, G5, G6, G7, G8, G9, G10\}$ interchangeably. For example, as seen in Figure 5.6 - bottom, the benchmark algorithm is affected by the mechanical torque modulation of the generator $G1$ leading to unstable results despite the quasi-sustained state.

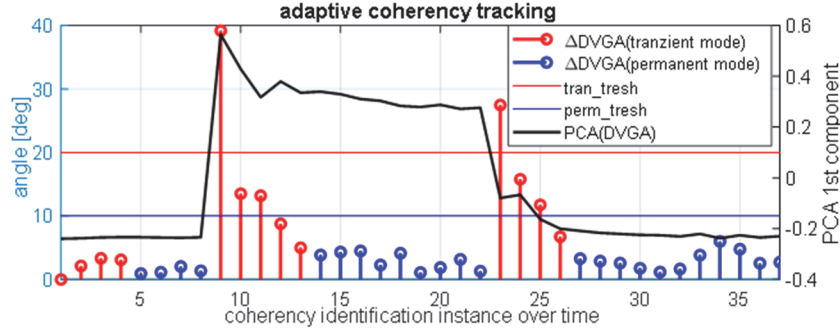


Figure 5.7: Coherency tracking progress of the preformed simulation, where the increase in angular deviation of two successive DVGA over the *tran_tresh* indicates a significant change in coherency following a disturbance. The red stems present transient mode coherency identification instances, while the blue stems present permanent mode coherency identification instances. The black line presents the PC1 of the past DVGAs.

B. APPLIED THREE-PHASE SELF-CLEARED FAULT ON BUS B25 WITH PERMANENT TRIPPING OF LINE B2-B25 AND DELAYED RECONNECTION

Following use-case *A* (mind the blue area in Table 5.2 between 9th and 22nd instance), first in use-case *B*, a three-phase 80 ms fault is applied on bus *B25* at 18.3 s of the simulation leading to permanent disconnection of the line *B2-B25*. The system perturbation following the event can be observed in Figure 5.8 - top and Figure 5.9. To clarify, the line disconnection changes the power system topology, which also affects the generator coherency. In this case, as indicated in Figure 5.8 - bottom, the proposed reverse data selectivity method identifies the interfering pre- and post-event coherency indices in the given observation window (mind the intersection between the black stems and red line in Figure 5.8 - bottom). In the next step, the method also identifies the transition point (mind the blue dot in Figure 5.8 - bottom) and discards the pre-event measurements (mind the red area in Figure 5.8 - top). In this way, only the post-event coherency indices are taken into account for further processing.

The change in generator coherency, caused by the topology change, can also be observed in Figure 5.7 as a jump in the PC1 (mind the black coloured line and its vertical increase from 8 to 9 in x-axis). Herby, an increase in $\Delta DVGA[9]$ above the *tran_tresh* triggers the activation of the *transient mode* for the following five coherency estimation instances (mind the red stems from 9 to 13 in x-axis). Afterwards, the adaptive tracking method switches back to *permanent mode* due to the new quasi-steady-state conditions (mind the blue stems from 14 to 22 in x-axis in Figure 5.7).

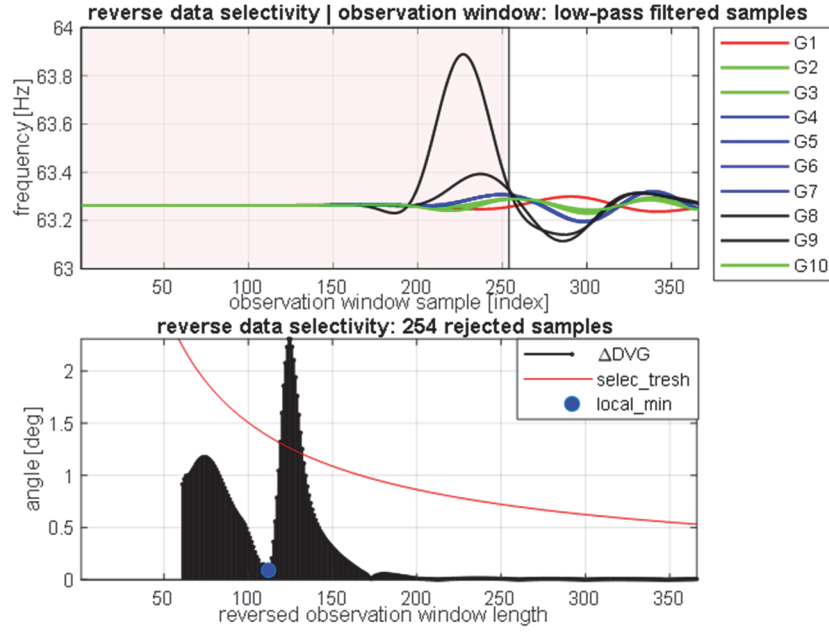


Figure 5.8: Detected interfering pre- and post-event coherency indices after the topology change (bottom); and the corresponding low-pass filtered frequency measurements (top). The red area marks the rejected pre-event measurements.

As seen in Figure 5.7, the PC1 gradually stabilise in new value after the initial jump indicating new quasi-sustained conditions and corresponding coherency configuration (mind the relatively narrow section of the black coloured line between 9 and 22 in x-axis). Immediately after the fault and line disconnection (see Figure 5.8 - top), the proposed algorithm identifies new four coherent groups as $c_1 = \{G1\}$, $c_2 = \{G2, G3, G10\}$, $c_3 = \{G4, G5, G6, G7\}$, and $c_4 = \{G8, G9\}$ continuously. Compared to the use-case *A* (pre-event), the generator *G8* of group c_2 and *G9* of group c_3 split from their existing groups (mind Figure 5.5 - top) and form a new independent group c_4 as a result of the topology change following the line disconnection.

On the contrary, the benchmark method identifies nine coherent groups with only generator *G6* and generator *G7* belonging to the same coherent group (see Figure 5.9 and Table 5.2). Similar occurs following five times (taking ~ 11 s) after the fault before it matches the results of the proposed algorithm. Yet, the benchmark method continues to produce variable results, while on the contrary, the proposed algorithm continuously identifies precisely the same groups as immediately after the line disconnection.

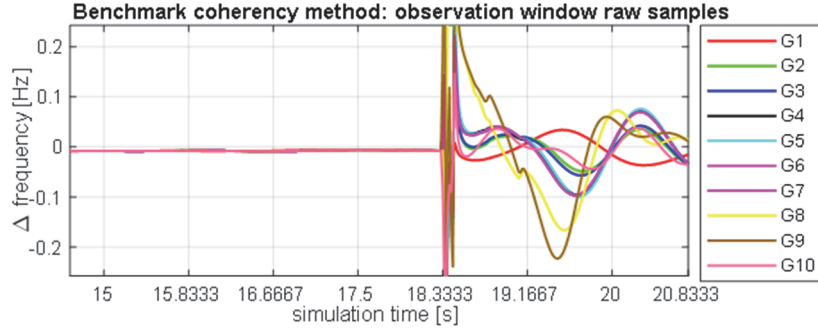


Figure 5.9: Applied fault resulting in the permanent line trip, where the benchmark method identifies nine groups of coherent generators (mind the legend colours).

Following 37 s of the simulation after the initial fault, the *B2-B25* line is reconnected, leading back to the same topology as in use-case *A* (mind the red area in Table 5.2 between 23rd and 32nd instance). Hereby, the proposed algorithm first identifies five groups of coherent generators (see Figure 5.10 - top) as $c_1 = \{G1\}$, $c_2 = \{G2, G3\}$, $c_3 = \{G4, G5, G6, G7\}$, $c_4 = \{G8, G10\}$, and $c_5 = \{G9\}$. This moment can be observed in Figure 5.7 at $\Delta DVGA[23]$ when the tracking algorithm switches to a *transient mode* due to the line reconnection. Also, in this use-case, the proposed algorithm identifies the interfering coherency indices due to the topology change (see Figure 5.10 - bottom). In the next three coherency identification instances, the algorithm identifies four groups of coherent generators (see Figure 5.10 - top) as $c_1 = \{G1\}$, $c_2 = \{G2, G3, G8, G10\}$, $c_3 = \{G4, G5, G6, G7\}$, $c_4 = \{G9\}$. Afterwards, the algorithm starts to identify the same groups as in use-case *A*, as a response of the generator *G9* resynchronisation with the group c_3 . This moment is seen in Figure 5.7, where the PC1 drops in steps and stabilise near its initial value of use-case *A* (mind the relatively narrow section of the black coloured line between 23 and 32 in x-axis).

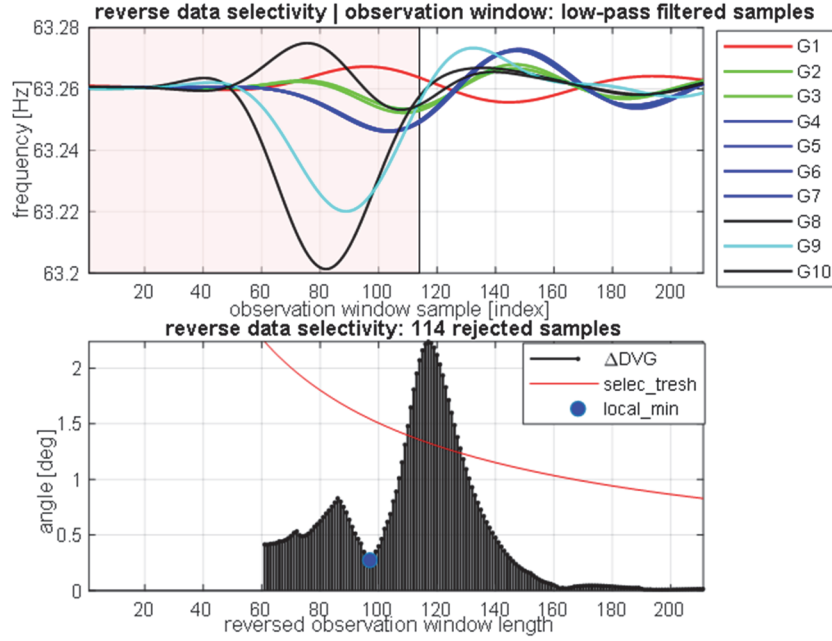


Figure 5.10: Detected interfering pre- and post-event coherency indices after the line reconnection (bottom); and corresponding low-pass filtered frequency measurements (top). The red area marks the rejected pre-event measurements.

On the other hand, after the line reconnection, the benchmark method first identifies the same nine groups as when the line $B2-B25$ is disconnected followed by producing variable results in time as seen in Table 5.2 (mind the red area). After five instances, the benchmark method matches with the proposed algorithm results.

C. THREE-PHASE SELF-CLEARED FAULT ON BUS B14

In this example (mind the green area in Table 5.2 between 33rd and 37th instance), quasi-steady-state conditions as in the use-case A , are followed by a three-phase 80 ms self-cleared fault on bus $B14$ at 78.1 s of the simulation leading to the system perturbation as seen in Figure 5.11 - top. As it can be seen in Figure 5.7 at $\Delta DVGA[33]$ and in PC1 (mind the narrow section of the black coloured line between 33 and 37 in x-axis), the slow coherency indices do not change significantly after the fault. This leads that the proposed algorithm continuously identifies the same groups of slow coherent generators $c_1 = \{G1\}$, $c_2 = \{G2, G3, G8, G10\}$, and $c_3 = \{G4, G5, G6, G7, G9\}$ precisely as in the use-case A and use-case B after the line reconnection.

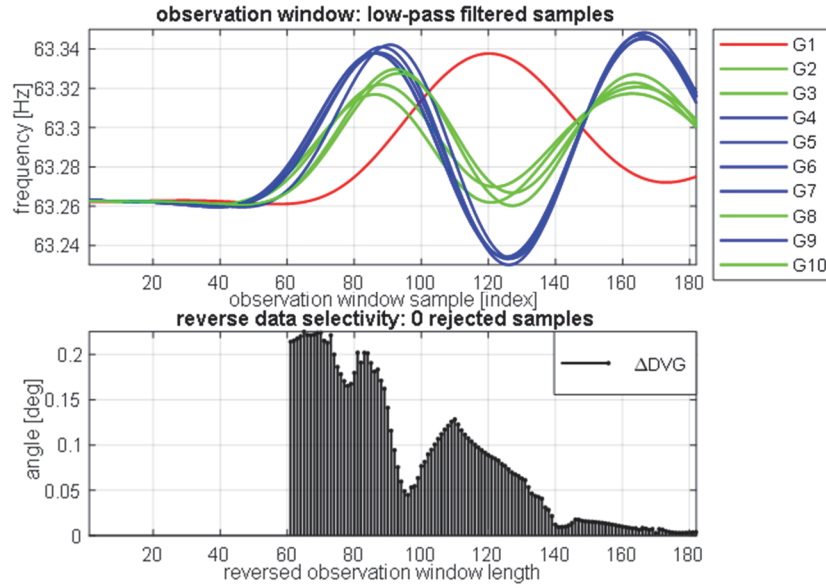


Figure 5.11: Continuously identified three coherent generator groups before and after the three-phase self-cleared fault (top); and corresponding reverse data selectivity (bottom) indicating no major coherency change after the event.

To clarify, the applied temporal fault does not affect the system structure permanently, leading to sustained slow coherency identification before and after the fault. This behaviour is expected and is in accordance with the slow coherency theory [181]. On the contrary, the benchmark method is significantly affected by the temporary fault perturbation resulting in identified nine coherent groups with only generator $G6$ and generator $G7$ belonging to the same group, following the variable results over time.

TABLE 5.2
Results of simulation

Instance (time)	Proposed algorithm	Benchmark method
1. (2.06 s)	{G1} {G2, G3, G8, G10} {G4, G5, G6, G7, G9}	{G1} {G2, G3, G4, G5, G6, G7, G8, G9, G10}
2. (3.75 s)	{G1} {G2, G3, G8, G10} {G4, G5, G6, G7, G9}	{G1} {G2, G3, G8, G10} {G4, G5, G6, G7, G9}
3. (5.03 s)	{G1} {G2, G3, G8, G10} {G4, G5, G6, G7, G9}	{G1} {G2, G3, G4, G5, G6, G7, G8, G9, G10}
4. (6.55 s)	{G1} {G2, G3, G8, G10} {G4, G5, G6, G7, G9}	{G1} {G2, G3, G4, G5, G6, G7, G8, G9, G10}
5. (8.5 s)	{G1} {G2, G3, G8, G10} {G4, G5, G6, G7, G9}	{G1} {G2, G3, G8, G10} {G4, G5, G6, G7, G9}
6. (10.46 s)	{G1} {G2, G3, G8, G10} {G4, G5, G6, G7, G9}	{G1} {G2, G3, G4, G5, G6, G7, G8, G9, G10}
7. (12.43 s)	{G1} {G2, G3, G8, G10} {G4, G5, G6, G7, G9}	{G1} {G2, G3, G4, G5, G6, G7, G8, G9, G10}
8. (14.05 s)	{G1} {G2, G3, G8, G10} {G4, G5, G6, G7, G9}	{G1} {G2, G3, G8, G10} {G4, G5, G6, G7, G9}
9. (19.81 s)	{G1} {G2, G3, G10} {G4, G5, G6, G7}	{G1} {G2} {G3} {G4} {G5} {G6, G7} {G8}

	{G8, G9}	{G9} {G10}
10. (21.85 s)	{G1} {G2, G3, G10} {G4, G5, G6, G7} {G8, G9}	{G1} {G2} {G3} {G4} {G5} {G6, G7} {G8} {G9} {G10}
11. (24.03 s)	{G1} {G2, G3, G10} {G4, G5, G6, G7} {G8, G9}	{G1} {G2} {G3} {G4} {G5} {G6, G7} {G8} {G9} {G10}
12. (26.43 s)	{G1} {G2, G3, G10} {G4, G5, G6, G7} {G8, G9}	{G1} {G2, G3} {G4, G5, G6, G7} {G8} {G9} {G10}
13. (28.55 s)	{G1} {G2, G3, G10} {G4, G5, G6, G7} {G8, G9}	{G1} {G2, G3, G4, G5, G6, G7, G10} {G8, G9}
14. (30.96 s)	{G1} {G2, G3, G10} {G4, G5, G6, G7} {G8, G9}	{G1} {G2, G3, G10} {G4, G5, G6, G7} {G8, G9}
15. (34.18 s)	{G1} {G2, G3, G10} {G4, G5, G6, G7} {G8, G9}	{G1} {G2, G3, G10} {G4, G5, G6, G7} {G8, G9}
16. (37.48 s)	{G1} {G2, G3, G10} {G4, G5, G6, G7} {G8, G9}	{G1} {G2, G3, G8, G9, G10} {G4, G5, G6, G7}
17. (40.2 s)	{G1} {G2, G3, G10} {G4, G5, G6, G7} {G8, G9}	{G1} {G2, G3, G10} {G4, G5, G6, G7, G8, G9}
18. (42.45 s)	{G1} {G2, G3, G10} {G4, G5, G6, G7} {G8, G9}	{G1} {G2, G3, G10} {G4, G5, G6, G7} {G8, G9}
19. (46.36 s)	{G1} {G2, G3, G10} {G4, G5, G6, G7} {G8, G9}	{G1} {G2, G3, G10} {G4, G5, G6, G7} {G8, G9}
20. (49.81 s)	{G1} {G2, G3, G10} {G4, G5, G6, G7} {G8, G9}	{G1} {G2, G3, G10} {G4, G5, G6, G7, G8, G9}
21. (51.55 s)	{G1} {G2, G3, G10} {G4, G5, G6, G7} {G8, G9}	{G1} {G2, G3, G10} {G4, G5, G6, G7} {G8, G9}
22. (53.43 s)	{G1} {G2, G3, G10} {G4, G5, G6, G7} {G8, G9}	{G1} {G2, G3, G10} {G4, G5, G6, G7} {G8, G9}
23. (57.1 s)	{G1} {G2, G3} {G4, G5, G6, G7} {G8, G10} {G9}	{G1} {G2} {G3} {G4} {G5} {G6, G7} {G8} {G9} {G10}
24. (59.01 s)	{G1} {G2, G3, G8, G10} {G4, G5, G6, G7} {G9}	{G1} {G2} {G3} {G4} {G5} {G6, G7} {G8} {G9} {G10}
25. (60.98 s)	{G1} {G2, G3, G8, G10} {G4, G5, G6, G7} {G9}	{G1} {G2, G3} {G4, G5, G6, G7} {G8, G10} {G9}
26. (62.96 s)	{G1} {G2, G3, G8, G10} {G4, G5, G6, G7} {G9}	{G1} {G2, G3, G8, G10} {G4, G5, G6, G7, G9}
27. (65.01 s)	{G1} {G2, G3, G8, G10} {G4, G5, G6, G7, G9}	{G1} {G2, G3, G4, G5, G6, G7, G8, G9, G10}
28. (66.65 s)	{G1} {G2, G3, G8, G10} {G4, G5, G6, G7, G9}	{G1} {G2, G3, G8, G10} {G4, G5, G6, G7, G9}
29. (69.18 s)	{G1} {G2, G3, G8, G10} {G4, G5, G6, G7, G9}	{G1} {G2, G3, G8, G10} {G4, G5, G6, G7, G9}
30. (71.75 s)	{G1} {G2, G3, G8, G10} {G4, G5, G6, G7, G9}	{G1} {G2, G3, G8, G10} {G4, G5, G6, G7, G9}
31. (74.11 s)	{G1} {G2, G3, G8, G10} {G4, G5, G6, G7, G9}	{G1} {G2, G3, G4, G5, G6, G7, G8, G9, G10}
32. (76.31 s)	{G1} {G2, G3, G8, G10} {G4, G5, G6, G7, G9}	{G1} {G2, G3, G8, G10} {G4, G5, G6, G7, G9}
33. (78.43 s)	{G1} {G2, G3, G8, G10} {G4, G5, G6, G7, G9}	{G1} {G2} {G3} {G4} {G5} {G6} {G7} {G8} {G9} {G10}
34. (80.53 s)	{G1} {G2, G3, G8, G10} {G4, G5, G6, G7, G9}	{G1} {G2} {G3} {G4} {G5} {G6, G7} {G8} {G9} {G10}
35. (81.78 s)	{G1} {G2, G3, G8, G10} {G4, G5, G6, G7, G9}	{G1} {G2} {G3} {G4} {G5} {G6, G7} {G8} {G9} {G10}
36. (83.18 s)	{G1} {G2, G3, G8, G10} {G4, G5, G6, G7, G9}	{G1} {G2} {G3} {G4} {G5} {G6, G7} {G8} {G9} {G10}
37. (84.56 s)	{G1} {G2, G3, G8, G10} {G4, G5, G6, G7, G9}	{G1} {G2, G3, G8, G10} {G4, G5, G6, G7} {G9}

5.4 DISCUSSION OF THE RESULTS

The first part of this section elaborates on the findings of the comparison between the proposed algorithm and the benchmark method. In the second part, a detailed performance assessment of the proposed method is conducted and articulated.

5.4.1 COMPARISON WITH THE BENCHMARK METHOD

The results, presented in Section 5.3, demonstrate that the proposed algorithm overcomes the limitations of the benchmark method for the purpose of ICI. In particular, the low-pass filtering of measurements (discussed in Section 5.2.2) of the proposed algorithm enables identification of slow coherent generator groups based on the superposition of the crucial inter-area oscillation modes only, while the benchmark method uses raw measurements containing higher frequency local modes and transients. As shown, the improved similarity method (discussed in Section 5.2.3) can assess the coherency indices in greater detail, leading to more sustained results and identification of slow coherent areas with different frequencies, while the benchmark method cannot distinguish different frequency zones (mind Figure 5.6). The adaptive observation window length method (discussed in Section 5.2.4) identifies the minimum number of processed samples for fast identification of generator slow coherent groups following a contingency, while the benchmark method uses a fixed observation window length. Especially, after a significant disturbance leading to the change in slow coherency, the proposed reverse data selectivity (discussed in Section 5.2.5) prevents mixing of interfering pre- and post-event coherency indices and retains only the measurements belonging to the post-event for more reliable results, while the benchmark method does not take that into account. The proposed adaptive tracking method (discussed in Section 5.2.6) makes the results more robust to temporal changes in coherency indices, while still permits adaptiveness of result in case of significant changes. On the contrary, the benchmark method does not perform adaptive tracking and produces results solely on identified most recent coherency indices (sometimes misleading), leading to altering results even during quasi-sustained power system state. As demonstrated in Figure 5.7, the applied PCA enables unprecedented visual demonstration of changes in generator slow coherency indices over time (discussed in Section 5.2.7). Finally, the fixed clustering parameter $\gamma_c = \gamma_r$ in the benchmark method leads to the high number of identified clusters following a disturbance, while the proposed AP preference parameter method can dynamically adapt to the present conditions (discussed in Section 5.2.8), leading to sustained and more robust results.

5.4.2 PROPOSED ALGORITHM'S REQUIREMENTS AND PERFORMANCE

This research work assumes that each generator unit is observed by a PMU installed at its terminal. However, in the case of the limited generator observability in practice, one could use a single PMU to monitor the behaviour of a generation region of electrically-short-connected slow coherent generators, such as large power plants. However, beforehand, a

comprehensive dynamic equivalencing analysis of the detailed power system model should be performed.

Moreover, 60 *fps* PMU reporting rate is used for the analysis, while in practice 30 *fps* or less might be available only. Nevertheless, the performed simulations (not part of this thesis) confirm that the proposed algorithm performance is not affected in the case of used 10, 15, or 30 *fps* PMU reporting rate. The readers are encouraged to run the offline simulation available on the *Code Ocean* [209] to obtain the corresponding results.

As observed in Figure 5.5, Figure 5.8, Figure 5.10 and Figure 5.11, the amplitudes of frequency measurements are altered as a side effect of the applied low-pass FIR filtering beforehand. This has no adverse effect on the results of the proposed algorithm.

During the simulation of all three use-cases (37 coherency identifications in total), a median observation window length of 113 samples (1.933 *s*) with 52 samples of standard deviation is determined automatically. It takes 0.36 *ms* execution time to process 950 samples of the median observation window (mind ten generators). After (5.8) is satisfied, it takes an additional 24.2 *ms* to perform reverse data selectivity, tracking, and generator clustering, while the benchmark method requires only 1.5 *ms* in total. In this case, the clustering takes 2.9 *ms* execution time. To summarise, the average coherency identification latency τ_{total} can be defined as:

$$\begin{aligned}\tau_{total} &= \tau_{PMU} + \tau_{comm} + \tau_{PDC} + \tau_{SADF} + \tau_{filt} + \tau_{win} + \tau_{proc} \\ &\approx 21 \text{ ms} + 1 \text{ ms} + 0.6 \text{ ms} + 1.5 \text{ ms} + 1.05 \text{ s} + 0.96 \text{ s} + 24.3 \text{ ms} \\ &= 2.05 \text{ s}\end{aligned}\quad (5.21)$$

where:

- τ_{PMU} is the PMU measurement delay;
- τ_{comm} is the delay between the PMU, Phasor Data Concentrator (PDC), and SADF;
- τ_{PDC} is the PDC processing delay;
- τ_{SADF} is SADF parsing delay of the PMU measurements;
- τ_{filt} is the low-pass filter delay;
- τ_{win} is the delay of an observation window centre ($M/2$);
- τ_{proc} is the proposed algorithm processing delay.

As observed in (5.21), the unavoidable low-pass filtering and observation window length are the most significant factors contributing to the overall latency. Still, this mostly outperforms the existing methods due to the relatively short observation window used.

Additionally, the required execution time of the proposed AP preference p parameter method together with the AP clustering is evaluated for a different number of nodes. For this, the median execution time of 100 iterations of randomly generated distance matrices concerning the increasing number of nodes to partition is compared. Hereby, the AP clustering automatically stops when the results of the last 20 iterations converge. The following Table 5.3 and Figure 5.12 present the obtained results. It can be observed that the

required execution time to cluster the nodes exponentially increases with the increasing number of nodes. The glitches in the figure are the result of the PC's internal processing of other tasks, resulting in increased processing time.

In summary, the adverse coherency identification latency, particularly affecting the supported closed-loop control applications, depends on many case dependent factors. Notably, one should consider delays associated with the PMU measurement, remote data acquisition, PDC time-aligning, coherency identification, application's processing, and final control signal conveying to remote actuators. It is essential to carefully assess overall latency to assure the adequate response of mission-critical applications in time.

TABLE 5.3
AP preference p method and AP clustering execution time

Number of nodes	Execution time [s]	Number of nodes	Execution time [s]
10	0.0028	160	0.2867
20	0.0041	180	0.4152
40	0.0087	200	0.5880
60	0.0180	220	0.8045
80	0.0345	240	1.0631
100	0.0634	260	1.4204
120	0.1076	280	1.8426
140	0.1863	300	2.3729

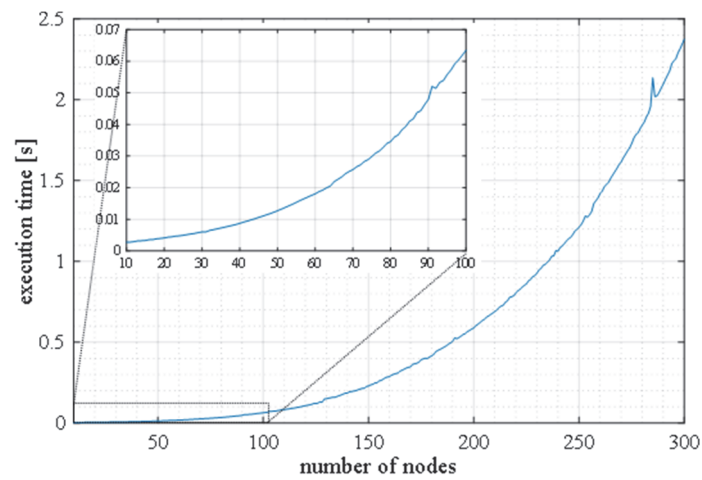


Figure 5.12: *Proposed preference adjustment parameter method and AP clustering execution time required concerning the increasing number of nodes to partition.*

5.5 CONCLUDING REMARKS

This chapter proposed a novel SMT supported algorithm for an online and near real-time tracking of grouping changes of the slow coherent generators in an interconnected power system. The conducted research work elaborated on the identified challenges and proposed the solutions to overcome them.

The outcome of this chapter research work is the measurement-based algorithm for online identification of groups of slow coherent generators. Hereby, the generators are partitioned into slow coherent groups based on the superposition of the inter-area oscillation modes during the quasi-steady-state and electromechanical transient period following a disturbance. The results of this research work show that the applied low-pass filtering of PMU frequency measurements is the crucial step for measurement-based generator slow coherency identification since it retains only the slow inter-area oscillation frequencies of interest. The research work built on top of the benchmark method and proposed the improved generator dissimilarity measure, which considers the direction and strength of electromechanical coupling between generators for thorough identification of coherency indices. This step, compared to the benchmark method, leads to more robust results and identification of generator regions with different frequencies. The new adaptive observation window method dynamically determines the minimum number of required measurement samples to be processed in an observation window. Compared to conventional methods with fixed observation window length, this step enables faster response and reduces the identification time delay. Especially during critical post-event conditions, the novel data selectivity algorithm detects mixing of interfering coherency indices of an observation window and retains only the measurements, containing post-event coherency indices, used for further clustering. This step significantly improves the accuracy of the crucial results immediately after the event. The novel adaptive coherency tracking method, which adapts to the present system state in order to suppress temporal coherency changes during quasi-steady-state while enables fast response during the electromechanical transient period following an event, makes the results more robust compared to the benchmark method. This chapter also addressed the challenge concerning the determination of an optimal number of coherent groups. The proposed AP preference p adjustment method enabled automatic identification of the outlier generators and adaptive determination of a finite number of coherent groups. In combination with the AP clustering, the proposed method enabled the efficient partition of the generators into corresponding coherent groups. Finally, the model-independent design and low-computational complexity of the proposed algorithm are unique properties, which make it suitable for online use in advanced SIPS, in particular as a part of ICI and PSS tuning applications. For ease of the result reproducibility, the *MATLAB* implementation of the proposed algorithm and the simulation dataset are available as an open-source on the *Code Ocean* platform. Future work may involve isolation of the dominant inter-area mode in an interconnected power system and partition the corresponding generators accordingly.

CHAPTER 6

CONCLUSIONS AND FURTHER RESEARCH DIRECTIONS

This thesis provided insight into required power system developments to overcome the emerging operational challenges imposed by the energy transition. In this context, the thesis presented the developed Synchronised Measurement Technology (SMT) supported cyber-physical experimental testbed and the proposed *MATLAB* implementation of the IEEE Std. C37.118.2-2011 specifications, enabling simplified design and online validation of Wide Area Monitoring, Protection, and Control (WAMPAC) applications. Finally, to improve situational awareness and facilitate the design of emergency control schemes, this thesis proposed two synchro-measurement supported algorithms for online disturbance detection and online identification of slow coherent generators, respectively. This final chapter concludes the thesis and addresses further research directions.

6.1 THESIS CONCLUSIONS

In the face of the technological pace related to the energy transition, there is hope that in the future, the energy supply will be entirely based on renewable, clean, sustainable and affordable energy sources.

“Technological progress comes from doing things differently in an unpredictable way. The future is not an extrapolation of the past.”

- Stanton Friedman

As history would have it, progress comes from doing things differently. The traditionally designed power systems have been continuously evolving into more efficient, decentralised, more sustainable and environmental-friendly interconnected power systems while incorporating a wide variety of technologies on the way to advance. Particularly, in the last decade, the power systems have been changing progressively as a result of the energy transition developments. In parallel, these developments have been imposing new challenges and requirements for the power system operation and control.

Chapter 1 discussed the existing and emerging operational and control challenges of modern power systems. As elaborated in the chapter, to prevent and mitigate power disruptions in the future, constructive actions reflected in new technological developments in combination with their profound integration into existing power systems, and radical adaptation of the operation and control procedures need to be considered.

“If you can’t measure it, you can’t manage it.”

- Peter Drucker

As discussed in the chapter, it is crucial not only to identify incipient technological advances to meet the operational requirements of today and the future power systems but above all, at an early stage, to provide a comprehensive and detailed insight into the power system state and operating boundaries. Notably, the lack of SMT supported system-wide observability and advanced situational awareness applications, hampers the ability of the power system operators to operate the grid effectively and proactively. Also, it limits the design of advanced protection and control schemes requiring such monitoring applications in their pre-step. Nevertheless, the lack of cutting-edge research and testing facilities to translate the theory into practice, in particular, enabling fast prototyping of new ideas into functionalities and products that are thoroughly validated on actual power system models, hampers the pace of innovation in the power systems. Hence, the primary research objective of this thesis was *to enhance the interconnected power system situational awareness with the aim of reinforcing the power systems reliability, and to develop a cyber-physical simulation testbed for online evaluation of the emerging WAMPAC applications under realistic conditions in real-time.*

In the face of the research objective, Chapter 2 provided an overview of the state-of-the-art SMT and its supported WAMPAC applications. As discussed in the chapter, the SMT provides unprecedented observability of power system phenomena compared to the traditional SCADA system. Especially, the increased resolution, accuracy, common time synchronisation and the relative phase angle of measurements make the SMT applicable for WAMPAC in large-scale interconnected power systems particularly. Nevertheless, as pinpointed, before being implemented into the real-world power systems, thorough assessment and validation of the WAMPAC applications under realistic conditions are required. Furthermore, the chapter elaborated on the high degree of complexity associated with WAMPAC and presented the essential implementation aspects to be considered. As concluded, the conventional software-based simulation tools are not applicable for mission-critical validation purposes of WAMPAC applications to guarantee their reliable operation. Hence, to serve this purpose, the chapter presented the developed WAMPAC-ready cyber-physical experimental testbed, enabling thorough validation of WAMPAC applications in the isolated and closed-loop supported simulation environment in real-time. Nevertheless, the testbed features HIL support, making it applicable for compliance testing of diverse power system monitoring, protection, and control devices and applications. Moreover, as a

part of the testbed, the chapter presented the developed web-based SMT monitoring platform. As demonstrated in Chapter 3 - 5, the experimental testbed can be used as a groundwork for future developments related to WAMPAC.

At the beginning of the research work of this thesis, there was a lack of user-friendly tools for development, validation, and seamless integration of WAMPAC applications into an SMT supported power system. Hence, the outcome of Chapter 3 is the Synchro-measurement Application Development Framework (SADF) software library, which for the first time enabled online receiving and parsing of machine-readable synchro-measurements into a human-readable format in the *MATLAB* programming environment in real-time. First, the chapter discussed the limitations of the conventional software bus measurements for the design and validation of WAMPAC applications. Moreover, the chapter motivated the seamless and online use of synchro-measurements for these delicate tasks. This research work filled the scientific gap between the IEEE Std. C37.118-2005 (communication part) and IEEE Std. C37.118.2-2011 specifications and their implementation by proposing a robust communication technique and efficient synchro-measurement data parsing method. Unique about this work is that SADF is the first open-source available implementation of the IEEE Std. C37.118.2-2011, which supports TCP, UDP, or combination of both for the online receiving of synchro-measurements. As demonstrated in Chapter 3, Chapter 4 and Chapter 5 of this thesis, combining the SADF library with *MATLAB*'s signal processing and visualisation functions enables the rapid prototyping of advanced online WAMPAC applications. To facilitate seamless and online use of synchro-measurements for the WAMPAC application design of the research community, the proposed SADF implementation is available as an open-source on *GitHub* repository. Further work is needed to convert the proposed SADF library into *C* or a similar high-performance programming language for industrial use.

To improve the situational awareness of power systems, Chapter 4 presented the SMT supported online disturbance detection, suitable for adaptive detection of disturbances in AC and HVDC power grids in near real-time. Unique about this work is that for the first time it made use of PMUs to deliver time-synchronised measurements of HVDC voltage and current. This made the proposed algorithm applicable in AC and HVDC power grids. As demonstrated, the algorithm is capable of identifying the disturbance occurrence and clearance measurement sample based on the adaptive threshold, driven by the measurement variance. This made the algorithm adaptive and robust to load fluctuations and noise. The algorithm is applicable as a pre-step of backup protection schemes or as a standalone situational awareness application. Further research work is needed to establish the automatic classification of identified disturbances.

Recent developments in the research community suggest the increasing trend in the design of distributed agent-based applications. However, it is important to note that some applications, e.g., addressing grid-wide stability challenges, often require centrally based

system-wide observability for their profound operation. For example, in Chapter 5, the proposed SMT supported algorithm for online identification of grouping changes of slow coherent generators for its operation requires centrally collected synchro-measurements from the generators' terminals. Since the inter-area modes of interest, in this case, often encompass multiple power systems, it is crucial to establish a safe and reliable PMU data exchange between all the utilities of an interconnected power system. Additionally, the continuously evolving power systems require constant online monitoring, in order to in time detect any newly excited, or any change in existing inter-area modes. However, despite the significant amount of earlier research work on the generator coherency topic, the existing methods are mostly not applicable for an online, direct, and reliable use in real-world power systems. Hence, to address the unresolved challenges, Chapter 5 proposed a novel SMT supported adaptive algorithm, suitable for near real-time tracking of grouping changes of slow coherent generators during quasi-steady-state and the electromechanical transient period following a disturbance in the grid. The conducted research presented in the chapter, first, identified the remaining challenges, which were then subsequently addressed by the proposed solutions, compounded into the algorithm. Unique about this work is the new data selectivity method, which for the first time prevented mixing of the interfering pre- and post-event coherency indices within a given observation window and retained only the post-event one. This step enabled more accurate results immediately after a critical event. Likewise, the novel adaptive tracking method enabled more robust results during quasi-steady-state and more responsive tracking during the electromechanical transient period following an event, when as a response, the groups of slow coherent generators might change. Further, it features an improved generator dissimilarity measure method, which enabled a more thorough assessment of the generator coherency indices as a direction and strength of the electromechanical coupling between generators. Also, the new preference adjustment method of AP clustering, which adaptively determined the optimal number groups and partitioned the outlier generators as independent clusters, was shown to be able to dynamically adapt to the present conditions, leading to improved accuracy of the results. All together in combination with the novel adaptive observation window method, which determined the minimum number of samples to be processed for near real-time coherency identification, fosters the design of fast-acting and adaptive SIPS, such as ICI. Further research is needed to separate inter-area oscillation modes, to identify the critical one and partition the generators accordingly.

"The diamond couldn't withstand the pain. I wonder what makes paper that strong."

- p\$K

As a final remark, the major challenge, faced in this thesis, was to design the measurement-based solutions, suitable for online and near real-time operation. This requirement came from the Author's personal belief that all the developments should be more or less directly applicable to real-world power systems. However, as discussed in Chapter 1, the power systems, or in other words, the heart of the modern world has been experiencing the

increasing number and severity of power outages, and is at risk due to the changes imposed by the energy transition. In order to prevent and mitigate power disruptions in the future and facilitate new developments towards more sustainable and environmental-friendly future power systems, closer cooperation between the research institutions and the industry is necessary. To put it differently; for the sake of our own good and generations to come, if not urgently before, now it is the high time to transfer the theory into practice, before being too late.

6.2 FURTHER RESEARCH DIRECTIONS

“The digitisation can propel the power systems in a way as the electrification did the industry.”

- Matija Naglič

The recent advancements in power system digitisation, in particular, the IEC Std. 61850 based digital substation, bring technological advances and unprecedented opportunities. One of the main gains of a digital substation is that the electrical signals are digitised at the source, leading to improved measurement accuracy. The abundance of microprocessor devices in digital substation's components enables real-time performance conditioning and ease of the device configuration remotely. The improved monitoring of components and high sampling rates advance the power system observability. Besides, the intra- and inter-substation peer-to-peer or peer-to-many IEC 61850 standard based communication enables the development of distributed and centralised intelligence. For example, this empowers the design of advanced protection and control schemes that are distributed amongst multiple IEDs within a substation or between multiple substations. Despite the many benefits and maturity of the digital substation technology, it rarely sees the light of day, but the gradual increase in recent deployments suggests its bright future.

“The triggering fact is that the EMS/SCADA developments are not in line with the power grid changes. The level of EMS/SCADA developments should always be one step ahead, to prepare the power system operators for future challenges. To think about, it may be that the current EMS/SCADA functionality imposes an overlooked time-bomb, manifested in an inability to adequately monitor, protect and control the power system in time.”

- Matija Naglič

A typical control centre, used nowadays to operate the power system, was initially designed to meet the operational requirements defined in the late 1960s. Despite the technological advances in SMT, digitalisation, high-speed telecommunication links, and increased computational capacity, the EMS/SCADA developments are not in line with the power network changes. The limited in time and space SCADA monitoring has a direct impact on

the observability of the power system phenomena. This affects the situational awareness of power system operators in a control room and in turn leads to a utopic misconception that the power system is under no stress predominantly. Also, the typical protection and control schemes, disseminated in remote substations, are primarily based on pre-determined and non-adaptive execution sequences that take into account only local information. This may, in combination with the increasing power system dynamics, trigger the undesired operation of conventional protection leading to cascading outages and devastating consequences. The lack of adaptive, fast response and system-wide coordinated control schemes may lead to unexpected instabilities and blackouts. To support the power system operators and prevent the out of hand situations, there is an increasing need for a *Control Room of Future* (CRoF) to meet the operation and control requirements of the today and the future power systems.

“The CRoF is relatively cost-efficient to build, but may be very expensive for society to do without.”

- Matija Naglič

The CRoF should decrease the workload of the power system operators and improve their response time, meanwhile enable proactive, more flexible, and economically efficient power system operation and control. Certainly, the real-time situational awareness should provide a holistic view and detailed insight into the power system state and operating boundaries, enabling immediate disturbance detection and comprehensive event analysis in real-time. Further, an improved primary- and backup protection system should self-adapt to the power system state changes in order to enable a reliable operation whenever needed, avoid unnecessary operations in case of harmless disturbances, and enable rigorous wide-area protection by taking system-wide considerations. Likewise, an adaptive and coordinated remedial-control system should timely execute a minimal number of the system-wide coordinated remedial actions to arrest and mitigate critical instabilities and bring the system to a stable state. Moreover, an advanced prediction system should enable proactive grid operation by performing advanced time-projection analysis of the online tuned digital power system model to reduce the occurrence of contingencies. An advanced decision-support system should assist the power system operators in improving their operational decisions in means of human-error reduction and power system optimisation. Also, it should reduce the power system operators' event response-time by automating the automation in means of advancing the existing emergency control procedures. This research field requires a broad spectrum of engineers with multidisciplinary expertise not only from the power system field, but also from the telecommunication and information systems, digital signal processing, data science, GUI design, and psychology.

“If we wait for the governments, it will be too little, too late. If we act as individuals, it will be too little. But if we act as communities, it might just be enough, just in time.”

- Rob Hopkins

The electric power sector has traditionally been served by large industrial companies selling hardware, of which developments have been mainly motivated throughout short-term financial gains. This not only limits the pace of innovation but also prevents the integration of hardware from other vendors due to vendor locked paradigm. However, the increasing trend in new often small high-tech companies adopting open-source tools shakes the conventional power market. Despite apparent benefits and potential, those companies lack trust due to the black-box paradigm, where advanced solutions are intentionally provided with no or limited knowledge of their internal workings. However, incipient open-source communities, featuring a neutral ground ecosystem, may ignite a new era of accelerated innovation and integration of advanced technologies in the energy sector. These communities, such as Linux Foundation Energy, promote open-source code of verified projects, developed by their members. The future seems to be in open-source. Yet, every innovation requires transparency and thorough validation before being applied.

“Dream big, act small.”

- Mart A.M.M. van der Meijden

6

The path of research and developments towards CRoF is full of unknowns, but every path has its start. Before being implemented into the grid, thorough vulnerability assessment and analyses on how the existing power systems accommodate the existing and emerging hardware and software components (further referred to as technologies) should be performed. The lack of advanced experimental testbeds, used to thoroughly verify the state-of-the-art technologies on a large-scale power system model, leads to mistrust of outside experts and in turn deflects the novel developments. To facilitate the use of state-of-the-art WAMPAC applications in existing power systems, and promote innovative developments towards CRoF, an advanced real-time capable cyber-physical experimental testbed is needed. The testbed should enable to perform sensitive simulations on large-scale power system models, critical analysis, and online testing of the existing and emerging technologies as hardware- and software-in-the-loop, respectively. Moreover, the testbed should encompass an actual control room for demonstration and training purposes of the power system operators. The operators would get acquainted with the performance of the newly developed algorithms, control room applications, and hardware components; perform complex operation scenarios; and practice closed-loop emergency control actions. This would enable a unique opportunity for the power system operators to meet, test, and adopt novel technologies thoroughly under realistic conditions in an isolated and flexible simulation environment, before being deployed in the real-world power systems. Moreover, this testbed would serve as a hub for the power utilities, vendors, and research organisations to promote their cooperation towards innovative developments.

“Some people call this artificial intelligence, but the reality is this technology will enhance us. So instead of artificial intelligence, I think we'll augment our intelligence.”

- Ginni Rometty

The increasing power system complexity (as a result of the energy transition) and observability of power system phenomena (as a result of the power system digitalisation) creates needs and opportunities, respectively, for the design of advanced algorithms to enhance power system modelling, protection, situational awareness, and controllability. There is a consensus that the ultramodern Machine Learning (ML) and big-data analytics are superior technologies to leverage information from datasets. Indeed, there are many possibilities for advancements, but an explicit match between the ML's strength and power system's problem to be solved must be identified beforehand. In combination with well-defined power system operating boundaries, the Artificial Intelligence (AI) technology, to which ML belongs, can be used to propel the EMS/SCADA functionality by automating the automation towards the CROF. For a start, transparency between the AI technology and the power system must be provided, to gain trust instead of another black-box. More thorough research is needed to investigate how the existing and emerging technologies influence the power systems and if/how they affect the critical cyber-security vulnerability. It is crucial to identify the power system operators' needs and to develop the related EMS/SCADA improvements to support them.

To conclude, more directly applicable scientific research is needed to support the power industry. Only if thoroughly and in time dealt with the identified challenges and requirements of modern power systems, the resulting innovative developments will expedite the energy transition towards more sustainable, environmental-friendly, efficient, reliable and self-healing power systems.

"The key to success is to imagine it first. The rest will follow."

- Matija Naglič

NOMENCLATURE

LIST OF ABBREVIATIONS

The following abbreviations are used in this thesis:

<i>Abbreviation</i>	<i>Explanation</i>
1-LG	Single Line-to-Ground
3-LG	Three-phase Line-to-Ground
AC	Alternating Current
ADC	Analog-to-Digital Converter
AI	Artificial Intelligence
AP	Affinity Propagation
ASCII	American Standard Code for Information Interchange
CPS	Cyber-Physical Systems
CRC	Cyclic Redundancy Check
CRoF	Control Room of Future
CSV	Comma Separated Value
DEG	Distributed Energy Generation
DFT	Discrete Fourier Transform
DSO	Distribution System Operator
DWT	Discrete Wavelet Transform
EMS	Energy Management System
EV	Electric Vehicles
FIR	Finite-duration Impulse Response
fps	frame per second
FRACSEC	Fraction of a Second
GE	General Electric
GLONASS	GLObal NAVigation Satellite System
GNSS	Global Navigation Satellite System

GPS	Global Positioning System
GUI	Graphical User Interface
HIL	Hardware-In-the-Loop
HVDC	High-Voltage Direct Current
ICI	Intentional Controlled Islanding
ICT	Information and Communications Technology
IEC	International Electrotechnical Commission
IED	Intelligent Electronic Device
IEEE	Institute of Electrical and Electronics Engineers
IESO	Independent Electricity System Operator
IET	Institution of Engineering and Technology
IETF	Internet Engineering Task Force
IIR	Infinite-duration Impulse Response
IoT	Internet of Things
IP	Internet Protocol
IP/MPLS	Internet Protocol/Multiprotocol Label Switching
IRIG-B	Inter-Range Instrumentation Group code-B
ITU	International Telecommunication Union
MAD	Median Absolute Deviation
ML	Machine Learning
MMC	Modular Multilevel Converter
MPLS	Multiprotocol Label Switching
MTU	Master Terminal Unit
NECRF	Next-generation EMS supported Control Room of the Future
OS	Operating System
PC	Principal Component
PC1	First (dominant) PC
PCA	Principal Component Analysis
PDC	Phasor Data Concentrators
PG	Pole-to-Ground
PMU	Phasor Measurement Unit
PP	Pole-to-Pole

PPS	Pulse Per Second
PSS	Power System Stabiliser
PTP	Precise Time Protocol
QoS	Quality of Service
RES	Renewable Energy Sources
RMS	Root Mean Square
ROCOF	Rate-Of-Change-Of-Frequency
RTU	Remote Terminal Unit
SADF	Synchro-measurement Application Development Framework
SCADA	Supervisory Control and Data Acquisition
SIL	Software-In-the-Loop
SIPS	System Integrity Protection Schemes
SLA	Service Level Agreement
SMT	Synchronised Measurement Technology
SOC	Second Of Century
SPS	Cyber-Physical Systems
SWT	Stationary Wavelet Transform
SyncE	Synchronous Ethernet
TCP	Transmission Control Protocol
TSO	Transmission System Operator
TUD	Delft University of Technology
TVE	Total Vector Error
UDP	User Datagram Protocol
URSES	Uncertainty Reduction in Smart Energy Systems
UTC	Universal Time Coordinated
WAMPAC	Wide Area Monitoring, Protection, and Control
WAN	Wide Area Network
WR	White Rabbit
WT	Wavelet Transform

LIST OF SYMBOLS AND NOTATIONS

Below follows a list of this thesis used symbols and notations.

<i>Abbreviation</i>	<i>Explanation</i>
$\bar{\cdot}$	conjugation of a complex value
$\mathbb{R}, \mathbb{R}^n, \mathbb{R}^{n \times n}$	the real number, set of n real number components of a vector, and set of n by n real number components of a matrix
\mathbb{N}	natural number
$ \cdot $	absolute value
\vee	logical OR
\wedge	logical AND
\cap	the intersection of a set
\sim	approximately
\approx	approximately equal
\neq	not equal to
$:=$	equal by definition
$==$	exactly equal
\in	element of
\notin	not element of
\leq	less than
\geq	greater than
$\arg \max$	the argument of a function for which it is maximum
\exists	there exists
\neg	logical negation

BIBLIOGRAPHY

- [1] M. Barrett, A. Belward, S. Bladen, T. Breeze *et al.*, *Living Planet Report 2018: Aiming Higher*. WWF, Oct. 2018. [Online]. Available: <https://www.worldwildlife.org/pages/living-planet-report-2018>
- [2] “Definition and Classification of Power System Stability IEEE/CIGRE Joint Task Force on Stability Terms and Definitions,” *IEEE Transactions on Power Systems*, vol. 19, no. 3, pp. 1387–1401, Aug. 2004.
- [3] J. Endrenyi, *Reliability Modelling in Electric Power Systems*. John Wiley & Sons Ltd, 1978. [Online]. Available: <https://books.google.nl/books?id=AlGRQgAACAAJ>
- [4] J. L. Carlson, R. A. Haffenden, G. W. Bassett, W. A. Buehring *et al.*, *Resilience: Theory and Application*. Department of Homeland Security, United States, Feb. 2012.
- [5] I. Adriano, Ed., *Flexible Resources for Flexible Transmission System Operation*. International Energy Agency, Oct. 2017. [Online]. Available: http://www.iea-pvps.org/-index.php?id=373&eID=dam_frontend_push&docID=4131
- [6] *Flexibility Use at Distribution Level*. Council of European Energy Regulators, 2018. [Online]. Available: <https://www.ceer.eu/documents/104400/-/-/e5186abe-67eb-4bb5-1eb2-2237e1997bbc>
- [7] E. Vaahedi, *Energy Management Systems*. John Wiley & Sons, Mar. 2014.
- [8] A. Polycarpou, “Power Quality and Voltage Sag Indices in Electrical Power Systems,” in *Electrical Generation and Distribution Systems and Power Quality Disturbances*, G. R. Rey and L. M. Muneta, Eds. IntechOpen, 2011, ch. 6.
- [9] U. Hager, C. Rehtanz, and N. Voropai, Eds., *Monitoring, Control and Protection of Interconnected Power Systems*. Springer, 2014.
- [10] P. Zhang, F. Li, and N. Bhatt, “Next-Generation Monitoring, Analysis, and Control for the Future Smart Control Center,” *IEEE Transactions on Smart Grid*, vol. 1, no. 2, pp. 186–192, Sep. 2010.
- [11] S. G. McCrady, *Designing SCADA Application Software: A Practical Approach*. Elsevier, 2013.
- [12] *Global Energy & CO2 Status Report 2017*. International Energy Agency, Mar. 2018, vol. 74.
- [13] V. Masson-Delmotte, P. Zhai, H. O. Portner, D. Roberts *et al.*, *Global warming of 1.5°C*. World Meteorological Organization, 2018. [Online]. Available: https://www.ipcc.ch/site/assets/uploads/sites/2/-2019/06/SR15_Full_Report_High_Res.pdf
- [14] D. J. Wuebbles, D. W. Fahey, K. A. Hibbard, D. J. Dokken, B. C. Stewart, T. K. Maycock *et al.*, “Our globally changing climate.” Washington, DC, USA: U.S. Global Change Research Program, 2017, pp. 35–72.
- [15] F. Harvey, “Rate of Ocean Acidification Due to Carbon Emissions Is at Highest for 300m Years,” 2013. [Online]. Available: <https://www.theguardian.com/environment/2013/oct/03/ocean-acidification-carbon-dioxide-emissions-levels>
- [16] M. A. M. M. van der Meijden, “A Sustainable and Reliable Electricity System; Inevitable and Challenging,” Delft University of Technology, Feb. 2012. [Online]. Available: <http://resolver.tudelft.nl/uuid:3d04f70f-38a1-47f4-898e-0330f528ad47>
- [17] *Connecting Europe: Electricity, 2018 Ten Year Network Development Plan, Executive Report*. ENTSO-E, Sep. 2018. [Online]. Available: https://tyndp.entsoe.eu/Documents/TYNDP%20documents/TYNDP2018/-consultation/Main%20Report/TYNDP2018_Executive%20Report.pdf

- [18] *World Energy Outlook 2018*. International Energy Agency, 2018. [Online]. Available: <https://www.oecd-ilibrary.org/content/publication/weo-2018-en>
- [19] E. Espe, V. Potdar, and E. Chang, "Prosumer Communities and Relationships in Smart Grids: A Literature Review, Evolution and Future Directions," *Energies*, vol. 11, no. 10, p. 2528, Sep. 2018.
- [20] A. Ghosh, V. Aggarwal, and H. Wan, "Strategic Prosumers: How to set the prices Dynamically in a Tiered Market?" *IEEE Transactions on Industrial Informatics*, vol. 15, no. 8, Aug. 2019.
- [21] I. Lampropoulos, G. M. A. Vanalme, and W. L. Kling, "A Methodology for Modeling the Behavior of Electricity Prosumers within the Smart Grid," in *Innovative Smart Grid Technologies Conference (ISGT)*. IEEE, Oct. 2010, pp. 1–8.
- [22] P. Kundur and N. J. Balu, *Power System Stability and Control*. McGraw-Hill, 1994.
- [23] J. Gooding, "Securing the Electric Grid with Common Cyber Security Services," 2014. [Online]. Available: <https://docplayer.net/10771861-Securing-the-electric-grid-with-common-cyber-security-services-jeff-gooding.html>
- [24] P. Tielens and D. V. Hertem, "Grid Inertia and Frequency Control in Power Systems with High Penetration of Renewables," in *Young Researchers Symposium in Electrical Power Engineering*, Jan. 2012.
- [25] L. Rutledge and D. Flynn, "Emulated Inertial Response From Wind Turbines: Gain Scheduling and Resource Coordination," *IEEE Transactions on Power Systems*, vol. 31, no. 5, pp. 3747–3755, Sep. 2016.
- [26] S. Eftekharij, V. Vittal, G. T. Heydt, B. Keel, and J. Loehr, "Small Signal Stability Assessment of Power Systems With Increased Penetration of Photovoltaic Generation: A Case Study," *IEEE Transactions on Sustainable Energy*, vol. 4, no. 4, pp. 960–967, Oct. 2013.
- [27] G. Lalor, A. Mullane, and M. O'Malley, "Frequency Control and Wind Turbine Technologies," *IEEE Transactions on Power Systems*, vol. 20, no. 4, pp. 1905–1913, Nov. 2005.
- [28] A. Ulbig, T. S. Borsche, and G. Andersson, "Impact of Low Rotational Inertia on Power System Stability and Operation," *IFAC Proceedings Volumes*, vol. 47, no. 3, pp. 7290–7297, 2014.
- [29] F. Milano, F. Dorfler, G. Hug, D. J. Hill, and G. Verbic, "Foundations and Challenges of Low-inertia Systems," in *IEEE Power Systems Computation Conference*, Jun. 2018, pp. 1–25.
- [30] W. Winter, K. Elkington, G. Bareux, and J. Kostevc, "Pushing the Limits: Europe's New Grid: Innovative Tools to Combat Transmission Bottlenecks and Reduced Inertia," *IEEE Power and Energy Magazine*, vol. 13, no. 1, pp. 60–74, Jan. 2015.
- [31] V. Telukunta, J. Pradhan, A. Agrawal, M. Singh, and S. G. Srivani, "Protection Challenges under Bulk Penetration of Renewable Energy Resources in Power Systems: A Review," *CSEE Journal of Power and Energy Systems*, vol. 3, no. 4, pp. 365–379, Dec. 2017.
- [32] S. Eftekharij, V. Vittal, Heydt, B. Keel, and J. Loehr, "Impact of Increased Penetration of Photovoltaic Generation on Power Systems," *IEEE Transactions on Power Systems*, vol. 28, no. 2, pp. 893–901, May 2013.
- [33] A. G. Phadke, W. A. L. L. Peter, D. I. N. G. Lei, and V. Terzija, "Improving the Performance of Power System Protection Using Wide Area Monitoring Systems," *Journal of Modern Power Systems and Clean Energy*, vol. 4, no. 3, pp. 319–331, Jul. 2016.
- [34] "Global power consumption trend over 1990 - 2018," Enerdata. [Online]. Available: <https://yearbook.enerdata.net/electricity/electricity-domestic-consumption-data.html>
- [35] E. D. Knapp, "Industrial Network Security," in *Securing Critical Infrastructure Networks for Smart Grid, SCADA, and Other Industrial Control Systems*, 2nd ed. Syngress, 2015.
- [36] X. Fang, S. Misra, G. Xue, and D. Yang, "Smart Grid - the New and Improved Power Grid: A Survey," *IEEE Communications Surveys & Tutorials*, vol. 14, no. 4, pp. 944–980, 2012.

- [37] V. Madani, M. Parashar, A. Jampala, and J. Giri, "Frontiers of Synchrophasor Solutions Deployment," in *International Conference on Power Systems (ICPS)*. IEEE, Dec. 2017.
- [38] A. Atputharajah and T. K. Saha, "Power System Blackouts - Literature Review," in *International Conference on Industrial and Information Systems (ICIIS)*. IEEE, Dec. 2009.
- [39] N. B. Soni and D. Mukherjee, "A Review Study on Power System Blackouts," *International Journal of Scientific and Research Publications (IJSRP)*, vol. 8, no. 5, May 2018.
- [40] Y. K. Wu, S. M. Chang, and Y. L. Hu, "Literature Review of Power System Blackouts," *Energy Procedia*, vol. 141, pp. 428–431, Dec. 2017.
- [41] H. H. Alhelou, M. Hamedani-Golshan, T. Njenda, and P. Siano, "A Survey on Power System Blackout and Cascading Events: Research Motivations and Challenges," *Energies*, vol. 12, no. 4, p. 682, Feb. 2019.
- [42] *The Third Industrial Revolution Roadmap Next Economy for the Metropolitan Region of Rotterdam and The Hague*. TIR Consulting Group, 2016. [Online]. Available: <https://mrdh.nl/sites/mrdh.nl/files/files/The-Third-Industrial-Revolution-Final-Report-RNE.pdf>
- [43] Bloomberg, "Digitalization of Energy Systems," Nov. 2017. [Online]. Available: <https://about.bnef.com/blog/digitalization-energy-systems/>
- [44] C. W. Gellings, M. Samotyj, and B. Howe, "The Future's Smart Delivery System," *IEEE Power and Energy Magazine*, vol. 2, no. 5, pp. 40–48, Sep. 2004.
- [45] V. Terzija, G. Valverde, D. Cai, P. Regulski *et al.*, "Wide-area Monitoring, Protection, and Control of Future Electric Power Networks," *Proceedings of the IEEE*, vol. 99, no. 1, pp. 80–93, 2011.
- [46] S. Nuthalapati, Ed., *Power System Grid Operation Using Synchrophasor Technology*. Springer International Publishing, 2019.
- [47] A. Phadke, J. Thorp, and M. Adamiak, "A New Measurement Technique for Tracking Voltage Phasors, Local System Frequency, and Rate of Change of Frequency," *IEEE Transactions on Power Apparatus and Systems*, vol. PAS-102, no. 5, pp. 1025–1038, May 1983.
- [48] A. G. Phadke and B. I. Tianshu, "Phasor Measurement Units, WAMS, and Their Applications in Protection and Control of Power Systems," *Journal of Modern Power Systems and Clean Energy*, vol. 6, no. 4, pp. 619–629, Jul. 2018.
- [49] A. G. Phadke and J. S. Thorp, *Synchronized Phasor Measurements and Their Applications*. Springer, 2017.
- [50] "IEEE Standard for Synchrophasor Measurements for Power Systems," *IEEE Std C37.118.1-2011*, pp. 1–61, Dec. 2011.
- [51] A. Derviskadic, "Synchronized Sensing for Wide-Area Situational Awareness of Electrical Grids in Non-Stationary Operating Conditions," 2019. [Online]. Available: <http://infoscience.epfl.ch/record/272131>
- [52] A. G. Phadke and B. Kasztenny, "Synchronized Phasor and Frequency Measurement under Transient Conditions," *IEEE Transactions on Power Delivery*, vol. 24, no. 1, pp. 89–95, Jan. 2009.
- [53] D. Macii, D. Fontanelli, G. Barchi, and D. Petri, "Impact of Acquisition Wideband Noise on Synchrophasor Measurements: A Design Perspective," *IEEE Transactions on Instrumentation and Measurement*, vol. 65, no. 10, pp. 2244–2253, Oct. 2016.
- [54] L. I. U. Hao, B. I. Tianshu, X. Chang, G. U. O. Xiaolong *et al.*, "Impacts of Subsynchronous and Supersynchronous Frequency Components on Synchrophasor Measurements," *Journal of Modern Power Systems and Clean Energy*, vol. 4, no. 3, pp. 362–369, Jul. 2016.
- [55] R. Lyons, "Using the DFT as a Filter: Correcting a Misconception," Feb. 2013. [Online]. Available: <https://www.dsprelated.com/showarticle/187.php>
- [56] A. Derviskadic, P. Romano, and M. Paolone, "Iterative-Interpolated DFT for Synchrophasor Estimation: A Single Algorithm for P- and M-Class Compliant PMUs," *IEEE Transactions on Instrumentation and Measurement*, vol. 67, no. 3, pp. 547–558, March 2018.

- [57] J. R. Razo-Hernandez, A. Mejia-Barron, D. Granados-Lieberman, M. Valtierra-Rodriguez, and J. F. Gomez-Aguilar, "A New Phasor Estimator for PMU Applications: P Class and M Class," *Journal of Modern Power Systems and Clean Energy*, vol. 8, no. 1, pp. 55–66, January 2020.
- [58] C. Thilakarathne, L. Meegahapola, and N. Fernando, "Improved Synchrophasor Models for Power System Dynamic Stability Evaluation Based on IEEE C37.118.1 Reference Architecture," *IEEE Transactions on Instrumentation and Measurement*, vol. 66, no. 11, pp. 2937–2947, Nov. 2017.
- [59] "IEEE Standard for Synchrophasors for Power Systems," *IEEE Std 1344-1995*, pp. i–, 1995.
- [60] "IEEE Standard for Synchrophasors for Power Systems," *IEEE Std C37.118-2005*, pp. 1–65, Mar. 2006.
- [61] "IEEE Standard for Synchrophasor Data Transfer for Power Systems," *IEEE Std C37.118.2-2011*, pp. 1–53, Dec. 2011.
- [62] "Communication Networks and Systems for Power Utility Automation – Part 90-5: Use of IEC 61850 to Transmit Synchrophasor Information According to IEEE C37.118," *IEC TR 61850 90-5*, 2012.
- [63] "IEEE Standard for Synchrophasor Measurements for Power Systems – Amendment 1: Modification of Selected Performance Requirements," *IEEE Std C37.118.1a-2014*, pp. 1–25, Apr. 2014.
- [64] M. Adamiak and B. Kasztenny, "Implementation and Performance of Synchrophasor Function within Microprocessor Based Relays," in *Protection and Control Journal*. GE Multilin, Dec. 2007, pp. 35–45.
- [65] M. U. Usman and M. O. Faruq, "Applications of Synchrophasor Technologies in Power Systems," *Journal of Modern Power Systems and Clean Energy*, vol. 7, no. 2, pp. 211–226, Oct. 2018.
- [66] M. Kezunovic, S. Meliopoulos, V. Venkatasubramanian, and V. Vittal, *Application of Time-Synchronized Measurements in Power System Transmission Networks*. Springer International Publishing, 2014, ch. Introduction, pp. 1–16.
- [67] *IRIG Standard 200 – 04, IRIG serial time code formats*, Range Commanders Council Std., Sep. 2004.
- [68] "IEEE Standard for a Precision Clock Synchronization Protocol for Networked Measurement and Control Systems," *IEEE Std 1588-2008*, pp. 1–300, Jul. 2008.
- [69] "IEEE Standard Profile for Use of IEEE 1588 Precision Time Protocol in Power System Applications," *IEEE Std C37.238-2017*, Jun. 2017.
- [70] CERN, "The White Rabbit Project." [Online]. Available: <http://white-rabbit.web.cern.ch/>
- [71] O. Ronen and M. Lipinski, "Enhanced Synchronization Accuracy in IEEE1588," in *2015 IEEE International Symposium on Precision Clock Synchronization for Measurement, Control, and Communication (ISPCS)*. IEEE, Oct 2015, pp. 76–81.
- [72] A. Derviskadic, R. Razzaghi, Q. Walger, and M. Paolone, "The White Rabbit Time Synchronization Protocol for Synchrophasor Networks," *IEEE Transactions on Smart Grid*, vol. 11, no. 1, pp. 726–738, Jan 2020.
- [73] T. Popovic, M. Kezunovic, and B. Krstajic, "IEEE Guide for Phasor Data Concentrator Requirements for Power System Protection, Control, and Monitoring," *IEEE Std C37.244-2013*, vol. 25, pp. 1–65, May 2013.
- [74] A. G. Phadke and J. S. Thorp, "Communication needs for Wide Area Measurement applications," in *2010 5th International Conference on Critical Infrastructure (CRIS)*. IEEE, Sep. 2010, pp. 1–7.
- [75] A. Derviskadic, P. Romano, M. Pignati, and M. Paolone, "Architecture and Experimental Validation of a Low-Latency Phasor Data Concentrator," *IEEE Transactions on Smart Grid*, vol. 9, no. 4, pp. 2885–2893, July 2018.
- [76] Y. Chompoobutrgool and L. Vanfretti, "Analysis of Time Delay Effects for Wide-area Damping Control Design Using Dominant Path Signals," in *Power and Energy Society General Meeting*. IEEE, Jul. 2014, pp. 1–5.
- [77] D. Roberson and J. F. O'Brien, "Loop Shaping of a Wide-Area Damping Controller Using HVDC," *IEEE Transactions on Power Systems*, vol. 32, no. 3, pp. 2354–2361, May 2017.

- [78] F. Bai, L. Zhu, Y. Liu, X. Wang *et al.*, "Design and Implementation of a Measurement-based Adaptive Wide-area Damping Controller Considering Time Delays," *Electric Power Systems Research*, vol. 130, pp. 1–9, Jan. 2016.
- [79] B. B. Gupta and T. Akhtar, "A Survey on Smart Power Grid: Frameworks, Tools, Security Issues, and Solutions," *Annals of Telecommunications*, vol. 72, no. 9, pp. 517–549, Oct. 2017.
- [80] S. Tan, D. De, W.-Z. Song, J. Yang, and S. K. Das, "Survey of Security Advances in Smart Grid: A Data Driven Approach," *IEEE Communications Surveys & Tutorials*, vol. 19, no. 1, pp. 397–422, 2017.
- [81] S. Borlase, *Smart Grids: Infrastructure, Technology, and Solutions*. CRC press, 2016.
- [82] V. Madani, J. Giri, D. Kosterev, D. Novosel, and D. Brancaccio, "Challenging Changing Landscapes: Implementing Synchrophasor Technology in Grid Operations in the WECC Region," *IEEE Power and Energy Magazine*, vol. 13, no. 5, pp. 18–28, Sep. 2015.
- [83] D. Novosel, V. Madani, B. Bhargave, K. Vu, and J. Cole, "Dawn of the Grid Synchronization," *IEEE Journals & Magazine*, vol. 6, no. 1, pp. 49–60, Jan. 2008.
- [84] F. Aminifar, M. Fotuhi-Firuzabad, A. Safdarian, A. Davoudi, and M. Shahidehpour, "Synchrophasor Measurement Technology in Power Systems: Panorama and State-of-the-art," *IEEE Access*, vol. 2, pp. 1607–1628, 2014.
- [85] *Wide Area Monitoring - Current Continental Europe TSOs Applications Overview*. System Protection & Dynamics Working Group, ENTSO-E, Sep. 2015.
- [86] M. Kezunovic, S. Meliopoulos, V. Venkatasubramanian, and V. Vittal, *Application of Time-synchronized Measurements in Power System Transmission Networks*. Springer, 2014.
- [87] C. Wang, Z. Qin, Y. Hou, and J. Yan, "Multi-area Dynamic State Estimation with PMU Measurements by an Equality Constrained Extended Kalman Filter," *IEEE Transactions on Smart Grid*, vol. 9, no. 2, pp. 900–910, Mar. 2018.
- [88] S. Datta and V. Vittal, "Operational Risk Metric for Dynamic Security Assessment of Renewable Generation," *IEEE Transactions on Power Systems*, vol. 32, no. 2, pp. 1389–1399, Mar. 2017.
- [89] Y. Zhang, Y. Xu, Z. Y. Dong, and R. Zhang, "A Hierarchical Self-adaptive Data-analytics Method for Real-time Power System Short-term Voltage Stability Assessment," *IEEE Transactions on Industrial Informatics*, vol. 15, no. 1, pp. 74–84, Jan. 2019.
- [90] J. Follum, J. W. Pierre, and R. Martin, "Simultaneous Estimation of Electromechanical Modes and Forced Oscillations," *IEEE Transactions on Power Systems*, vol. 32, no. 5, pp. 3958–3967, Sep. 2017.
- [91] G. Coletta, A. Vaccaro, and D. Villacci, "A Review of the Enabling Methodologies for PMUs-based Dynamic Thermal Rating of Power Transmission Lines," *Electric Power Systems Research*, vol. 152, pp. 257–270, Nov. 2017.
- [92] M. M. Esfahani and G. R. Yousefi, "Real Time Congestion Management in Power Systems Considering Quasi-dynamic Thermal Rating and Congestion Clearing Time," *IEEE Transactions on Industrial Informatics*, vol. 12, no. 2, pp. 745–754, Apr. 2016.
- [93] A. Pal, P. Chatterjee, J. S. Thorp, and V. A. Centeno, "Online Calibration of Voltage Transformers Using Synchrophasor Measurements," *IEEE Transactions on Power Delivery*, vol. 31, no. 1, pp. 370–380, Feb. 2016.
- [94] S. Thale, V. Agarwal, and S. Gore, "Adaptive Protection Scheme with Fault Detection, Classification and Isolation Features for Off-grid Distributed Generation System," in *IEEE International Conference on Power Electronics, Drives and Energy Systems (PEDES)*. IEEE, Dec. 2012, pp. 1–6.
- [95] P. M. Ashton, C. S. Saunders, G. A. Taylor, A. M. Carter, and M. E. Bradley, "Inertia Estimation of the GB Power System Using Synchrophasor Measurements," *IEEE Transactions on Power Systems*, vol. 30, no. 2, pp. 701–709, Mar. 2015.

- [96] Y. Liu, K. Sun, and Y. Liu, "A Measurement-based Power System Model for Dynamic Response Estimation and Instability Warning," *Electric Power Systems Research*, vol. 124, pp. 1–9, 2015.
- [97] M. Naglic, L. Liu, I. Tyuryukanov, M. Popov, M. A. M. van der Meijden, and V. Terzija, "Synchronized Measurement Technology Supported AC and HVDC Online Disturbance Detection," *Electric Power Systems Research*, vol. 160, pp. 308–317, Jul. 2018.
- [98] H. Gharavi and B. Hu, "Space-time Approach for Disturbance Detection and Classification," *IEEE Transactions on Smart Grid*, vol. 9, no. 5, pp. 5132–5140, Sep. 2018.
- [99] I. Niazazari and H. Livani, "A PMU-data-driven Disruptive Event Classification in Distribution Systems," *Electric Power Systems Research*, vol. 157, pp. 251–260, Apr. 2018.
- [100] F. Bai, Y. Liu, Y. Liu, K. Sun *et al.*, "A Measurement-based Approach for Power System Instability Early Warning," *Protection and Control of Modern Power Systems*, vol. 1, no. 1, p. 4, Jun. 2016.
- [101] A. Pal, I. Singh, and B. Bhargava, "Stress Assessment in Power Systems and Its Visualization Using Synchrophasor Based Metrics," in *2014 North American Power Symposium (NAPS)*. IEEE, Sep. 2014, pp. 1–6.
- [102] *Diagnosing Equipment Health and Mis-operations with PMU Data*, North American Synchrophasor Initiative (NASPI), May 2015. [Online]. Available: <https://www.naspi.org/node/365>
- [103] S. A. M. Javadian, R. Tamizkar, and M.-R. Haghifam, "A Protection and Reconfiguration Scheme for Distribution Networks with DG," in *PowerTech*. IEEE, Jun. 2009, pp. 1–8.
- [104] J. O'Brien, A. Deronja, A. Apostolov, A. Arana, M. Begovic *et al.*, "Use of Synchrophasor Measurements in Protective Relaying Applications," *IEEE PSRC System Protection Subcommittee Working Group C14*, 2014. [Online]. Available: http://www.pes-psrc.org/kb/published/reports/-Use%20of%20Synchrophasor%20Measurements%20in%20Protective%20Relaying%20Applications_final.pdf
- [105] M. K. Jena, S. R. Samantaray, and B. K. Panigrahi, "A New Adaptive Dependability-security Approach to Enhance Wide Area Back-up Protection of Transmission System," *IEEE Transactions on Smart Grid*, vol. 9, no. 6, pp. 6378–6386, Nov. 2018.
- [106] J. He, L. Liu, W. Li, and M. Zhang, "Development and Research on Integrated Protection System Based on Redundant Information Analysis," *Protection and Control of Modern Power Systems*, vol. 1, no. 1, p. 13, Oct. 2016.
- [107] P. Gopakumar, B. Mallikajuna, M. J. B. Reddy, and D. K. Mohanta, "Remote Monitoring System for Real Time Detection and Classification of Transmission Line Faults in a Power Grid Using PMU Measurements," *Protection and Control of Modern Power Systems*, vol. 3, no. 1, p. 16, Jun. 2018.
- [108] M. Pignati, L. Zanni, P. Romano, R. Cherkaoui, and M. Paolone, "Fault Detection and Faulted Line Identification in Active Distribution Networks Using Synchrophasors-Based Real-Time State Estimation," *IEEE Transactions on Power Delivery*, vol. 32, no. 1, pp. 381–392, Feb 2017.
- [109] V. Madani, D. Novosel, S. Horowitz, M. Adamiak *et al.*, "IEEE PSRC Report on Global Industry Experiences With System Integrity Protection Schemes (SIPS)," *IEEE Transactions on Power Delivery*, vol. 25, no. 4, pp. 2143–2155, Oct. 2010.
- [110] X. Liu, J. M. Kennedy, D. M. Lavery, D. J. Morrow *et al.*, "Wide-area Phase-angle Measurements for Islanding Detection – An Adaptive Nonlinear Approach," *IEEE Transactions on Power Delivery*, vol. 31, no. 4, pp. 1901–1911, Aug. 2016.
- [111] P. Mahat, Z. Chen, and B. Bak-Jensen, "Review on Islanding Operation of Distribution System with Distributed Generation," in *Power and Energy Society General Meeting*. IEEE, Jul. 2011, pp. 1–8.
- [112] H. You, V. Vittal, and X. Wang, "Slow Coherency-based Islanding," *IEEE Transactions on Power Systems*, vol. 19, no. 1, pp. 483–491, 2004.

- [113] L. Ding, Y. Guo, P. Wall, K. Sun, and V. Terzija, "Identifying the Timing of Controlled Islanding Using a Controlling UEP Based Method," *IEEE Transactions on Power Systems*, vol. 33, no. 6, pp. 5913–5922, Nov. 2018.
- [114] U. Rudez and R. Mihalic, "WAMS-based Underfrequency Load Shedding with Short-term Frequency Prediction," *IEEE Transactions on Power Delivery*, vol. 31, no. 4, pp. 1912–1920, Aug. 2016.
- [115] Y. Lpiu, R. Fan, and V. Terzija, "Power System Restoration: A Literature Review from 2006 to 2016," *Journal of Modern Power Systems and Clean Energy*, vol. 4, no. 3, pp. 332–341, Jul. 2016.
- [116] C. Basu, A. Agrawal, J. Hazra, A. Kumar *et al.*, "Understanding Events for Wide-area Situational Awareness," in *Innovative Smart Grid Technologies Conference (ISGT)*. IEEE, Feb. 2014, pp. 1–5.
- [117] C. Basu, M. Padmanaban, S. Guillon, L. Cauchon, M. D. Montigny, and I. Kamwa, "Situational Awareness for the Electrical Power Grid," *IBM Journal of Research and Development*, vol. 60, no. 1, pp. 10:1–10:11, Jan. 2016.
- [118] W. Sattinger and G. Giannuzzi, "Monitoring Continental Europe: An Overview of WAM Systems Used in Italy and Switzerland," *IEEE Power and Energy Magazine*, vol. 13, no. 5, pp. 41–48, Sep. 2015.
- [119] A. G. Phadke, H. Volskis, R. M. de Moraes, T. Bi *et al.*, "The Wide World of Wide-area Measurement," *IEEE Power and Energy Magazine*, vol. 6, no. 5, pp. 52–65, Sep. 2008.
- [120] T. Rauhala, K. Saarinen, M. Latvala, M. Laasonen, and M. Uusitalo, "Applications of Phasor Measurement Units and Wide-area Measurement System in Finland," in *PowerTech*. IEEE, Jun. 2011, pp. 1–8.
- [121] B. Heimisson, "Automatic Controls Using WAMs," in *SGTech*, Mar. 2017.
- [122] "GE Power to Deliver World's Largest Wide Area Monitoring System (WAMS)," Webpage, Jul. 2018. [Online]. Available: <https://www.genewsroom.com/press-releases/ge-power-deliver-world%E2%80%99s-largest-wide-area-monitoring-system-wams-284429>
- [123] S. Sarkar, G. Saha, G. Pal, and T. Karmakar, "Indian Experience on Smart Grid Application in Blackout Control," in *National Systems Conference (NSC)*. IEEE, Dec. 2015, pp. 1–6.
- [124] C. Huang, L. I. Fangxing, Z. H. O. U. Dao, G. U. O. Jiahui *et al.*, "Data Quality Issues for Synchrophasor Applications Part I: A Review," *Journal of Modern Power Systems and Clean Energy*, vol. 4, no. 3, pp. 342–352, Jul. 2016.
- [125] P. Palensky, A. A. V. D. Meer, C. D. Lopez, A. Joseph, and K. Pan, "Cosimulation of Intelligent Power Systems: Fundamentals, Software Architecture, Numerics, and Coupling," *IEEE Industrial Electronics Magazine*, vol. 11, no. 1, pp. 34–50, Mar. 2017.
- [126] A. W. Colombo, S. Kamouskos, O. Kaynak, Y. Shi, and S. Yin, "Industrial Cyberphysical Systems: A Backbone of the Fourth Industrial Revolution," *IEEE Industrial Electronics Magazine*, vol. 11, no. 1, pp. 6–16, Mar. 2017.
- [127] M. Stifter, J. Cordova, J. Kazmi, and R. Arghandeh, "Real-Time Simulation and Hardware-in-the-Loop Testbed for Distribution Synchrophasor Applications," *Energies*, vol. 11, no. 4, p. 876, Apr. 2018.
- [128] S. S. Biswas, J. H. Kim, and A. K. Srivastava, "Development of a Smart Grid Test Bed and Applications in PMU and PDC Testing," in *2012 North American Power Symposium (NAPS)*. IEEE, Sep. 2012, pp. 1–6.
- [129] C. Liu, Z. H. Rather, N. Stearn, Z. Chen, C. L. Bak, and P. Thogersen, "Practical Testing and Performance Analysis of Phasor Measurement Unit Using Real Time Digital Simulator (RTDS)," in *IEEE International Energy Conference (ENERGYCON)*, Sep. 2012, pp. 408–414.
- [130] F. L. Grando, A. E. Lazzaretti, G. W. Denardin, M. Moreto, and H. V. Neto, "A Synchrophasor Test Platform for Development and Assessment of Phasor Measurement Units," *IEEE Transactions on Industry Applications*, vol. 54, no. 4, pp. 3122–3131, Jul. 2018.

- [131] J. Kilter, I. Palu, M. S. Almas, and L. Vanfretti, "Experiences with Dynamic PMU Compliance Testing Using Standard Relay Testing Equipment," in *Innovative Smart Grid Technologies Conference (ISGT)*. IEEE, Feb. 2015, pp. 1–5.
- [132] D. Colangelo, D. Hoogenboom, E. Dierikx, G. Rietveld, and G. Frigo, "Metrological Characterization of a PMU Calibrator in the 25 Hz to 3 kHz Range," in *PowerTech*. IEEE, Jun. 2017, pp. 1–6.
- [133] P. Castello, C. Muscas, P. A. Pegoraro, and S. Sulis, "Automated Test System to Assess Reporting Latency in PMUs," in *IEEE International Instrumentation and Measurement Technology Conference*. IEEE, May 2016, pp. 1–6.
- [134] B. Chen, K. L. Butler-Purpy, A. Goulart, and D. Kundur, "Implementing a Real-time Cyber-physical System Test Bed in RTDS and OPNET," in *2014 North American Power Symposium (NAPS)*. IEEE, Sep. 2014, pp. 1–6.
- [135] D. R. Gurusinge, D. Ouellette, and A. D. Rajapakse, "Development of a Test Platform for Synchrophasor Applications with Real-time Digital Simulator," in *2016 Electrical Engineering Conference (EECon)*. IEEE, Dec. 2016, pp. 13–18.
- [136] A. S. Leger, J. Spruce, T. Banwell, and M. Collins, "Smart Grid Testbed for Wide-Area Monitoring and Control Systems," in *IEEE/PES Transmission and Distribution Conference and Exposition*. IEEE, May 2016, pp. 1–5.
- [137] L. Vanfretti, V. H. Aarstrand, M. S. Almas, V. S. Peric, and J. O. Gjerde, "A Software Development Toolkit for Real-time Synchrophasor Applications," in *IEEE Grenoble Conference*. IEEE, Jun. 2013, pp. 1–6.
- [138] M. S. Almas, L. Vanfretti, and M. Baudette, "BabelFish – Tools for IEEE C37.118.2-compliant Real-time Synchrophasor Data Mediation," *SoftwareX*, vol. 6, pp. 209–216, 2017.
- [139] M. S. Almas, M. Baudette, L. Vanfretti, S. Lovlund, and J. O. Gjerde, "Synchrophasor Network, Laboratory and Software Applications Developed in the STRONG2rid Project," in *Power and Energy Society General Meeting*. IEEE, Jul. 2014, pp. 1–5.
- [140] U. Adhikari, T. Morris, and S. Pan, "WAMS Cyber-physical Test Bed for Power System, Cybersecurity Study, and Data Mining," *IEEE Transactions on Smart Grid*, vol. 8, no. 6, pp. 2744–2753, Nov. 2017.
- [141] RTDS, *RSCAD 5.003 Manuals*, 2018.
- [142] RTDS, *Company Profile*, 2019. [Online]. Available: <https://www.rtds.com/about/company-profile/>
- [143] "Synchrophasor Measurement Test Suite Specification–version 2," *IEEE TSS – v2*, pp. 1–43, Sep. 2015.
- [144] "MATLAB Central," Jul. 2019. [Online]. Available: <http://www.mathworks.com/matlabcentral>
- [145] J. Warichet, T. Sezi, and J.-C. Maun, "Considerations about Synchrophasors Measurement in Dynamic System Conditions," *International Journal of Electrical Power & Energy Systems*, vol. 31, no. 9, pp. 452–464, Oct. 2009.
- [146] S. Maharjan, J. C.-H. Peng, J. E. Martinez, W. Xiao *et al.*, "Improved Sample Value Adjustment for Synchrophasor Estimation at Off-nominal Power System Conditions," *IEEE Transactions on Power Delivery*, vol. 32, no. 1, pp. 33–44, Feb. 2017.
- [147] D. Macii, D. Petri, and A. Zorat, "Accuracy Analysis and Enhancement of DFT-based Synchrophasor Estimators in Off-nominal Conditions," *IEEE Transactions on Instrumentation and Measurement*, vol. 61, no. 10, pp. 2653–2664, Oct. 2012.
- [148] G. Barchi, D. Macii, and D. Petri, "Synchrophasor Estimators Accuracy: A Comparative Analysis," *IEEE Transactions on Instrumentation and Measurement*, vol. 62, no. 5, pp. 963–973, May 2013.
- [149] A. J. Roscoe, "Exploring the Relative Performance of Frequency-tracking and Fixed-filter Phasor Measurement Unit Algorithms under C37.118 Test Procedures, the Effects of Interharmonics, and Initial Attempts at Merging P-class Response with M-class Filtering," *IEEE Transactions on Instrumentation and Measurement*, vol. 62, no. 8, pp. 2140–2153, Aug. 2013.

- [150] N. Pandit and K. Khandeparkar, "Design and Implementation of IEEE C37.118 based Phasor Data Concentrator & PMU Simulator for Wide Area Measurement System," Tech. Rep., May 2012. [Online]. Available: <https://sourceforge.net/projects/iitbpd/files/Technical%20Document.pdf>
- [151] S. Sandi, B. Krstajic, and T. Popovic, "pyPMU – Open Source Python Package for Synchrophasor Data Transfer," in *2016 24th Telecommunications Forum (TELFOR)*. IEEE, Nov. 2016, pp. 1–4.
- [152] "Grid Protection Alliance," Dec. 2017. [Online]. Available: <https://www.gridprotectionalliance.org>
- [153] W. R. Stevens, *TCP/IP Illustrated, Volume 1: The Protocols*. Addison-Wesley Professional, Jan. 1994.
- [154] W. R. Stevens and G. R. Wright, *TCP/IP Illustrated, Volume 2: The Implementation*. Addison-Wesley Professional, Jan. 1995.
- [155] M. Naglic, "Synchro-measurement Application Development Framework: An IEEE Standard C37.118.2-2011 Supported MATLAB Library," GitHub, 2018. [Online]. Available: https://github.com/matijanaglich/SADF_IEEE_C37.118.2-2011
- [156] "IEEE Recommended Practice for Monitoring Electric Power Quality," *IEEE Std 1159-2009 (Revision of IEEE Std 1159-1995)*, pp. 1–81, Jun. 2009.
- [157] M. V. Ribeiro, J. Szczupak, M. R. Iravani, I. Y. H. Gu *et al.*, "Emerging Signal Processing Techniques for Power Quality Applications," *EURASIP Journal on Advances in Signal Processing*, vol. 2007, no. 1, p. 087425, Dec. 2007.
- [158] M. H. Bollen and I. Gu, *Signal Processing of Power Quality Disturbances*. John Wiley & Sons, 2006.
- [159] H. Eristi, Ö. Yildrm, B. Eristi, and Y. Demir, "Optimal Feature Selection for Classification of the Power Quality Events Using Wavelet Transform and Least Squares Support Vector Machines," *International Journal of Electrical Power & Energy Systems*, vol. 49, pp. 95–103, 2013.
- [160] Z. L. Gaing, "Wavelet-based Neural Network for Power Disturbance Recognition and Classification," *IEEE Transactions on Power Delivery*, vol. 19, no. 4, pp. 1560–1568, 2004.
- [161] M. Caujolle, M. Petit, G. Fleury, and L. Berthet, "Reliable Power Disturbance Detection Using Wavelet Decomposition or Harmonic Model Based Kalman Filtering," in *International Conference on Harmonics and Quality of Power (ICHQP)*. IEEE, 2010, pp. 1–6.
- [162] K. Thirumala, A. C. Umarikar, and T. Jain, "Estimation of Single-phase and Three-phase Power-quality Indices Using Empirical Wavelet Transform," *IEEE Transactions on Power Delivery*, vol. 30, no. 1, pp. 445–454, 2015.
- [163] M. S. Azam, F. Tu, K. R. Pattipati, and R. Karanam, "A Dependency Model-based Approach for Identifying and Evaluating Power Quality Problems," *IEEE Transactions on Power Delivery*, vol. 19, no. 3, pp. 1154–1166, 2004.
- [164] S. Santoso, W. M. Grady, E. J. Powers, J. Lamoree, and S. C. Bhatt, "Characterization of Distribution Power Quality Events with Fourier and Wavelet Transforms," *IEEE Transactions on Power Delivery*, vol. 15, no. 1, pp. 247–254, 2000.
- [165] S. Mishra, C. N. Bhende, and B. K. Panigrahi, "Detection and Classification of Power Quality Disturbances Using S-transform and Probabilistic Neural Network," *IEEE Transactions on Power Delivery*, vol. 23, no. 1, pp. 280–287, 2008.
- [166] S. Suja and J. Jerome, "Pattern Recognition of Power Signal Disturbances Using S Transform and TT Transform," *International Journal of Electrical Power & Energy Systems*, vol. 32, no. 1, pp. 37–53, 2010.
- [167] S. Mallat and W. L. Hwang, "Singularity Detection and Processing with Wavelets," *IEEE Transactions on Information Theory*, vol. 38, no. 2, pp. 617–643, 1992.
- [168] K. De Kerf, K. Srivastava, M. Reza, D. Bekaert *et al.*, "Wavelet-based Protection Strategy for DC Faults in Multi-terminal VSC HVDC Systems," *IET Generation, Transmission & Distribution*, vol. 5, no. 4, pp. 496–503, 2011.

- [169] L. Liu, M. Popov, M. Van Der Meijden, and V. Terzija, "A Wavelet Transform-based Protection Scheme of Multi-terminal HVDC System," in *International Conference on Power System Technology (POWERCON)*. IEEE, 2016, pp. 1–6.
- [170] Y. Yang, T. Pierce, and J. Carbonell, "A Study of Retrospective and On-line Event Detection," in *International ACM SIGIR conference on Research and development in information retrieval*. ACM, 1998, pp. 28–36.
- [171] A. J. Allen, S. W. Sohn, S. Santoso, and W. M. Grady, "Algorithm for Screening PMU Data for Power System Events," in *Innovative Smart Grid Technologies Conference (ISGT)*. IEEE, 2012, pp. 1–6.
- [172] S. Li and X. Wang, "Monitoring Disturbances in Smart Grids Using Distributed Sequential Change Detection," in *Computational Advances in Multi-Sensor Adaptive Processing (CAMSAP)*. IEEE, 2013, pp. 432–435.
- [173] J. Ma, Y. V. Makarov, R. Diao, P. V. Etingov, J. E. Dagle, and E. De Tuglie, "The Characteristic Ellipsoid Methodology and Its Application in Power Systems," *IEEE Transactions on Power Systems*, vol. 27, no. 4, pp. 2206–2214, 2012.
- [174] Y. Ge, A. J. Flueck, D.-K. Kim, J.-B. Ahn *et al.*, "Power System Real-time Event Detection and Associated Data Archival Reduction Based on Synchrophasors," *IEEE Transactions on Smart Grid*, vol. 6, no. 4, pp. 2088–2097, 2015.
- [175] Y. Seyedi, H. Karimi, and J. M. Guerrero, "Centralized Disturbance Detection in Smart Microgrids with Noisy and Intermittent Synchrophasor Data," *IEEE Transactions on Smart Grid*, vol. 8, no. 6, pp. 2775–2783, 2017.
- [176] C. Leys, C. Ley, O. Klein, P. Bernard, and L. Licata, "Detecting Outliers: Do Not Use Standard Deviation around the Mean, Use Absolute Deviation around the Median," *Journal of Experimental Social Psychology*, vol. 49, no. 4, pp. 764–766, 2013.
- [177] M. Naglic, "Synchronized Measurement Technology Supported AC and HVDC Online Disturbance Detection," GitHub, 2020. [Online]. Available: https://github.com/matijanaglich/SMT_disturbance_detection
- [178] P. M. Anderson and A. A. Fouad, *Power System Control and Stability*, 2nd ed. Wiley-Interscience, 2003.
- [179] D. Schoenwald, F. Wilches-Bernal, D. Trudnowski, B. Pierre, and R. Elliott, "Data Considerations in Real-Time PMU Feedback Control Systems," *North American SynchroPhasor Initiative (NASPI)*, Apr. 2019. [Online]. Available: https://www.naspi.org/sites/default/files/2019-04/01_snl_schoenwald_data_considerations_20190416.pdf
- [180] M. Klein, G. J. Rogers, and P. Kundur, "A Fundamental Study of Inter-area Oscillations in Power Systems," *IEEE Transactions on Power Systems*, vol. 6, no. 3, pp. 914–921, 1991.
- [181] J. H. Chow, *Power System Coherency and Model Reduction*. Springer, 2013.
- [182] I. Tyuryukanov, M. Naglic, M. Popov, and M. A. M. M. van der Meijden, *Implementation of Slow Coherency Based Controlled Islanding Using DIgSILENT PowerFactory and MATLAB*. Springer New York, 2018.
- [183] B. P. Padhy, S. C. Srivastava, and N. K. Verma, "A Coherency-Based Approach for Signal Selection for Wide Area Stabilizing Control in Power Systems," *IEEE Systems Journal*, vol. 7, no. 4, pp. 807–816, Dec. 2013.
- [184] R. Podmore, "Identification of Coherent Generators for Dynamic Equivalents," *IEEE Transactions on Power Apparatus and Systems*, no. 4, pp. 1344–1354, 1978.
- [185] "Analysis and Control of Power System Oscillations," in *Technical Brochure C4.111*. CIGRE, 1996. [Online]. Available: <https://e-cigre.org/publication/111-analysis-and-control-of-power-system-oscillations>
- [186] R. Singh, M. Elizondo, and S. Lu, "A Review of Dynamic Generator Reduction Methods for Transient Stability Studies," in *Power and Energy Society General Meeting*. IEEE, 2011, pp. 1–8.

- [187] A. M. Khalil and R. Iravani, "A Dynamic Coherency Identification Method Based on Frequency Deviation Signals," *IEEE Transactions on Power Systems*, vol. 31, no. 3, pp. 1779–1787, 2016.
- [188] M. A. M. Ariff and B. C. Pal, "Coherency Identification in Interconnected Power System - An Independent Component Analysis Approach," *IEEE Transactions on Power Systems*, vol. 28, no. 2, pp. 1747–1755, May 2013.
- [189] Y. Li, D. Yang, F. Liu, Y. Cao, and C. Rehtanz, *Theoretical Foundation of Low-Frequency Oscillations*. Springer, 2016.
- [190] M. Jonsson, M. Begovic, and J. Daalder, "A New Method Suitable for Real-time Generator Coherency Determination," *IEEE Transactions on Power Systems*, vol. 19, no. 3, pp. 1473–1482, Aug. 2004.
- [191] D. J. Trudnowski and J. W. Pierre, "Overview of Algorithms for Estimating Swing Modes from Measured Responses," in *Power and Energy Society General Meeting*. IEEE, Jul. 2009, pp. 1–8.
- [192] N. Senroy, "Generator Coherency Using the Hilbert-Huang Transform," *IEEE Transactions on Power Systems*, vol. 23, no. 4, pp. 1701–1708, Nov. 2008.
- [193] F. Raak, Y. Susuki, and T. Hikiara, "Data-Driven Partitioning of Power Networks Via Koopman Mode Analysis," *IEEE Transactions on Power Systems*, vol. 31, no. 4, pp. 2799–2808, Jul. 2016.
- [194] A. Vahidnia, G. Ledwich, E. Palmer, and A. Ghosh, "Generator Coherency and Area Detection in Large Power Systems," *IET Generation, Transmission & Distribution*, vol. 6, no. 9, pp. 874–883, 2012.
- [195] T. Guo and J. V. Milanovic, "Online Identification of Power System Dynamic Signature Using PMU Measurements and Data Mining," *IEEE Transactions on Power Systems*, vol. 31, no. 3, pp. 1760–1768, May 2016.
- [196] Z. Lin, F. Wen, Y. Ding, and Y. Xue, "Data-driven Coherency Identification for Generators Based on Spectral Clustering," *IEEE Transactions on Industrial Informatics*, vol. 14, no. 3, pp. 1275–1285, Mar. 2018.
- [197] Z. Lin, F. Wen, Y. Ding, Y. Xue *et al.*, "WAMS-Based Coherency Detection for Situational Awareness in Power Systems With Renewables," *IEEE Transactions on Power Systems*, vol. 33, no. 5, pp. 5410–5426, Sep. 2018.
- [198] A. M. Khalil and R. Iravani, "Power System Coherency Identification Under High Depth of Penetration of Wind Power," *IEEE Transactions on Power Systems*, vol. 33, no. 5, pp. 5401–5409, Sep. 2018.
- [199] D. J. Trudnowski, "Estimating Electromechanical Mode Shape From Synchrophasor Measurements," *IEEE Transactions on Power Systems*, vol. 23, no. 3, pp. 1188–1195, Aug. 2008.
- [200] P. V. Kokotovic, B. Avramovic, J. H. Chow, and J. R. Winkelman, "Coherency Based Decomposition and Aggregation," *Automatica*, vol. 18, no. 1, pp. 47–56, 1982.
- [201] L. Vanfretti, S. Bengtsson, and J. O. Gjerde, "Preprocessing Synchronized Phasor Measurement Data for Spectral Analysis of Electromechanical Oscillations in the Nordic Grid," *International Transactions on Electrical Energy Systems*, vol. 25, no. 2, pp. 348–358, 2015.
- [202] V. K. Madisetti, *The Digital Signal Processing Handbook*, 2nd ed. CRC Press, Inc., Dec. 2009.
- [203] S. Aghabozorgi, A. S. Shirkhorshidi, and T. Y. Wah, "Time-series Clustering – A Decade Review," *Information Systems*, vol. 53, pp. 16–38, 2015.
- [204] D. Francois, V. Wertz, and M. Verleysen, "The Concentration of Fractional Distances," *IEEE Transactions on Knowledge and Data Engineering*, vol. 19, no. 7, pp. 873–886, 2007.
- [205] "Principal Component Analysis," Wikipedia, Jun. 2019. [Online]. Available: https://en.wikipedia.org/w/index.php?title=Principal_component_analysis&oldid=915680157
- [206] B. J. Frey and D. Dueck, "Clustering by Passing Messages Between Data Points," *Science*, vol. 315, no. 5814, pp. 972–976, 2007.

- [207] P. Li, H. Ji, B. Wang, Z. Huang, and H. Li, “Adjustable Preference Affinity Propagation Clustering,” *Pattern Recognition Letters*, vol. 85, pp. 72–78, 2017.
- [208] RTDS, *RSCAD 5.003 Manuals: Real-time Simulation Model of IEEE 39-bus Power System*, 2018.
- [209] M. Naglic, “Synchronized Measurement Technology Supported Online Generator Slow Coherency Identification and Adaptive Tracking,” Code Ocean, 2020. [Online]. Available: <https://doi.org/10.24433/CO.3369095.v1>

ACKNOWLEDGEMENTS

The research work of this thesis could not be possible without the financial support from Dutch Scientific Council NWO and Shell International B.V., and the in-kind contributions from TenneT TSO B.V., Dutch Metrology Institute VSL, General Electric, and Schweitzer Engineering Laboratories, which I very gratefully acknowledge.

First, I would like to express my deepest appreciation and sincere thanks to my promoters Prof. ir. Mart A.M.M. van der Meijden and Dr. Dipl.-Ing. Marjan Popov for their support and encouragement throughout this work.

Mart, you have been the utmost remarkable Mentor (yes, with the capital *M*) to me. Thank you for the trust in me, numerous challenging, learning, and inspiring debates, the opportunities to prove myself, and your genuine support and encouragements when needed. I got to a realisation that pushing the limits during a Ph.D. research is not only about excellent results, but at most in enormous personal development for which I am incredibly grateful to you.

Marjan, without you, I would not experience this extraordinary life-changing journey. I am deeply grateful to you for offering me the Ph.D. research position, and your very warm welcome on the first day we met. I would like to express my appreciation for your trust in my competences, the opportunities to gain international experiences, and the nomination in the first place. Thank you for the invaluable guidance during the publication of our research and throughout this thesis.

I would also like to express a special thank you to Prof. Dr. Vladimir Terzija, The University of Manchester, for your active participation in the publications. I am confident to say that our future as cutting-edge researchers on the WAMPAC topic is more than bright. I am looking forward to our next collaboration.

My sincere gratitude goes to all members of the doctoral examination committee for the efforts spent on this thesis, invaluable feedback, and participation in my defence. It has been an absolute honour and pleasure for me to have such first-class experts on board.

I would like to thank Dr. Leo J. Korstanje for chairing of the URSES project meetings, and to all unnamed participants of the URSES project consortium for successful collaboration.

Furthermore, I would like to thank you Dr. Janko Kosmač, ELES, and Mag. Andrej Souvent, EIMV, for your trust in me and the encouragements with starting the Ph.D. research abroad. I hope we will further nourish our continued relationship.

I am truly grateful for the involvement and the support that I have received during my Ph.D. research, both from my colleagues at the TUD as well as from other interesting people that I have had the opportunity to meet. I consider myself fortunate that some of

them perceive me as a close friend. To all the friends, colleagues and others, please accept my warmest appreciation and thanks for the great moments we have spent together. I am looking forward to our next life path crossings and joint adventures.

Last and foremost, my deepest appreciation and thanks go to both families in Slovenia, especially to my parents Zdenka and Miran, for their endless support and believing in me. Special thanks go to my dear wife Tina for her unconditional encouragements and support in all means. Tina, you and our son Mark are the brightest stars in the universe, my true inspiration to follow.

Matija Naglič

Delft, February 2020

BIOGRAPHY



Matija Naglič was born on the 8th of January 1987 in Kranj, Slovenia. He received uni. dipl. inž. degree in Electrical Engineering, study filed Telecommunications, grade 10, from the Faculty of Electrical Engineering, University of Ljubljana, Ljubljana, Slovenia in 2011.

From 2011 to 2014 he was a researcher with the Milan Vidmar Electric Power Research Institute, Ljubljana, Slovenia. From 2014 to 2019, he was a Doctoral Researcher in the Intelligent Electrical Power Grids group at Faculty of Electrical Engineering, Mathematics and Computers Science, Delft University of Technology, Delft, The Netherlands. In 2020, he joined TenneT TSO B.V., Arnhem, The Netherlands, to pursue on the automation of power systems.

Publications related to this thesis:

- Journal papers:

1. M. Naglic, M. Popov, M. A. M. M. van der Meijden, and V. Terzija, “Synchronized Measurement Technology Supported Online Generator Slow Coherency Identification and Adaptive Tracking”, *IEEE Transactions on Smart Grid*, early access, Dec. 2019.
2. M. Naglic, M. Popov, M. A. M. M. van der Meijden, and V. Terzija, “Synchro-measurement Application Development Framework: an IEEE Standard C37.118.2-2011 Supported *MATLAB* Library,” *IEEE Transactions on Instrumentation and Measurement*, vol. 67, no. 8, pp. 1804–1814, Aug. 2018.
3. M. Naglic, L. Liu, I. Tyuryukanov, M. Popov, M. A. M. M. van der Meijden, and V. Terzija, “Synchronized Measurement Technology Supported AC and HVDC Online Disturbance Detection,” *Electric Power Systems Research*, vol. 160, pp. 308–317, Jul. 2018.
4. P. Ceferin, M. Naglic, A. Souvent, “WAMS Systems and ICT Networks”, *CIGRE Science & Engineering Journal*, vol. 6, pp. 109–118, Jun. 2016.

- International conference papers:

1. M. Naglic, L. Lian, I. Tyuryukanov, M. Popov, M. A. M. M. van der Meijden, and V. Terzija, “Synchronized Measurement Technology Supported AC and HVDC Online Disturbance Detection”, *International Conference on Power Systems Transients (IPST 2017)*, Seoul, Republic of Korea, Jul. 2017.
2. M. Naglic, I. Tyuryukanov, M. Popov, M. A. M. M. van der Meijden, and V. Terzija, “WAMPAC-ready Platform For Online Evaluation Of Corrective Control Algorithms,” *Mediterranean Conference on Power Generation, Transmission, Distribution and Energy Conversion (MedPower 2016)*, IEEE, Belgrade, Serbia, Sep. 2016.

- Book chapters:

1. M. Naglic, A. Joseph, K. Pan, M. Popov, M. A. M. M. van der Meijden, and P. Palensky, “Grid Awareness Under Normal Conditions and Cyber-Threats,” in *Intelligent Integrated Energy Systems*, Springer, pp. 55–75, Oct. 2018.

- Open-source software:

1. Synchro-measurement Application Development Framework: an IEEE Standard C37.118.2-2011 Supported *MATLAB* Library, GitHub, 2018, [Online]. Available: https://github.com/matijanaglich/SADF_IEEE_C37.118.2-2011
2. Synchronized Measurement Technology Supported AC and HVDC Online Disturbance Detection, GitHub, 2020, [Online]. Available: https://github.com/matijanaglich/SMT_disturbance_detection
3. Synchronized Measurement Technology Supported Online Generator Slow Coherency Identification and Adaptive Tracking, Code Ocean, 2020, [Online]. Available: <https://doi.org/10.24433/CO.3369095.v1>

- Patent applications:

1. M. Naglic, M. Popov, and M. A. M. M. van der Meijden, “Synchronized Measurement Technology Supported Online Generator Slow-coherency Identification and Dynamic Tracking”, *ref: P6077250NL*, Netherlands, under process.

Other publications:**- International conferences:**


1. I. Radevic, M. Naglic, O. Mansour, D. Bijwaard, and M. Popov, "Smart DFT Based PMU Prototype," *International Conference on Smart Grid Synchronized Measurements and Analytics (SGSMA)*, IEEE, Texas, USA, May 2019.
2. I. Tyuryukanov, J. Quiros-Tortos, M. Naglic, M. Popov, M. A. M. M. van der Meijden, and V. Terzija, "A Post-processing Methodology For Robust Spectral Embedded Clustering Of Power Networks," *International Conference on Smart Technologies (EUROCON 2017)*, IEEE, Ohrid, Macedonia, Jul. 2017.
3. I. Tyuryukanov, J. Quiros-Tortos, M. Naglic, M. Popov, M. A. M. M. van der Meijden, and V. Terzija, "Controlled Islanding Of Power Networks Based On Graph Reduction And Spectral Clustering", *Mediterranean Conference on Power Generation, Transmission, Distribution and Energy Conversion (MedPower 2016)*, IEEE, Belgrade, Serbia, Sep. 2016.

- Book Chapters:

1. I. Tyuryukanov, M. Naglic, M. Popov, and M. A. M. M. van der Meijden, "Implementation of Slow Coherency Based Controlled Islanding Using DIGSILENT PowerFactory and *MATLAB*," *Advanced Smart Grid Functionalities Based on PowerFactory*. Gonzalez-Longatt, F. & Rueda Torres, J. L. (eds.). Cham: Springer International Publishing AG, p. 279-299, Dec. 2017.

Distinctions related to this thesis:

1. 2018 Apple prize for "pioneering and innovative work supported by excellent research and education results" on the topic of Power System Control Room of Future, Department of Electrical Sustainable Energy, Faculty of Electrical Engineering, Mathematics and Computer Science, TU Delft, Dec. 2018.
2. The conference paper presented in International Conference on Power Systems Transients (IPST 2017) was selected for invited publication in Electric Power Systems Research journal.



This thesis aims to provide insight into the necessary power system operation and control developments to facilitate a sustainable, safe and reliable electric power supply now and in the future. The primary objective is to enhance the interconnected power system situational awareness with the aim of reinforcing the reliability of power systems. First, the thesis elaborates on the existing and emerging operational challenges of modern power systems and identifies the required power system developments to overcome them. Next, it focuses on state-of-the-art Synchronised Measurement Technology (SMT) supported Wide-area Monitoring Protection and Control (WAMPAC) of power systems. In this context, a cyber-physical experimental testbed for online evaluation of the emerging WAMPAC applications under realistic conditions is developed. Following, to fill the scientific gap between the IEEE Std. C37.118-2005 (communication part) and IEEE Std. C37.118.2-2011 specifications and their implementation, the MATLAB supported Synchro-measurement Application Development Framework is developed. Next, to improve situational awareness of power systems, two SMT-supported algorithms are proposed. The first algorithm is suitable for online detection of disturbances, observed as excursions in SMT measurements, in AC and HVDC power grids. Whereas the second algorithm is suitable for online identification of grouping changes of slow coherent generators in an interconnected power system during quasi-steady-state and the electromechanical transient period following a disturbance. Finally, further research directions towards the Control Room of Future are presented.